Late Holocene development of a polygon mire in NW Yakutia inferred from plant macrofossil and lithological analysis

Diplomarbeit

Universität Potsdam

Institut für Erd- und Umweltwissenschaften - Geoökologie

Eingereicht von

Juliane Wolter

1. Gutachterin : Prof. Dr. Ulrike Herzschuh

Universität Potsdam;

Alfred-Wegener-Institut Potsdam

2. Gutachter:

PD Dr. Bernhard Dieckmann

Alfred-Wegener-Institut Potsdam

Potsdam, im November 2010

Contents

List of figures

List of tables

Kurzfassung

Das untersuchte Polygonmoor gehört zu einem Moorkomplex in einem verlandeten Altarm des Anabar in der Waldtundra des Nordsibirischen Tieflandes. Ziel der Diplomarbeit ist einerseits die Beschreibung dieses Polygonmoors, andererseits die Rekonstruktion seiner Entwicklung während der vergangenen 1500 Jahre. Dazu wurden morphologische, sedimentologische, isotopengeochemische, botanische und paläobotanische Analysen vorgenommen. Morphologie und Vegetation des Moors wurden während der Expedition im August 2007 vor Ort untersucht. Für sedimentologische, isotopengeochemische und paläobotanische Analysen wurden Proben entlang einer Oberflächentransekte, aus je einem Bodenprofil vom Polygonwall und dem Übergangsbereich zwischen Wall und Mitte sowie aus einem Kurzkern aus der Moormitte entnommen.

Das Polygonmoor misst etwa 13 m im Durchmesser und besteht aus von polygonförmig angeordneten Eiskeilen emporgehobenen Sedimentwällen, die eine etwa 0,6 m tiefer liegende Mulde umgeben, in der sich Wasser staut. Die kleinteiligen Änderungen der Mikrotopograpie bringen ein Mosaik von Pflanzenhabitaten hervor. Zwischen der typischen Tundravegetation auf dem Polygonwall und der Moorvegetation im Zentrum liegen nur wenige Meter. Dazwischen finden sich Übergangsgesellschaften. Auch die anderen untersuchten Parameter zeigen typische Veränderungen vom Wall hin zum Zentrum. In der Mitte des Moores ist die Auftauschicht am mächtigsten, die Bodentemperatur am höchsten. Relativ geringe TOC-Gehalte und C/N-Verhältnisse sind bedingt durch die aquatische Vegetation. Die Bedingungen im Polygonwall sind nicht so einheitlich wie in der Moormitte. Besonders die Auftautiefen sind hier variabel. Die Bodentemperaturen sind niedrig, der pH-Wert schwach sauer, TOC und C/N aufgrund der terrestrischen Vegetation hoch. Im Übergangsbereich finden sich intermediäre Bedingungen. Diese Erkenntnisse ermöglichen eine Rekonstruktion vergangener Bedingungen aus dem abgelagerten torfreichen Sediment.

Die ältesten Proben stammen aus der Zeit um das 5. Jh. n. Chr. und zeigen relativ trockene Bedingungen in Wall und Übergang. Etwa um das 15. Jh. n.Chr. beginnt eine kühlere Phase mit erhöhtem Wasserspiegel im Polygon. In den jüngsten Proben zeichnet sich eine erneute Erwärmung sowie ein sinkender Wasserspiegel ab. Polygonmoore sind ausgezeichnete paläoökologische Archive, es muss jedoch beachtet werden, dass Sedimentparameter und Vegetation innerhalb der Polygone eine große Variabilität zeigen. Multidisziplinäre Untersuchungen und ein genaues Verständnis der Funktionsweise von Polygonmooren helfen bei der Rekonstruktion vergangener Umweltparameter.

Moore speichern große Mengen Kohlenstoff, der im Verlauf der klimatischen Erwärmung der Arktis als Kohlenstoffdioxid und Methan in die Atmosphäre gelangen könnte. Speicherfunktion und Regulationsmechanismen der Polygonmoore, besonders in diesem immer noch wenig erforschten Teil Sibiriens, sind bislang nicht hinreichend verstanden.

1 Introduction

Polygon mires are the typical mire type of the Arctic. They develop in polygonal nets of ice wedges and cover 3 % of the arctic land area (Minke et al. 2007). Moisture, temperature and active-layer dynamics define habitats in arctic environments (ACIA 2005) and are determined by topography (Brown et al. 1980, Webber et al. 1980). Polygon mires diversify the microtopography and provide a series of more or less favourable microhabitats for life in an otherwise hostile environment (ACIA 2005). They are also of central importance in the carbon and methane balance of the Arctic tundra (Hobbie et al. 2000, Wagner et al. 2003, 2005, Kutzbach et al. 2004), where the largest climate change is expected (ACIA 2005). Polygon mires are especially susceptible to climate change (ACIA 2005) and may release substantial amounts of greenhouse gases into the atmosphere when the air temperature rises and especially when they dry up (Smol & Douglas 2007, Sachs et al. 2008). Small intrapolygonal ponds are particularly endangered of falling dry because of their small water volume and low depth (Smol & Douglas 2007). The recent desiccation of ponds observed in the Canadian Arctic has been associated with climate warming (Smol & Douglas 2007). Once the peat has dried up decomposition accelerates and the mire is consequently eroded.

Sediments accumulating in polygon mires under anaerobic conditions preserve plant and animal remains as well as sedimentological characteristics and ultimately the environmental history of the site, which may be inferred from these proxies (Fortier & Allard 2004, Ellis & Rochefort 2006, Minke et al. 2007). Moreover, active ice wedges are restricted to the zone of continuous permafrost (French 2007), and their presence is in itself evidence for extremely cold and dry winters (Washburn 1980). The ice-rich sediment sequences called ice complex developed from polygonal tundra and provide the most important palaeoenvironmental archives covering the Holocene and Pleistocene in the Arctic (Kienel et al. 1999, Schirrmeister et al. 2002, Andreev et al. 2004, Eisner et al. 2005).

Relatively few studies have been carried out on Siberian polygon mires, and the processes controlling polygon mires are still not completely understood (e.g. Minke et al. 2007). Studies of the past development of polygon mires may also provide insights into their possible reaction to changes in climate.

During August 2007, a polygon mire north of Saskylakh near the eastern bank of the Anabar river (72.07° N and 113.92° E) was studied. In the field, a vegetation survey was carried out, and ground surface elevation, active layer depth and soil temperature were determined. pH and conductivity were measured along a transect through the polygon. Surface samples were

taken from the transect and two profiles were dug, one on top of the polygon ridge and one in the transition between ridge and centre. Additionally, a short core was taken from the submerged centre of the mire. Plant macrofossil analysis was carried out for the surface transect and the two profiles. Organic matter composition (TOC, TC, TN, C/N), grain size and stable carbon isotopes ($\delta^{13}C$) were analyzed for all taken samples.

The objectives of this work are:

- to characterise the morphology, sedimentology and vegetation in a Northwest Yakutian polygon mire,
- to understand the relationship between the studied parameters and the respective conditions in the polygon ridge, ridge-centre transition and centre,
- to explore the representation of the polygon vegetation in the macrofossil assemblage in a surface transect through the mire,
- to study the development of the polygon mire and its vegetation, hydrological regime and climate during the last 1500 years, and
- to possibly be able to understand the reaction of polygon mires to a changing climate.

2 Study Area

2.1 Regional setting

The study area is situated in the Anabar Region in Northwest Yakutia, Siberia (see Fig. 1). Yakutia is a scarcely inhabited Russian republic with only 0.3 inhabitants per square kilometer on average. Its size of 3.1 million square kilometers is comparable to India, but only 950,000 people live there (Federal State Statistics Service Russia 2009). About two third of the population live in urban surroundings, so that most of the land is virtually uninhabited.

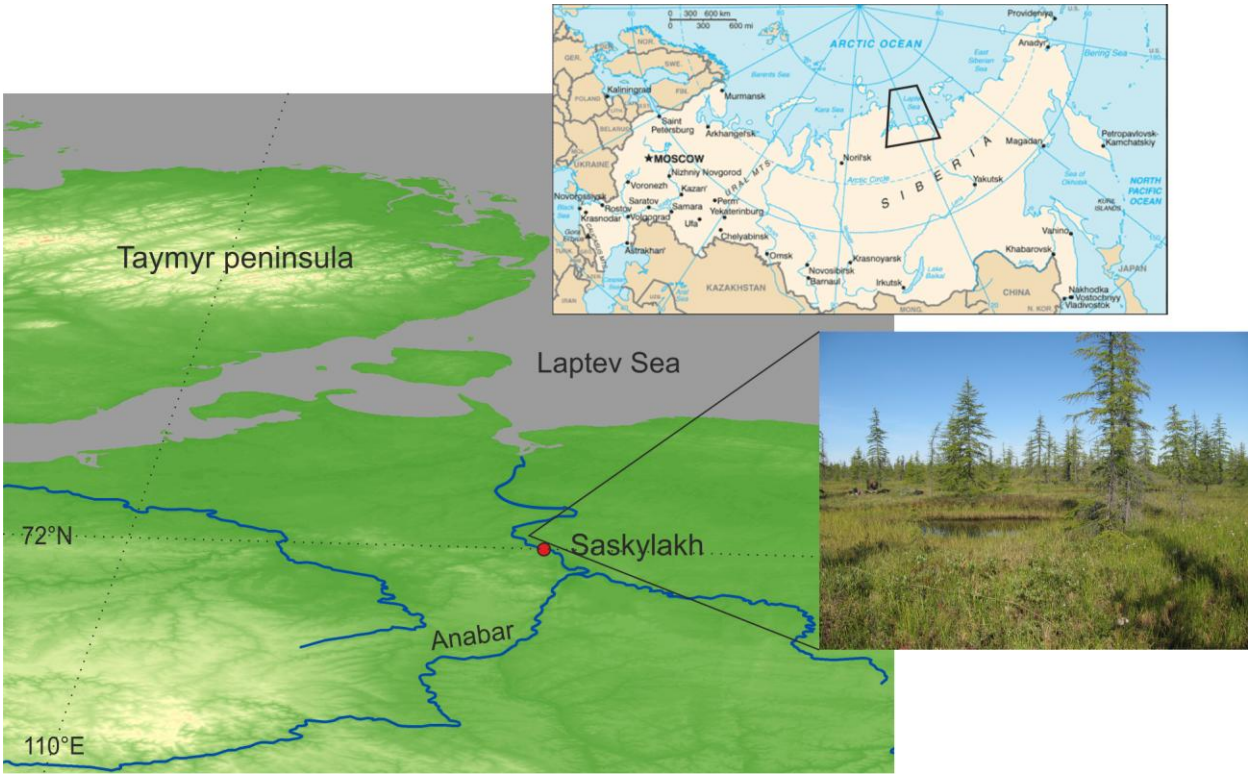

Fig. 1 Study area in the North Siberian Lowland; the polygon mire is situated about 50 km north of the town Saskylakh and east of the Anabar River, which flows into the Laptev Sea, a marginal sea of the Arctic Ocean; the photograph shows the studied polygon with intrapolygonal pond and *Larix gmelinii* growing on elevated ridges (small map: The World Factbook, Anabar map: Yongbo Wang, Alfred-Wegener Institute Potsdam, photograph: Ulrike Herzschuh, Alfred-Wegener Institute Potsdam)

The studied polygon mire is located about 50 km to the north of Saskylakh, the administrative centre of the district Anabarsky ulus ("Anabar region"). The Anabar region has 4,000 inhabitants, the majority living in four settlements on 181,700 km², which is about half the size of Germany. The northern part of the region (north of Saskylakh) belongs to the North Siberian Lowland, the southern part (south of Saskylakh) to the Central Siberian Plateau.

The main river is the Anabar, which has its source in the Central Siberian Plateau and flows north to the Laptev Sea in the Arctic Ocean. Only 150 of its 939 km length are navigable during the summer months (Huh & Edmond 1999). In winter, it freezes to the bottom (Huh & Edmond 1999, Koronkevich 2002), and the river's average discharge of roughly 500 m^3/s occurs solely during the snowmelt and until the end of summer, concentrating on the months May to July (see Fig. 2).

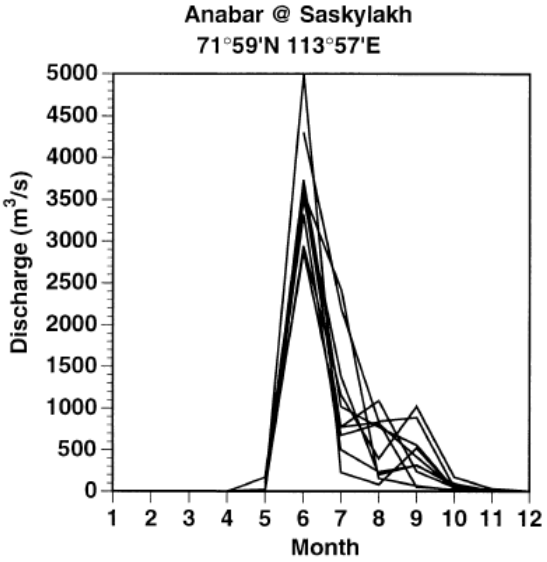

During the last glacial maximum (LGM) the Anabar region was not glaciated; local ice shields occurred in the Verkhoyansk mountains in the east, the Putorana Mountains in the west and along the northern fringe of the Taymyr peninsula in the north (Svendsen et al. 2004).

Fig. 2 Multi-year hydrograph showing average monthly discharge of Anabar river (Huh & Edmond (1999) using data from UNESCO (1979))

2.2 Geology and soils

The main geological structures in Yakutia are the Verkhoyansk-Kolyma orogen in the east and the Siberian Craton in the west (see Fig. 3). Archaean gneiss rocks form the basement of the craton, outcrops of which are found in the Anabar shield (e.g. Koronovsky 2002), the Aldan-Stanovoy shield and the Yenisey and Baikal uplifts (e.g. Huh & Edmond 1999). The remainder of the craton is covered by sediments of different geneses. The study area is situated in the lowland part of the Anabar region, which is relatively flat in relief and covered by silty and sandy alluvial and glaciomarine Quaternary deposits as well as Mesozoic marine, continental and lagoon sediments (Sokolov et al. 2004). Abundant thermokarst lakes, pingos, ice wedge polygons and other cryogenic landforms diversify the microrelief. In the FAO classification (IUSS 2007), all Yakutian soils are cryosols, i.e. soils with permafrost within 1m depth. The perennially frozen subsoil impedes drainage, and low soil oxygen and temperatures lead to slow mineralization and accumulation of organic matter. In the freeze-thaw top layer, the so-called "active layer", cryogenic processes such as thermal cracking, cryogenic sorting or cryoturbation are visible (IUSS 2007). Stagnating soil water with changing water levels leads to gleying of the soil in the active layer. The diverse Yakutian

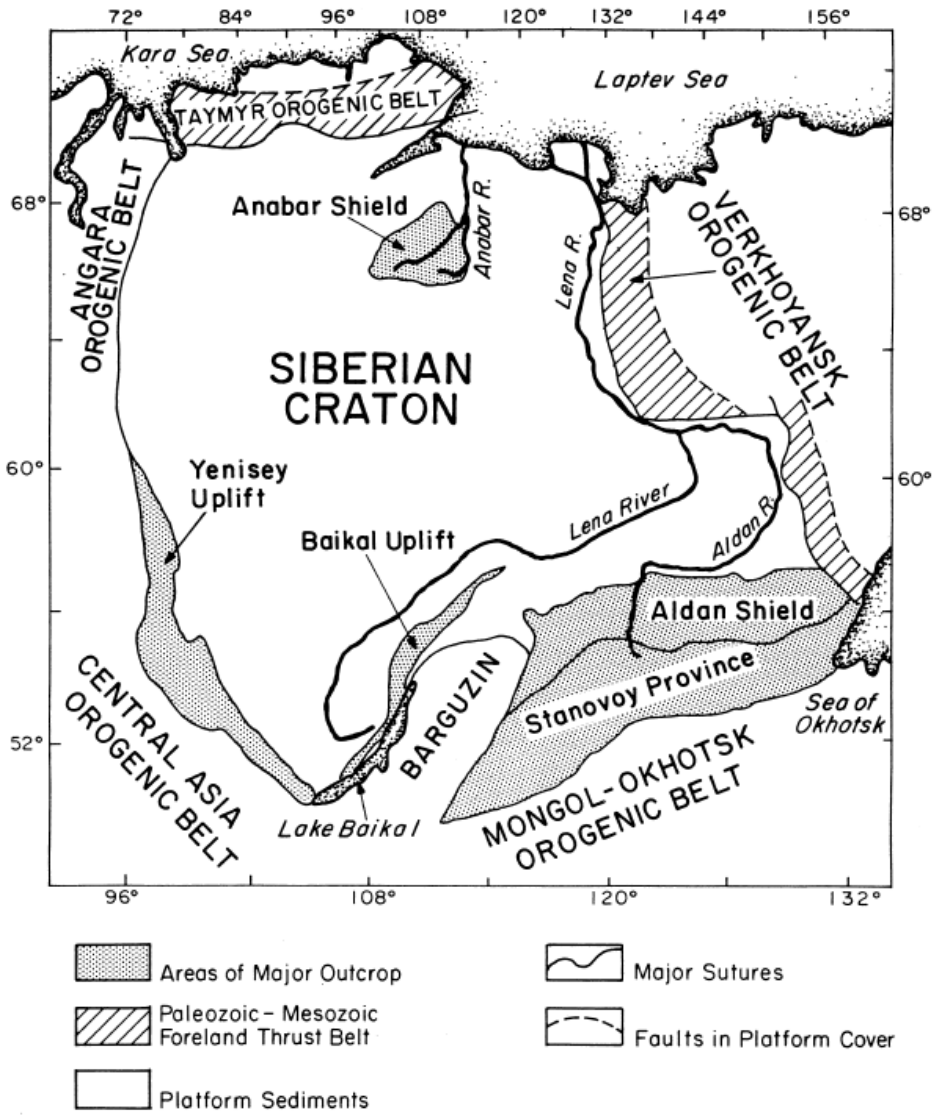

Fig. 3 Geotectonic map of the Siberian Craton with the Anabar River and Shield in the north (Huh & Edmond (1999), adapted from Rosen et al. 1994)

microtopography creates complex soil cover patterns, however, and soils associated with cryosols are histosols, gleysols and podzols with various modifications. Hydromorphic and acidic soils prevail throughout the Anabar region (Sokolov et al. 2004). Peat soils forming in cryogenic depressions, in lowlands and on floodplains are historthels and aquiturbels (United States Department of Agriculture (USDA) 1998, Kutzbach et al. 2004).

2.3 Climate

The Climate in Eastern Siberia is sharply continental, with low precipitation rates, large seasonal differences in air temperature and extremely low winter temperatures. This continentality is caused by the huge land mass of the Eurasian continent isolating its inner

parts from oceanic influence. The proximity to the Arctic Ocean does not milden conditions much, because the Arctic Ocean remains frozen for most of the year, reducing thermal conduction from the water (Shahgedanova 2002, Weischet & Endlicher 2000). Winter cooling is enhanced by lack of clouds and a relatively thin snow cover, allowing temperature fluctuations to penetrate the snow (Nicholson & Granberg 1973), but still producing albedo values of up to 80 % (Weischet & Endlicher 2000) during nine months of the year.

The general atmospheric circulation over Eastern Siberia is relatively simple, with a conspicuous change between summer and winter. During winter, radiational cooling of the earth surface promotes the development of high pressure. The "Siberian high" dominates the lower part of the northeast Asian atmosphere between November and March. High pressure starts to build up around the end of August and peaks in February, beginning to weaken in early April (Shahgedanova 2002). As it is thermally induced, the Siberian high does not reach higher than approximately 850 hPa. Above this height, a trough linking the Icelandic and Aleutian lows is prevalent (Shahgedanova 2002 and Weischet & Endlicher 2000). Generally, cyclonic activity declines eastwards and depressions reach areas east of the Yenisey River infrequently (Shahgedanova 2002). Temperatures are therefore controlled by radiative loss of energy rather than by the atmospheric circulation (Shahgedanova 2002). In winter, moist cyclonic airmasses are deflected to the north by the strong Siberian anticyclone. As cyclones are the main providers of moisture in Yakutia (Gavrilova 1993), dry and cloudless conditions ensue.

High insolation and the resulting heating of air masses lets the Siberian high dissipate towards summer (Franz 1973), to be replaced by a weak low pressure zone by the beginning of June. The pressure difference enhances the transport of moist Atlantic air and cyclones from the Sea of Okhotsk. The resulting summer precipitation maximum can be observed for the whole of northeast Asia (Mock et al. 1998).

The study area is located about 560 km north of the polar circle. At this high latitude, the Polar day lasts from May to August, the polar night lasts from November to January. The average winter snow height ranges from 20 cm in the North to 50 cm in the south (Agricultural Atlas of the Republic Sakha (Yakutia) 1989). Snowmelt usually starts around the beginning of June, and the growing season lasts from the middle of June to the middle of September (Boike et al. 2008), when a continuous snow cover is established. About 40-50 percent of the annual precipitation fall as rain during the growing season. Still, precipitation amounts during that time are small, in Saskylakh they average between 34mm in July and 54mm in August. During the months June to August potential evapotranspiration

exceeds precipitation (Rivas-Martínez 2007), and plant-available soil moisture is mainly provided by snow and permafrost melt (Popp 2006).

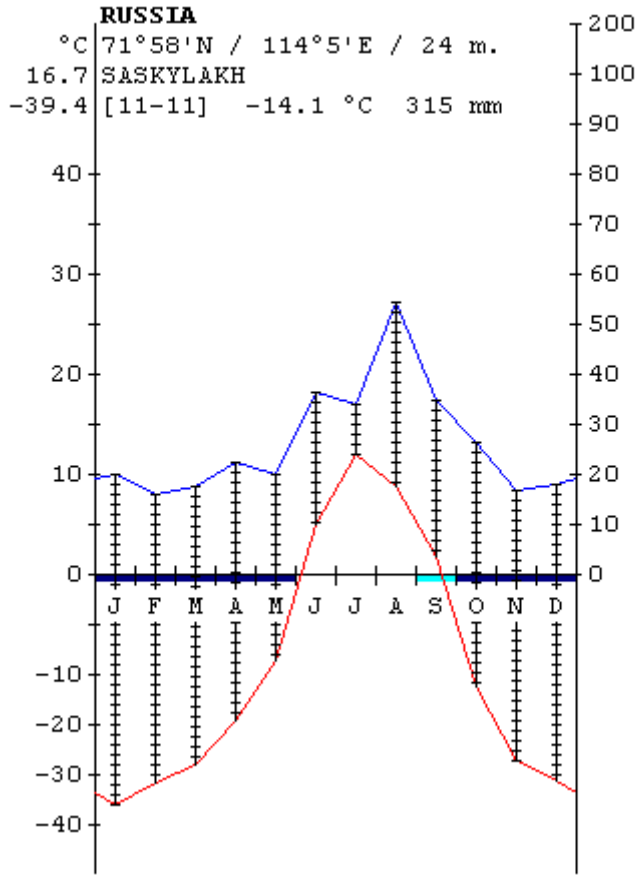

Fig. 4. Climate diagram from the meteorological station in Saskylakh (Rivas-Martinez 2007), mean annual precipitation and temperature averaged from data for the observation period 1984-1994

A climate diagram from the meteorological station in Saskylakh, which is located about 50 km south of the studied polygon, is shown in Fig. 4. The mean annual temperature in Saskylakh is -14°C, with an average of 12°C in July, and -36.1°C in January. The absolute maximum temperature of the warmest month is 32.2°C, while the absolute minimum temperature of the coldest month is -57.2°C. The large temperature amplitude of ~ 90 K marks the extreme continentality of the location. Mean annual precipitation is at 315 mm. Precipitation is highest in summer and lowest in winter, and about half the annual precipitation is measured during the months June to September.

2.4 Vegetation

Plants have to cope with rather difficult conditions in the far north. Extreme winter cold, strong wind and associated snow abrasion, a very short and cool growing season and lack or excess of plant-available water are just some of the hardships facing them (Marchand 1996). Direct human influence, however, is minimal in large areas.

Vegetation in general is characterized by low growth and low biodiversity. The regional biome is the tundra, with the polar desert adjoining to the north and the forest-tundra to the south. The tundra zone is comprised of the three subzones arctic tundra, typical tundra and southern tundra (see Fig. 5).

A detailed vegetation description was made for the adjacent Taymyr peninsula (Matveyeva 1994), where all three subzones of the tundra are present, with polar desert in the north and forest tundra in the south. The author suggests the value of this classification as a representative of the entire Siberian arctic.

Typical and southern tundra are the main vegetation subzones in the Anabar region. To the north, the typical tundra extends to the July 5°C-isotherm, bordering on the arctic tundra zone or the Arctic Ocean. The border between the typical and southern tundra is marked by the July isotherms 8-10°C. Arctic tundra is found in the northern part of the Taymyr peninsula, with local occurrences along the Anabar river shore. Polygonal stands of dwarf-shrub-moss communities mostly grow less than 10 cm tall, *Hylocomium splendens* being the characteristic moss and *Salix polaris, S. arctica* and *Dryas* the only dwarf shrubs present (Matveyeva 1994). This zone remained treeless during the entire Holocene (Aleksandrova 1980).

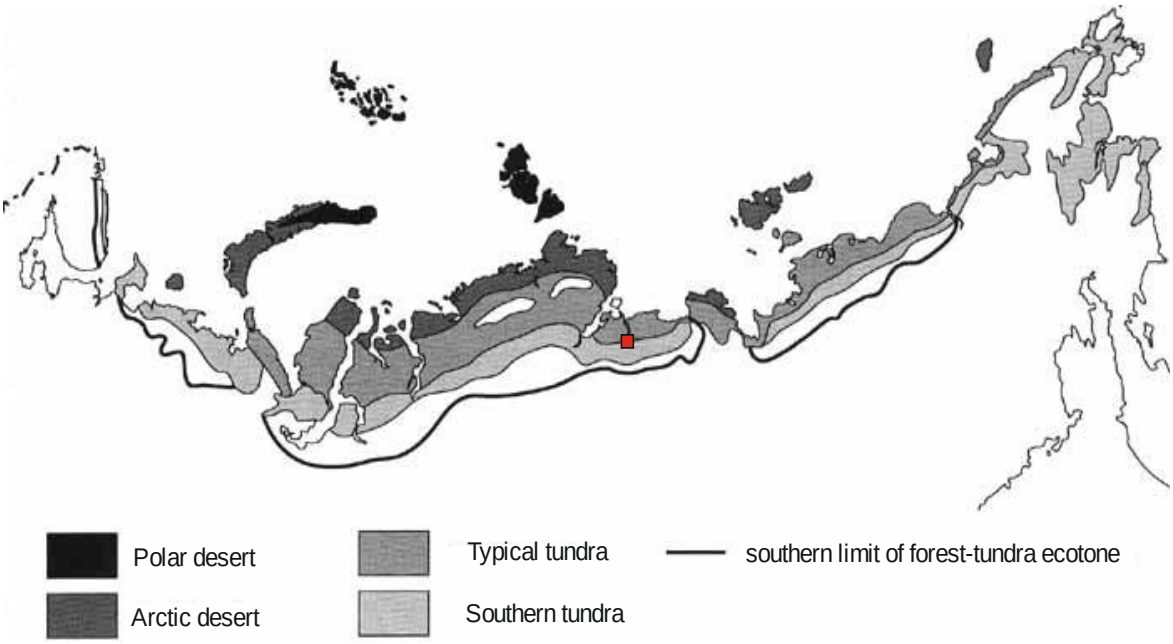

Fig. 5 Map of vegetation zones of the Russian Arctic (modified after Shahgedanova & Kuznetsov 2002); the red square indicates the position of the studied polygon in the southern tundra subzone

The typical tundra, also referred to as sedge-moss-tundra, is characterized by a continuous vegetation cover made up mostly of mosses, lichens, shrubs and sedges, typical species include *Hylocomium splendens* and *Carex ensifolia ssp. Arctisibirica*; and *Betula nana* and different Ericaceae occur (Matveyeva 1994). Plants of the typical tundra rely on snow to survive the harsh winters and seldom grow higher than the protective snow cover (20-50 cm). In the southern tundra, which is also called forest tundra, bushes grow slightly higher and individual trees appear, *Larix gmelinii* forming the tree-line (Shahgedanova & Kuznetsov 2002). Along rivers, patches of woodland occur. The ground level is comprised of a continuous and species-rich moss cover and grasses and dwarf-shrubs thrive beneath the bushes. *Alnaster fruticosa*, *Betula nana* and *Eriophorum vaginatum* are species characteristic to this subzone (Matveyeva 1994).

Plant communities typical to the three subzones occur mostly on plakors, one of the five major habitats named by Matveyeva (1994), as the hydrothermal regime in these flat or gently sloping, well-drained sites reflects the macroclimatic conditions of the subzones. The main zonal association occurring on plakors in the tundra zone is *Carici arctisibiricae - Hylocomietum alaskanii*.

On snowbeds, fellfields, south-facing slopes and in wetlands, different types of plant communities are found (Matveyeva 1994). On snowbeds, varying types of herb-moss or

lichen-moss communities are found. Fellfields are covered by dwarfshrub communities dominated by *Dryas punctata*. On south-facing slopes, herb-grass meadows prevail. Mires and bogs are the most widespread non-plakor habitats and cover roughly 560,000 km² of the typical and southern tundra (Bliss & Matveyeva 1992). Plant communities on wetlands are moss-rich communities with an herb layer and sometimes low shrubs growing atop the moss turf. On Taymyr, wetland communities of the class *Scheuchzerio-Caricetea nigrae* belong to the order *Tofieldietalia*, for which Matveyeva (1994) proposed the new alliance *Caricion stantis*. In mire depressions, which maintain a moist soil throughout the entire vegetation period, such as the mires in low-centred polygons, plant communities of the association *Meesio triquetris-Caricetum stantis* prevail. The studied polygon mire is part of the southern tundra zone's wetlands (see Fig. 5).

2.5 Permafrost

In the unglaciated regions of the Arctic, permafrost is one of the main factors determining soil formation and plant growth. Permafrost is defined as ground whose temperature does not exceed 0°C for at least two consecutive years (Harris et al. 1988). Weise (1983) specifies two types of permafrost: dry permafrost, containing practically no water (e.g. rocks) and ice-rich permafrost, which may have ice contents of up to 50 - 80 %, for example the silty and sandy loams of the Lena Terraces. This kind of ice-rich sediment is called "Ice Complex" (Brouchkov et al. 2004).

Permafrost extends over about one fourth of the earths land area (Anisimov & Nelson 1996), and roughly half of it is classified as continuous permafrost, where 90-100 percent of the subsoil are frozen. Yakutia is completely underlain by continuous permafrost (see Fig. 6), and its depths range from 300 m in the south to 600 m in the north, exceeding 1000 m in the northern part of the Central Siberian Plateau (Geocryology of the USSR: Eastern Siberia and the Far East 1989). Generally, permafrost in the mountains reaches deeper than in lowlands because of the higher thermal conductivity of rocks (French 2007). One of the largest known permafrost thicknesses of 1200-1470 m was found in the Anabar tableland (Geocryology of the USSR: Eastern Siberia and the Far East 1989).

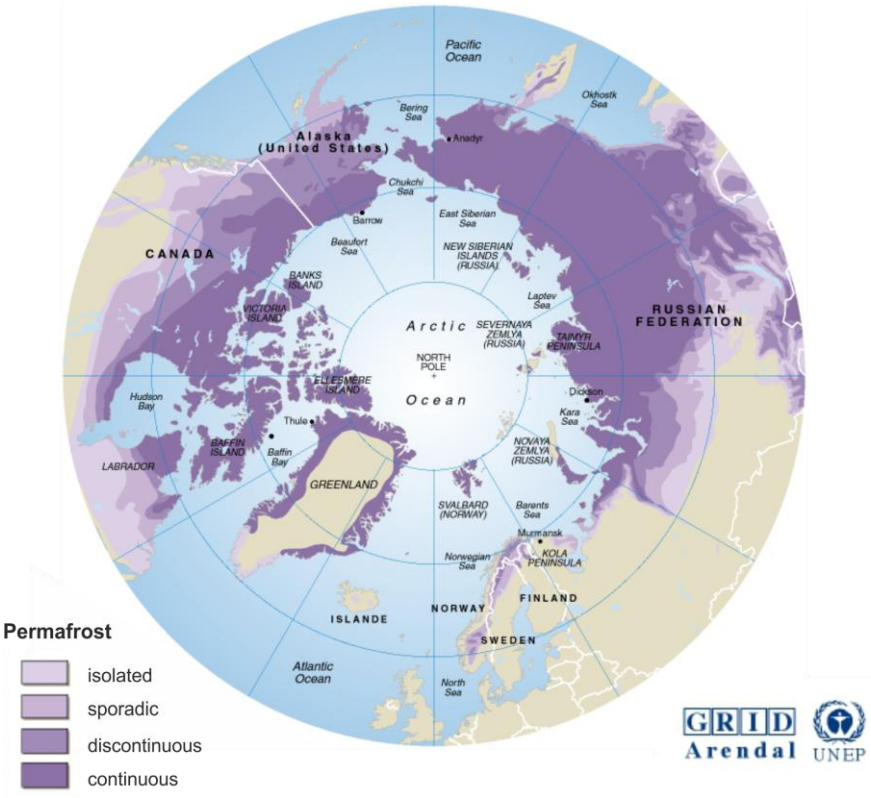

Fig. 6 Circumpolar map of permafrost distribution (International Permafrost Association 1998)

The upper part of the permafrost soil, which thaws in summer and freezes in winter, is called the active layer. Yakutian active layer depths commonly range from 0.2 m (peat soils of the north) to 2.5 m (coarsely textured mineral substrates of the south), depending mainly on latitude, substrate and vegetation cover (Sokolov et al. 2004).

In the Anabar region, permafrost is promoted by the surface vegetation cover, usually mosses, which prevents summer heating (Gavrilova 1993), and the relatively thin snow cover of only 20 to 50 cm (Agricultural Atlas of the Republic Sakha (Yakutia) 1989), which does not insulate the ground efficiently (cf. Nicholson & Granberg 1973), but reflects incoming radiation, causing extreme cooling of the ground during winter.

In permafrost soils, successive freeze and thaw events cause processes such as ice segregation, cryoturbation, cryogenic sorting, frost heave, frost shattering of rocks, mass wasting on slopes and thaw-related thermokarst. This brings forth the typical periglacial landforms such as patterned ground, palsas and pingos, thermokarst depressions and ice wedge polygons.

2.6 Polygon mires

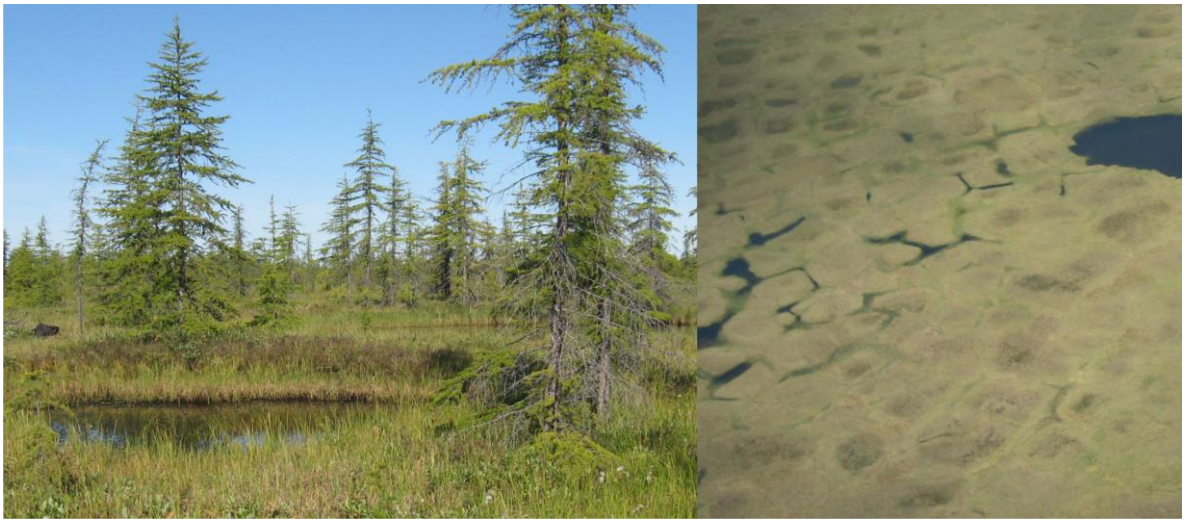

Fig. 7 Studied polygon with intrapolygonal pond and *Larix gmelinii* trees on the elevated ridges; the photograph on the right shows polygonal tundra in the Anabar region (Ulrike Herzschuh, Alfred-Wegener-Institute Potsdam)

Polygon mires are the characteristic mire type of the tundra lowlands of the Arctic. Minke et al. (2007) estimate that 3% of the Arctic land mass, about 250,000 km^2, are covered by polygon mires. They exist in the arctic coastal plains of Alaska, the middle and low Arctic of Canada (Mackenzie delta) and in northern Siberia (Minke et al. 2007) (see Fig. 8). Outside these regions, incidental occurrences may be found. In Siberia, they are abundant in the southern, low-lying parts of the Taymyr peninsula, the Yenisey lowlands, the Lena delta and the Yana-Indigirka and Kolyma lowlands (Botch & Masing 1983, Naumov 2004), where they occur most frequently on flat watersheds, river terraces and floodplains as well as on the bottom of drained lakes (Boch 1974). A photograph of the studied polygon is shown in Fig. 7. Polygon mires can be either low-centred or high-centred. Low-centred polygons have elevated ridges around a central depression, while high-centred polygons are surrounded by trenches which develop when ridges collapse due to ice wedge melt (Minke et al. 2007). High-centred polygons are eroded readily. The trenches serve as drainage channels, and the dried peat is eventually oxidized or blown away (Zoltai & Pollett 1983). In low-centred polygons, however, peat accumulates continuously. The studied polygon is low-centred, which is also the most common type.

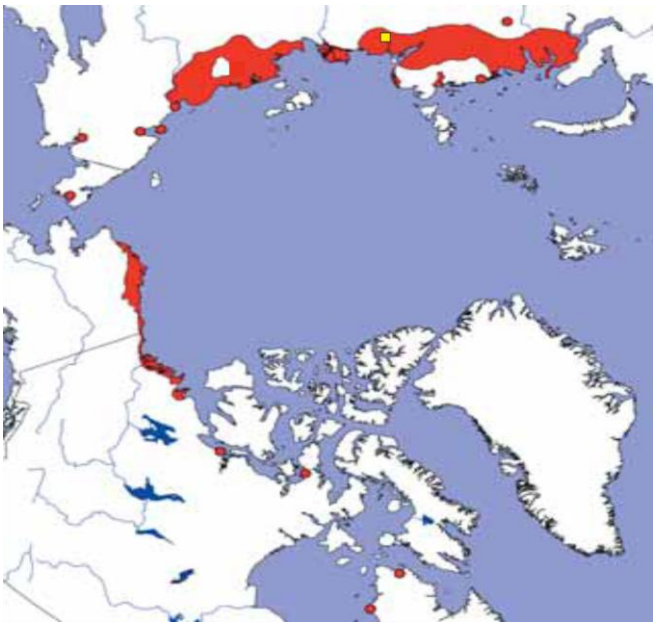

Fig. 8 Circumpolar map of polygon mires; extensive occurrences in red, incidental occurrences given as red dots, yellow dot represents the studied polygon near Saskylakh, NW Yakutia (modified after Minke et al. 2007, based on Quickbird satellite images)

The polygonal shape of this type of nonsorted patterned ground (sensu Washburn 1980) is the result of the formation of ice wedges in the ground. Wedge ice forms from initial ice veins in frost cracks: Thermal contraction at subfreezing temperatures opens frost cracks in the ground (Washburn 1980), which fill with thaw water upon snow melt (see Fig. 9 a). Frost heave enlarges the veins with each freeze-thaw iteration, and eventually an ice wedge develops when several ice veins meld. Adjacent ice wedges usually join at right or slightly obtuse angles, so that tetragonal to polygonal nets of ice wedges form (French 2007). Impeded drainage due to underlying permafrost and surrounding ice wedges encourages the development of mires in the polygon centre's water-saturated soils. Intrapolygonal ponds are typical at this stage (see Fig. 9 b). Degradation of the polygon ridges promotes the formation of interpolygonal ponds at the junctions of ice wedges and along the frost cracks (see Fig. 9 c). In a final stage of degradation, the polygonal structures are intertwined with thaw lakes (see Fig. 9 d). These thermokarst lakes continue to grow in depth and size, reaching water depths of up to 5 meters (Wetterich 2008). The ice-rich sequences known as ice complex were produced by late Pleistocene polygonal ice wedge systems (e.g. Kunitsky 1989).

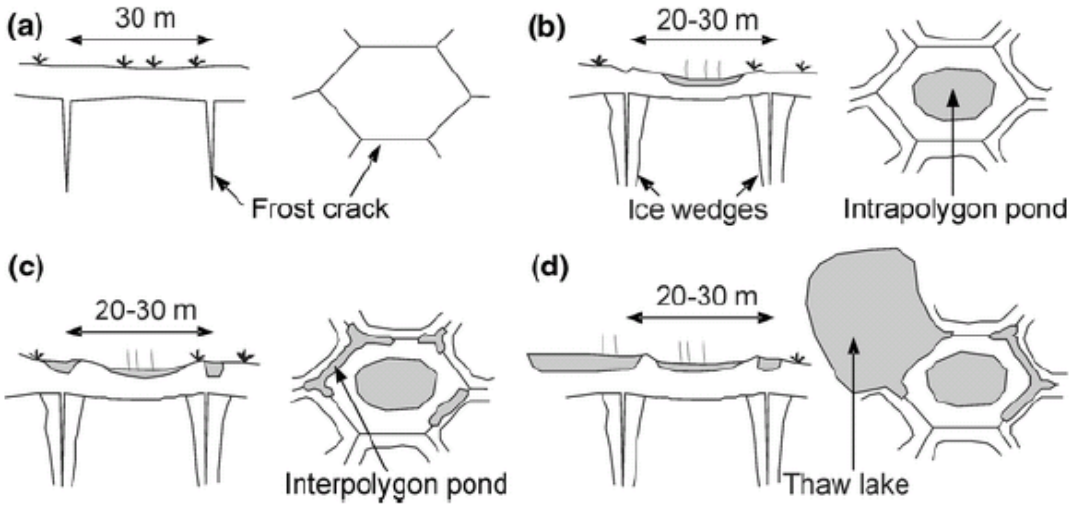

Fig. 9 Development of ice wedge polygons and their degradation states, (a) juvenile polygon, very small height differences and no water body, (b) mature low-centred polygon with intrapolygonal pond, height differences between wall and centre 0.5 m to 1 m, (c) initial degradation: polygon with interpolygonal ponds, (d) final degradation: height differences up to 1.5 m, presence of polygonal thaw lake (Wetterich 2008, modified after Meyer 2003)

The polygons measure between 7 and 40 m in diameter (French 2007, Chernov & Matveyeva 1997). The soil on the ridges is lifted slightly above the water table and is consequently drier than the waterlogged or submerged soil in the polygon centre. Ridge soils have been classified as typic aquiturbels (Kutzbach et al. 2004, United States Department of Agriculture (USDA) 1998). They are usually silty and loamy sands with low organic matter contents (Wagner et al. 2005). The soils in polygon centres are typic historthels (Kutzbach et al. 2004, United States Department of Agriculture (USDA) 1998). Under the anaerobic conditions in the waterlogged silty sand organic matter accumulates (Boike et al. 2008).

The diverse microrelief in polygon mires supports a rather diverse vegetation as compared to other arctic environments (Minke et al. 2007). Plant communities of polygon mires on Taymyr are two-layered, mosses and lichens growing about 5 cm high and vascular plants growing 20-30 cm high (Kutzbach et al. 2004). The peat layer is about 10 - 15 cm thick and roots generally reach the mineral substrate. The field layer is made up of *Salix reptans* and the hydrophilic sedge *Carex aquatilis* (*Carex stans*). The latter may reach a dominance of up to 80%. Boike et al. (2008) studied polygon mires in the Lena River delta, where *Carex aquatilis* reaches a dominance of 25% in the polygon centres, and 8 % on the rims. An intermediate layer of the low *Carex* species *C. rariflora* and *C. chordorrhiza* growing about 10 cm high may be found locally, and the moss layer is characterized by a fine mosaic of species (about

15-35) all growing together in a confined space (Boike et al. 2008). In polygon mires in the Lena River Delta the mosses *Limprichtia revolvens* and *Meesia longiseta* are found in the polygon centres, while *Hylocomnium splendens* and *Timmia austriaca* are typical ridge mosses (Kutzbach et al. 2004). The polygon ridges are dominated by mosses and mesophytic dwarf shrubs such as *Dryas octopetala* and in the polygon centres mosses and *Carex aquatilis* grow.

In polygon mires on Taymyr the herbs *Carex rariflora*, *Comarum palustre*, and *Eriophorum angustifolium* are characteristic, and mosses *Drepanocladus exannulatus*, *D. revolvens* and *Tomentypnum nitens* are abundant (Matveyeva 1994).

Sediments in ice-wedge polygons are valuable for palaeoecological studies (Fortier & Allard 2004, Ellis & Rochefort 2006, Minke et al. 2007), such as sedimentological analyses and the study of plant and animal remains, which are usually well-preserved in the mires. Polygon ponds are especially susceptible to the effects of climatic change because of their small water volume and large surface area to depth ratio (Smol & Douglas 2007).

3. Methods

3.1 Field work

In the course of the "Anabar expedition" in the summer 2007 a polygon mire was sampled by Ulrike Herzschuh (Alfred-Wegener Institute Potsdam), Ljudmila Pestryakova (Yakutian State University) and Stefanie Müller (Freie Universität Berlin). The studied polygon is located at 72.07° N and 113.92° E and 14m height above sea level.

The polygon was divided in a grid of 12 x 13 m with 1 m spacing, along which measurements were taken. Cords were stretched across the polygon from ridge to ridge to produce a reference surface from which the elevation of the polygon's ground surface was determined. A thin metal rod was pushed into the ground to determine the depth of the active layer. Both ground surface elevation and elevation of the active layer are given as distances from the water table. Soil temperatures were measured using a soil thermometer (ama-digit ad 17th, Amarell). The vegetation survey was conducted by Stefanie Müller, following the Braun-Blanquet floristic approach.

Along a transect through the middle of the polygon, 13 surface samples were taken. Two soil profiles were dug, one at the rim (profile A, 42 cm deep) and one at the transition between rim and flat bottom (profile B, 50 cm deep). These were sampled at 2.3 cm intervals, profile A yielding 18 samples and profile B yielding 22 samples. In the middle of the mire a short core was taken using a plastic tube of 30 cm length. During coring core C was compressed slightly, so that when it was sampled at 1 cm intervals, 27 samples were obtained. pH and conductivity were measured along the surface transect using a multi parameter handheld meter (WTW Multi 350i).

3.2 Plant macrofossil analysis

For the extraction of plant macrofossils, subsamples of 25 cm^3 were taken from each sample from the surface transect and the profiles A and B, and washed through sieves of 125, 250 and 850 µm mesh sizes with water. The material retained by the sieves was stored in water at 3-6 °C until the residue from the 250 µm and 850 µm meshes was picked under a stereo microscope (Stemi 2000-C, Zeiss). A few random samples of the 125 µm fraction were checked, but as they did not contain any identifiable plant remains, not all were picked. For identification reference atlases and seed identification manuals (Anderberg 1994, Beijerinck 1947, Berggren 1969, Berggren 1981, Katz et al. 1965) and a reference collection were used

with the assistance of Frank Kienast (Senckenberg research station for Quaternary Palaeontology Weimar).
During macrofossil extraction, *Daphnia* ephippiae were found and picked and the presence or absence of sklerotia of the ektomycorrhizal fungus *Cenococcum geophilum* was recorded.
Mosses were not identified in this study.

3.3 Laboratory analyses

Laboratory analyses were performed at the Alfred-Wegener-Institute for Polar and Marine Research in Potsdam, Germany.

3.3.1 Geochemical analysis

The analysis of organic matter, and especially of the parameters total carbon (TC), total organic carbon (TOC), and total nitrogen (TN) can give information about the conditions under which it was produced and deposited. TOC reflects the biomass production in the mire and the ratio of carbon to nitrogen (C/N, calculated as TC divided by TN) provides an insight into the source of organic carbon (e.g. Meyers 1994) and its degree of decomposition (e.g. Schirrmeister et al. in press).
The analysis of TOC, TC and TN was carried out using an elemental analyzer (Vario EL III, Elementar). The method is based on combustion at high temperatures and subsequent measuring of the combustion products on a gas-phase chromatograph. The sediment samples were freeze dried (Zirbus sublimator 3-4-5) and finely ground (Fritsch planetary mill). In order to measure TOC (amount of carbon bound in organic compounds), inorganic carbon had to be removed from the samples. Carbonates were dissolved by adding ~4% hydrochloric acid (HCL) and heating each sample to 97°C for three hours. Dissolved carbonates were washed out with water and the samples were dried in a cabinet drier (Memmert ULM 700).
Five milligrams of prepared sediment were weighed into tin capsules and entered into an automatic sampler. The vario EL III manual recognizes three stages during the measurement: digestion of the sample and removal of foreign gases, separation of measurement components, and detection (Elementaranalysator vario EL III – Bedienungsanleitung, 2005). Jet injection of oxygen ensures complete combustion of the samples at 1150° C. Foreign gases such as volatile halogens are removed. Helium is used as a carrier gas to transport the produced gas through adsorption columns in order to separate its mixed components carbon, nitrogen and sulphur. Sulphur concentrations were not measured. The respective gas mixtures of He/CO_2 and He/N_2 flow through a measurement cell, while a constant helium flow travels through a

reference measuring cell. Detection limits for both carbon and nitrogen detection are 0.1 %. Each sample was measured twice, and the standard deviation was used as a means to assess and control the measurements. A number of calibration standards was applied to each measurement cycle and additional control standards were used on every twentieth sample.

3.3.2 Stable carbon isotope analysis

Two stable isotopes occur in natural carbon: ^{12}C and ^{13}C, and their natural ratio is 98.89 % / 1.11%. The characteristic carbon isotope ratio a plant has at its death is stored in sediments and can give information about the conditions at the plant's death.

$\delta^{13}C$ values of C3 plants like those growing in arctic polygon mires indicate variations in soil moisture and precipitation (Schleser 1995).

$\delta^{13}C$ is the ratio of $^{12}C/^{13}C$ as compared to a standard sediment called PeeDee belemnite (PDB), which is a limestone from the PeeDee formation in South Carolina, USA (see Eq. 1).

$$\delta^{13}C_{\mathrm{Sample}} = \left(\frac{^{13}C/^{12}C_{\mathrm{Sample}}}{^{13}C/^{12}C_{\mathrm{PDB}}} - 1 \right) \cdot 1000$$

Eq. 1 Stable carbon isotope ratio

$\delta^{13}C$ was measured on carbonate-free samples (for procedure see above) to ensure finding the isotopic composition of the organic carbon portion of the sediment. Carbon isotope ratios were obtained from the samples using a Thermo Finnigan MAT Delta-S mass spectrometer to which an element analyzer (Flash EA 1112 Series, Thermo Finnigan) and a gas mixing system (CONFLO III) were connected to ensure the samples are in a gaseous state (CO_2).

An appropriate amount of carbonate-free sample material was enclosed in tin capsules (see Eq. 2) and released into an automatic sampler (AS 200).

$$\text{sample weight [g]} = \frac{45}{\mathrm{TOC}}$$

Eq. 2 Calculation of sample weight

Standard CO_2 with known isotope ratio was measured first to provide a means of comparison. Combustion to CO_2 took place in an oxygen-enriched atmosphere at 950°C. The sample gas was ionized upon entering the mass spectrometer, accelerated in an electrostatic field and focussed into a single beam, which was measured in a magnetic analyzer. Isotope ratios were calculated from the mass-specific electrical peaks recorded when the ions separated by the magnetic field hit a collector.

Control measurements were inserted after every seventh measurement to ensure reproducibility of the data, and the standard deviation for all measurements was less than 0.15 ‰.

3.3.3 Grain size distribution analysis

Texture, the relative proportion of different grain sizes, is one of the main soil properties.
Grain size distribution analysis was conducted using a laser diffraction particle sizer (Beckman Coulter LS 200). Subsamples of 1 to 17.5 g of wet sediment were used from each sample. As the aim of the analysis is to determine the grain size distribution of the inorganic fraction, organic particles were removed from the samples. For that purpose 100 ml of 3 % hydrogen peroxide (H_2O_2) were added to each sample. Samples were then placed on a gyrotory platform shaker (New Brunswick Scientific Innova 2300) and tested for reaction to an additional 10 ml of concentrated hydrogen peroxide thrice a week. This procedure was repeated for two to four weeks, until none of the samples showed a reaction. When samples were organic-free, 100 ml of 10 % acetic acid were added to dissolve carbonates. They were then washed, centrifuged (Heraeus Cryofuge 8500 and Multifuge 3S) and dried in a cabinet drier (Memmert ULM 700). Of the dry, organic- and carbonate-free sediment, 0.3 to 6 g were dispersed using about 5 g tetrasodium pyrophosphate decahydrate and about 650 -750 ml 0.0001% ammonia solution. After spending a minimum of 6 hours in an elution shaker (Gerhardt Rotoshake RS 12), samples were divided into eight subsamples by means of a rotary sample divider (Fritsch Laborette 27). In order to achieve a concentration of 8 to 12 % in the laser diffraction analyzer, 1 to 8 of these subsamples were used per measurement. If the use of one subsample still yielded too high concentrations, 4 of the 8 were divided once more. Apart from the six samples with too little material for more than one measurement each sample was measured at least twice, and further calculations were based on the mean of all measurements. The measured diffraction pattern was transformed into grain size distribution using the Fraunhofer diffraction theory, which seems to represent the clay fraction, and non-spherical particles in general, better than the also commonly used Mie Theory (e.g. Loizeau et al. 1994, Konert & Vandenberghe 1997). The Fraunhofer theory considers only diffraction and no refraction, which may occur especially in organic matter. As the sediment is made organic-free, refraction may be neglected. Grain size classes are displayed in Table 1, lithological classes after Shepard (1954) are illustrated in the ternary diagram in Fig. 10.

Table 1 Fine grain size classes (after Scheffer & Schachtschabel 2002)

	clay	silt			sand		
mm µm	< 0.002 < 2	< 0.0063 < 6.3 Fine	< 0.02 < 20 Medium	< 0.063 < 63 Coarse	< 0.2 < 200 Fine	< 0.63 < 630 Medium	< 2 < 2000 Coarse

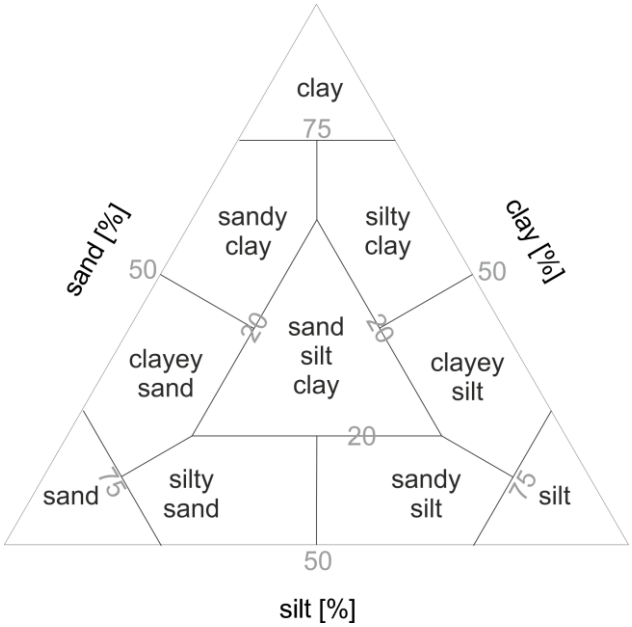

Fig. 10 Lithological classes after Shepard (1954), displayed in ternary diagram

3.3.4 Accelerator Mass Spectrometry (AMS) dating

Accelerator mass spectrometry (AMS) dating was conducted by the Leibniz-Laboratory for Radiometric Dating and Stable Isotope Research Kiel. The laboratory uses a 3 million Volt Tandetron 4130 AMS system (High Voltage Engineering) with a single caesium sputter ion source.

In the course of this study four samples were dated: the bottommost samples of cores A and B (A-18, B-22), the second lowest sample from core C (C-26), and an additional sample from the middle part of core A (A-09). Leaves, seeds and wood were picked from the samples for dating. The sample from core C was not picked for macrofossils, because it contained only very small amounts of suitable material. Instead, an entire portion of the peaty sediment was used.

Samples were checked for visible contamination under the microscope and the best seeds, wood and leaves were selected. To remove contaminating carbon, samples were subjected to

acid-alkali-acid (AAA) cleaning with 1% hydrochloric acid and 1% sodium hydroxide. CO_2 was obtained from the samples by combustion at 900°C in an evacuated quartz tube with copper oxide and silver wool. It was then reduced with H_2 on a catalyst of about 2 mg of iron powder in a modular reduction system. The resulting graphite-iron mixture was pressed into a pellet in an aluminium target holder.

^{14}C concentrations were measured by comparing the ^{14}C, ^{13}C and ^{12}C beams of the samples with those of oxalic acid standard CO_2 and coal background material. The $^{13}C/^{12}C$ ratio was used for $\delta^{13}C$ correction. Conventional ^{14}C ages were calculated according to Stuiver and Polach (1977). Calendar ages were calculated using "CALIB rev 5.01" (data set: IntCal04, Reimer et al. 2004). Measuring uncertainty was expressed in terms of standard deviation σ, the 1 σ range being the best estimate for the measurement.

4. Results

Measuring and observation results obtained in the field and the laboratory are listed in the Appendix.

4.1 Polygon setting, morphology and vegetation

Polygon setting and morphology

The studied polygon mire is situated at 72.07 °N, 113.92 °E and 14 m height above sea level in the North Siberian Lowland. It belongs to a polygon mire complex about 50 km to the north of the town Saskylakh, in an abandoned meander east of the river Anabar. The adjacent polygons are of irregular shapes, and not all of them have intrapolygonal ponds. There is some anthropogenic influence in the area due to the adjacency of the small town, but utilization of the mire complex is restricted to the occasional removal of trees.

The studied low-centred polygon (sensu Zoltai and Tarnocai 1975, Billings and Peterson 1980, Mackay 2000) consists of a central depression surrounded by low ridges. One of the ridges is collapsed (see blue coloured grid cells along the right edge of figure 11 b). Here, the ice wedge is laid bare. The water surface measures 5 x 7 m. The polygon ridge rises to a maximum of 44 cm above the water table, and the maximum height distance between ground surface levels is 61 cm, as the water is up to 17 cm deep. In the degraded ridge the maximum depth is -62 cm.

Active layer thickness ranges from 21 cm to 83 cm, averaging to 48.5 cm. It is generally lower on the ridges and higher under the water in the central depression of the polygon, although the highest values occur on the ridges as well. In comparison, the thickness of the active layer is rather homogeneous at or below the water table, values ranging from 52 to 71 cm and averaging to 60.8 cm. The elevation of the ice surface follows closely that of the ground surface (Fig. 11 a and b). The difference between the deepest and highest point of the ice surface is 104 cm. In the ridges the ice surface actually rises above the water table, whereas it is lowest under the water in the middle of the polygon.

This pattern is continued in the soil temperatures (see Fig. 11 c), which range from 1°C to 10.4°C. The lowest values are found in the ridges and the highest values under the water. For the coordinates L2 through L10 no soil temperatures are available because there was no soil above the ice wedge. Soil temperatures are significantly higher in the low-lying middle of the

polygon, averaging 8.73°C in the middle, 5.5°C in the transition (surface elevations of 0 to 15 cm) and 3.08 °C in the ridges.

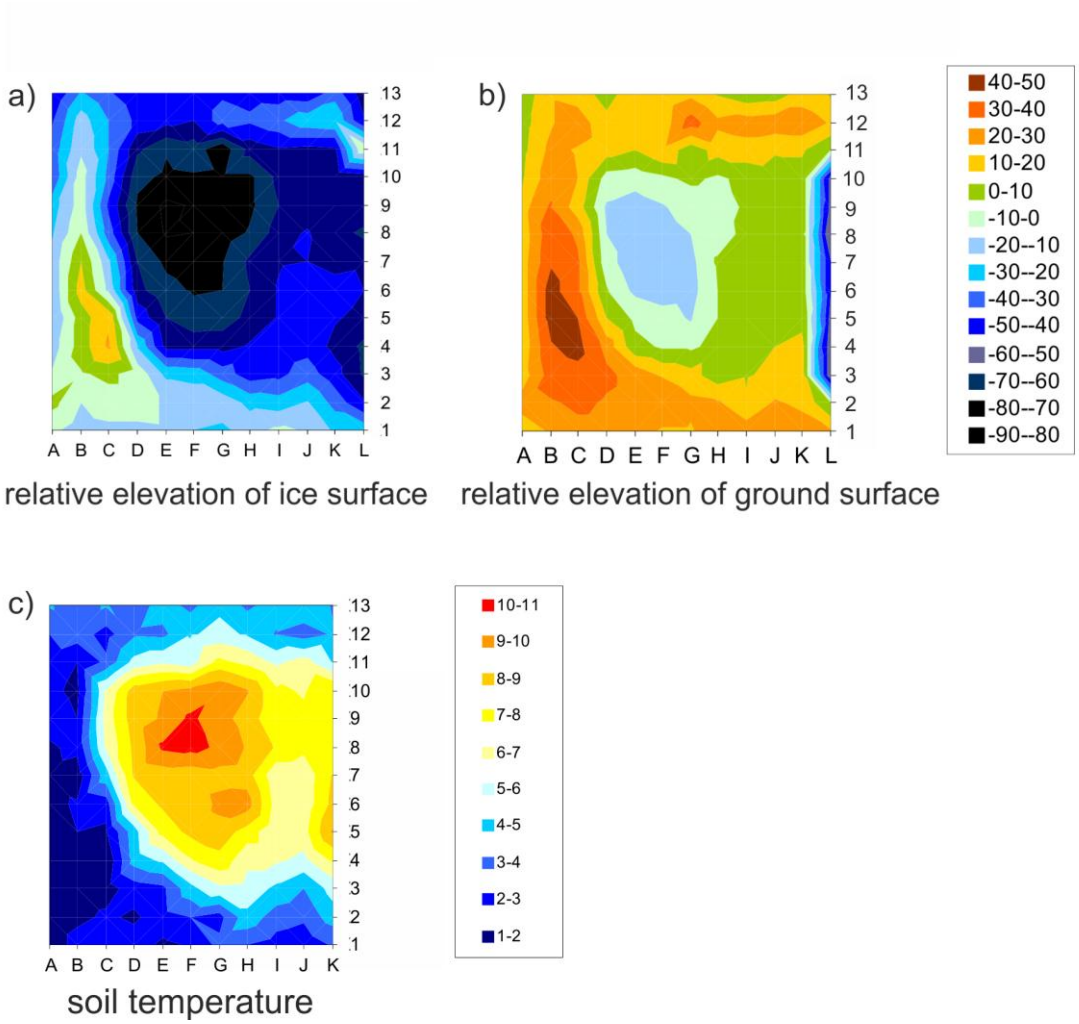

Fig. 11 Ice surface elevation (a), ground surface elevation (b) and soil temperature (c); elevations are given in cm, temperatures are given in °C; note that column L of the soil temperatures has not been displayed because no data is available for coordinates L2 to L10

Polygon vegetation

Fig. 12 displays the distribution of plant taxa relative to the ground surface elevation in the studied polygon. The vegetation survey was conducted after the flowering season and it was not always possible to identify species in the field. Instead, different types have been discerned or the plants have been identified to genus (*Pedicularis*, *Vaccinium*, *Polygonum*, *Dicranium*) or family level (Poaceae). Two types each of *Salix* and *Carex* have been differentiated, which will be called *Salix* type A and B and *Carex* type A and B (*Carex* type B is smaller than type A). Apart from the moss *Dicranium*, three types of mosses have been mapped and called moss type A, moss type B and aquatic moss.

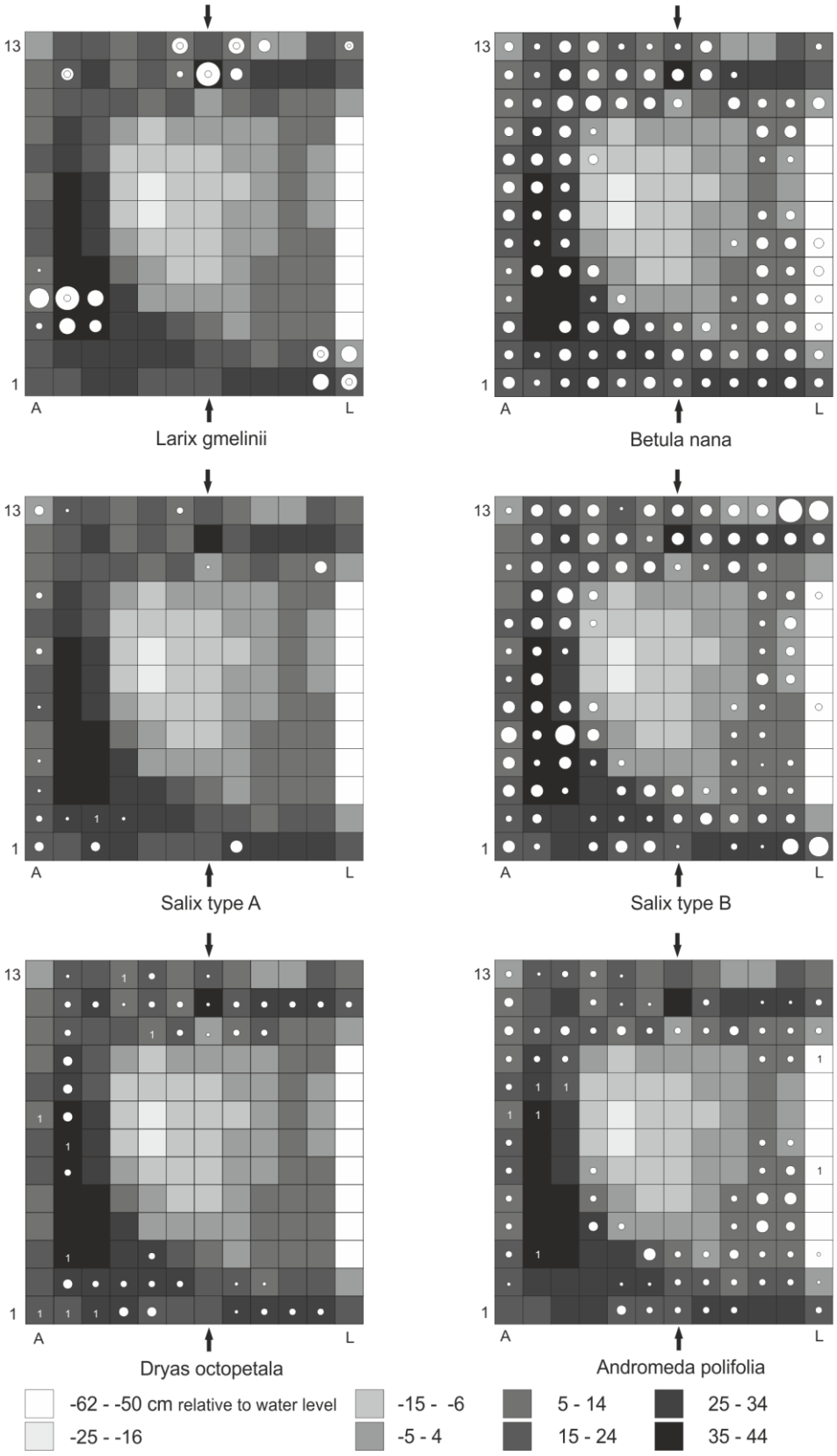

Fig. 12 Plant taxa distribution in cover-abundance classes after Braun-Blanquet (1964) vs. ground surface elevation; Plain circles represent cover-abundance classes, the double circles used for *Larix* indicate location of trees. The number 1 symbol stands for single occurrences. Arrows show the position of the surface transect.

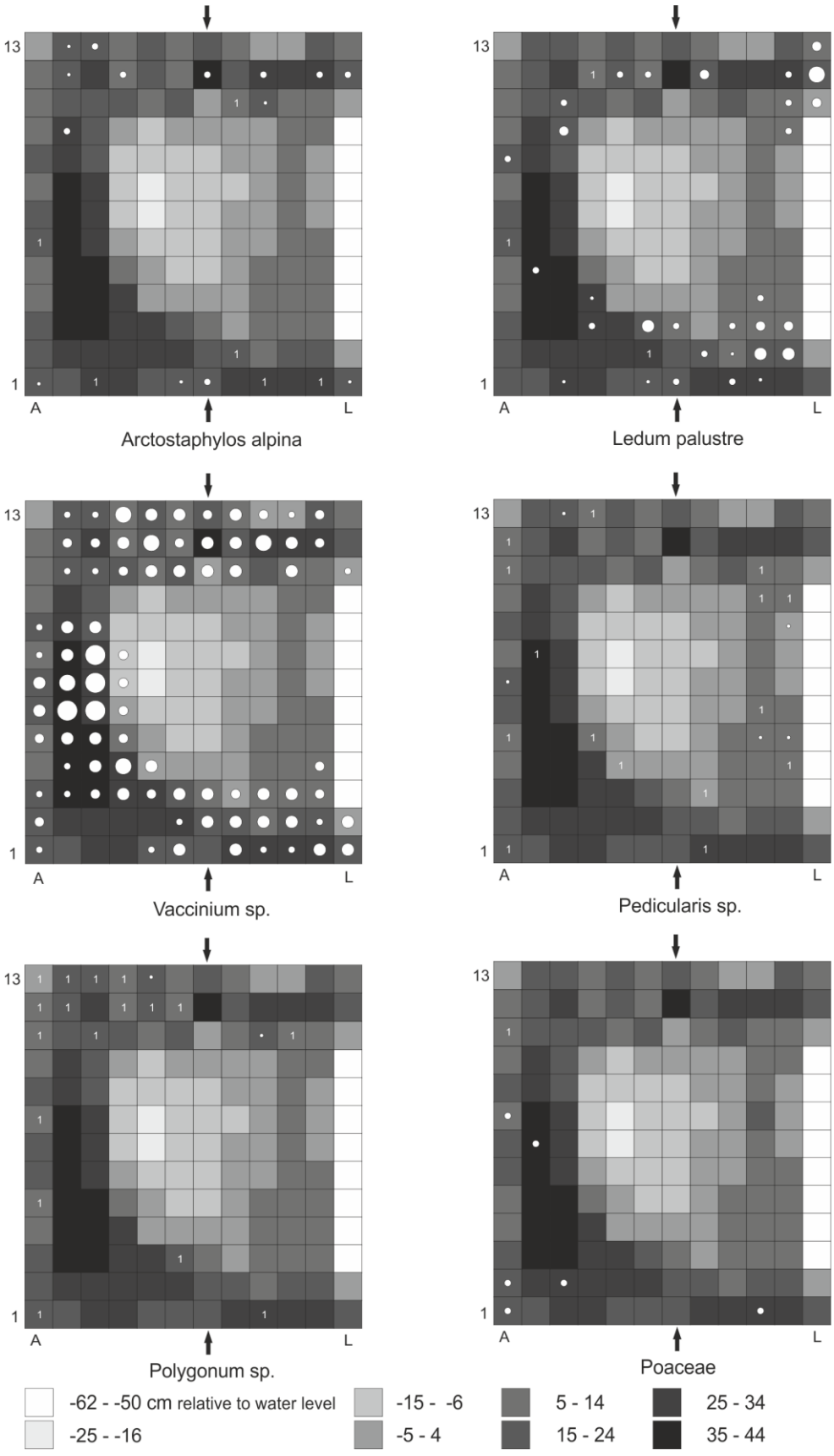

Fig. 12 continued

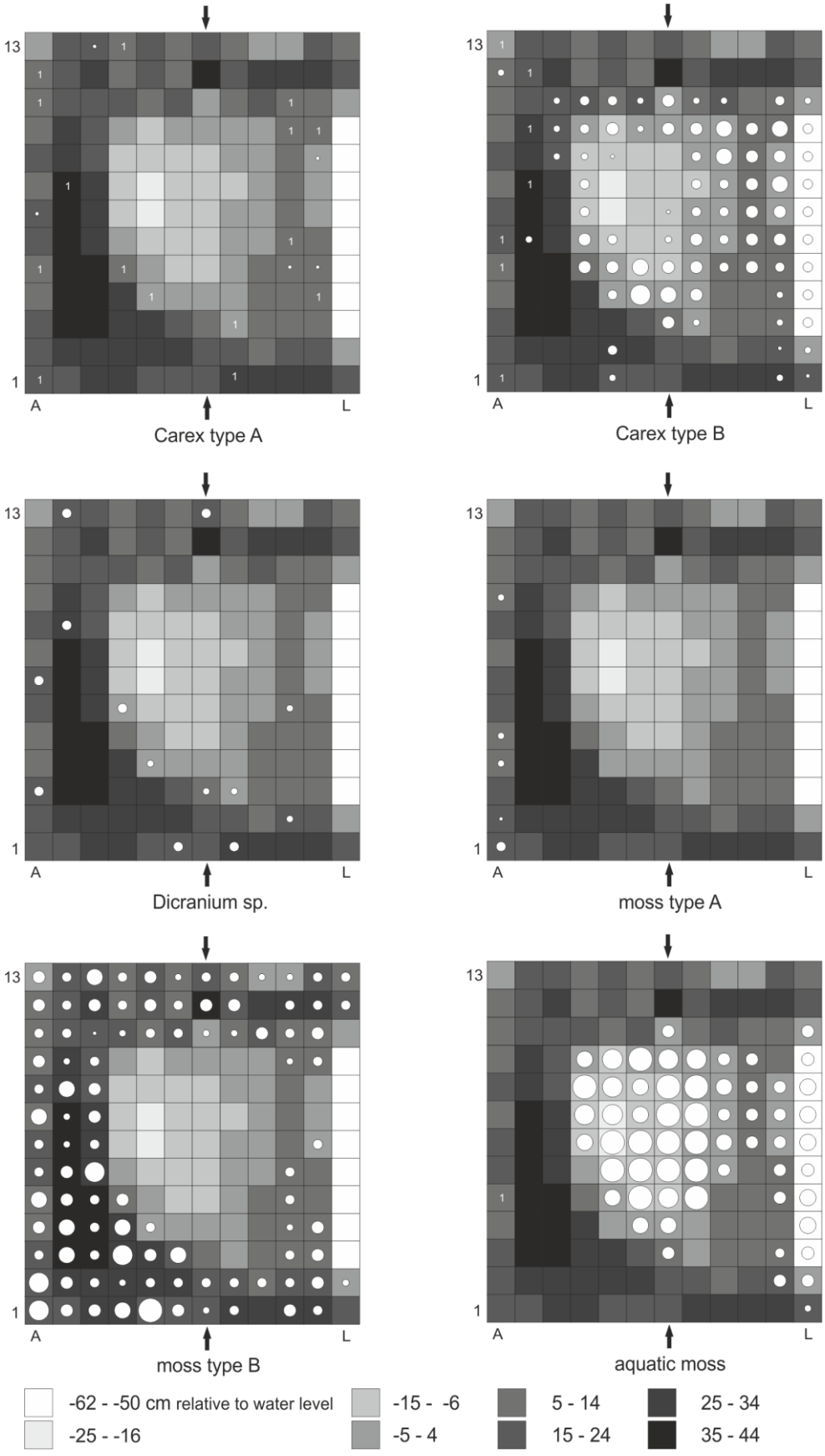

Fig. 12 continued

Larix gmelinii, *Salix* type A, *Arctostaphylos alpina*, *Dryas octopetala*, *Polygonum viviparum* and Poaceae are restricted to the ridges, while *Betula nana*, *Salix* type B, *Vaccinium*, *Ledum palustre*, and *Carex* type A are found both on ridges and in the transition. *Andromeda polifolia* and *Pedicularis* seem to favour the transition between ridge and centre. In the submerged centre only the two *Carex* types and aquatic mosses are found. Where the water is deeper than a few centimeters only aquatic mosses are present. The moss type A grows on the somewhat lower part of one of the ridges, the moss type B is found both on the ridges and in the transition, and *Dicranium* is found in the transition and the lower parts of ridges.

4.2 surface transect

The maximum elevation difference in the surface transect is 49 cm, the deepest point lying 14 cm below the water table and the highest point 35 cm above it (cf. Fig. 13). Ground and ice surface elevation, active layer thickness and soil temperatures are illustrated in Fig. 17.

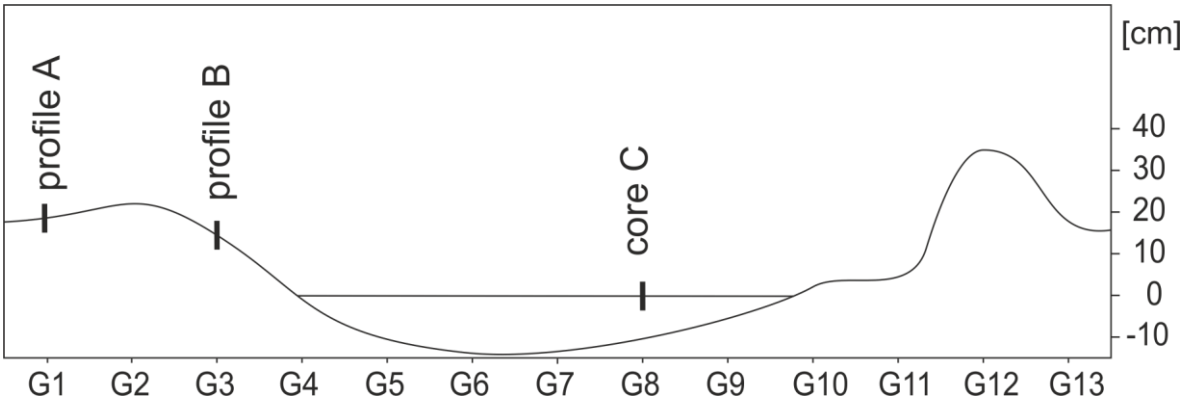

Fig. 13 Schematic height profile of the studied polygon viewed along the surface transect; ground surface elevation relative to the water surface is indicated on the right side of the sketch, grid cell names are given below; the position of profiles A and B and of core C is marked

Recent vegetation and plant macrofossils

Vegetation along the transect follows the general patterns found in the polygon: most of the mapped plant taxa (*Larix*, *Betula*, *Salix*, *Dryas*, different Ericaceae, *Carex* type A and mosses) grow on the ridges and some in transitional ranges (mainly *Carex* Type A and B and aquatic mosses), but in the submerged middle only aquatic mosses are present (for full vegetational data see Fig. 12 above).

This distribution is reflected in the macrofossil data (see Fig. 14). The least amounts of plant macrofossils (other than *Larix* needles) and the lowest taxa numbers were found in the samples 04 - 09, below the water table. *Larix gmelinii* needles occur in high numbers in all

samples, but *Larix gmelinii* seeds are practically absent from the low-lying middle of the polygon. Short shoots and a complete cone were found directly under the tree and in the adjacent sample (samples 12 and 13). *Betula* remains occur scattered along the transect, but in the submerged part only one *Betula nana* fruit, one leaf and no catkin scales were found. Leaf numbers were conspicuously higher on the ridges. An entire *Betula nana* catkin was obtained from sample 01. *Salix* leaves were found in ridge and transitional samples and only one leaf was obtained from the centre. *Salix* capsules were recovered from one of the ridges, and a single leaf of *Salix polaris* was found in a ridge sample (sample 13). Two single leaves of *Dryas octopetala* were found in one transitional sample (sample 11) and one sample from the opposite ridge (sample 02). *Andromeda polifolia* leaf numbers are high on ridges and at transitional ranges, but only single leaves were obtained from centre samples. Seeds are absent from the submerged middle. *Arctostaphylos alpina* leaves and seeds are present only where the actual plants grow. *Vaccinium microcarpum* leaves occur solely at transitional ranges. *Vaccinium vitis-idaea* and *V. uliginosum* remains were found on ridges. Two *Vaccinium* seeds that could not be identified to a lower level were found in the submerged centre. Single seeds of *Luzula* species were recovered from two of the centre samples, and one seed of *Potentilla palustris* was found on one of the ridges. *Carex* seeds occur in all samples but the deepest one, but numbers are higher on ridges and in transitional ranges. *Eriophorum angustifolium* and *Eriophorum russeolum* seeds were found on ridges and in transitional ranges. No fossils of *Ledum* were found, although *Ledum* grows in low dominance on one of the ridges (in grid cells G1 and G3).

Daphnia ephippiae are absent from the ridges, but occur in most other samples. Sclerotia of the mykorrhiza fungus *Cenococcum geophilum* are only present in the ridge samples 01 and 02. Sclerotia were not counted.

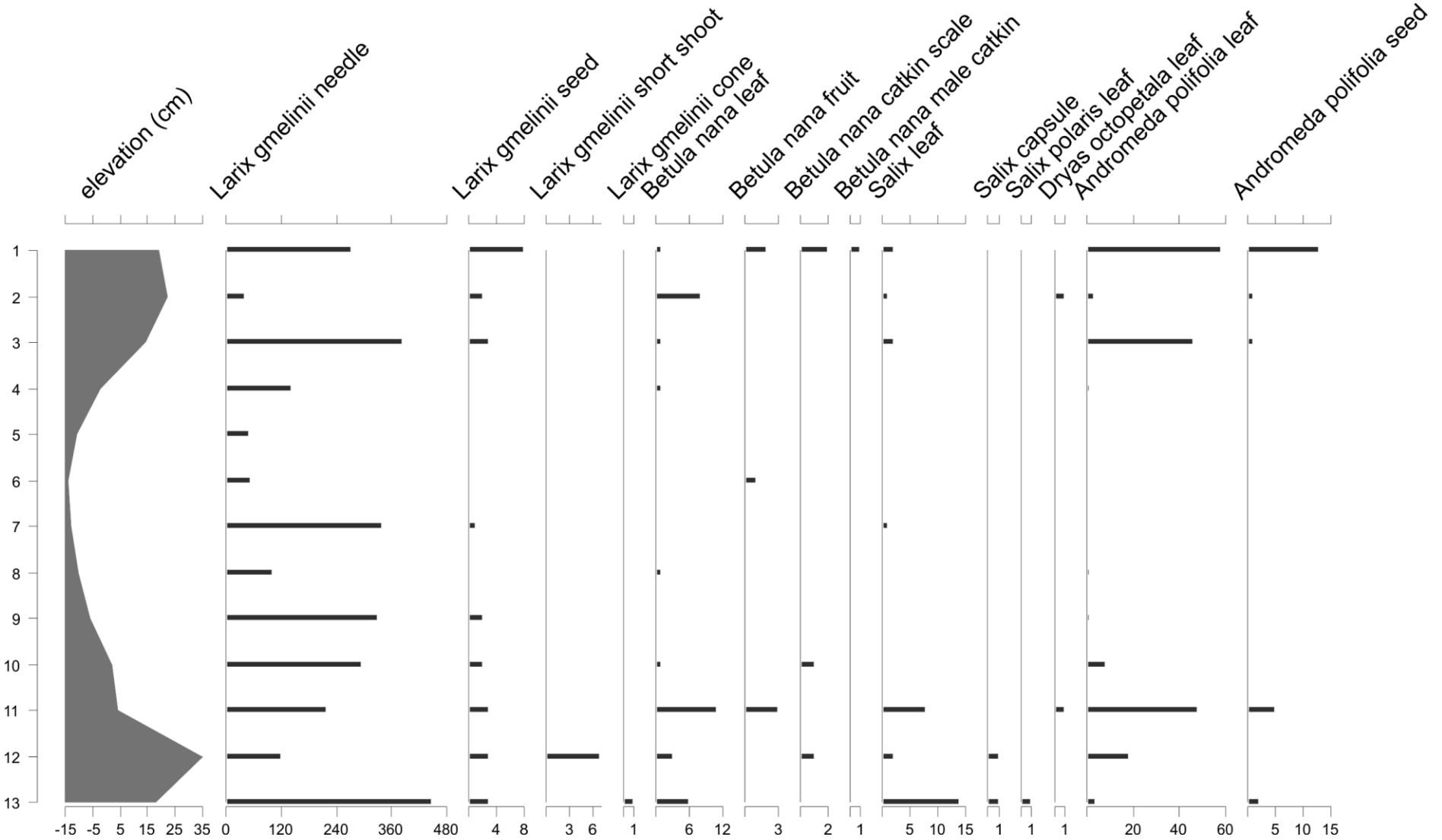

Fig. 14 Plant macrofossil diagram showing the distribution of plant macrofossil types along the surface transect

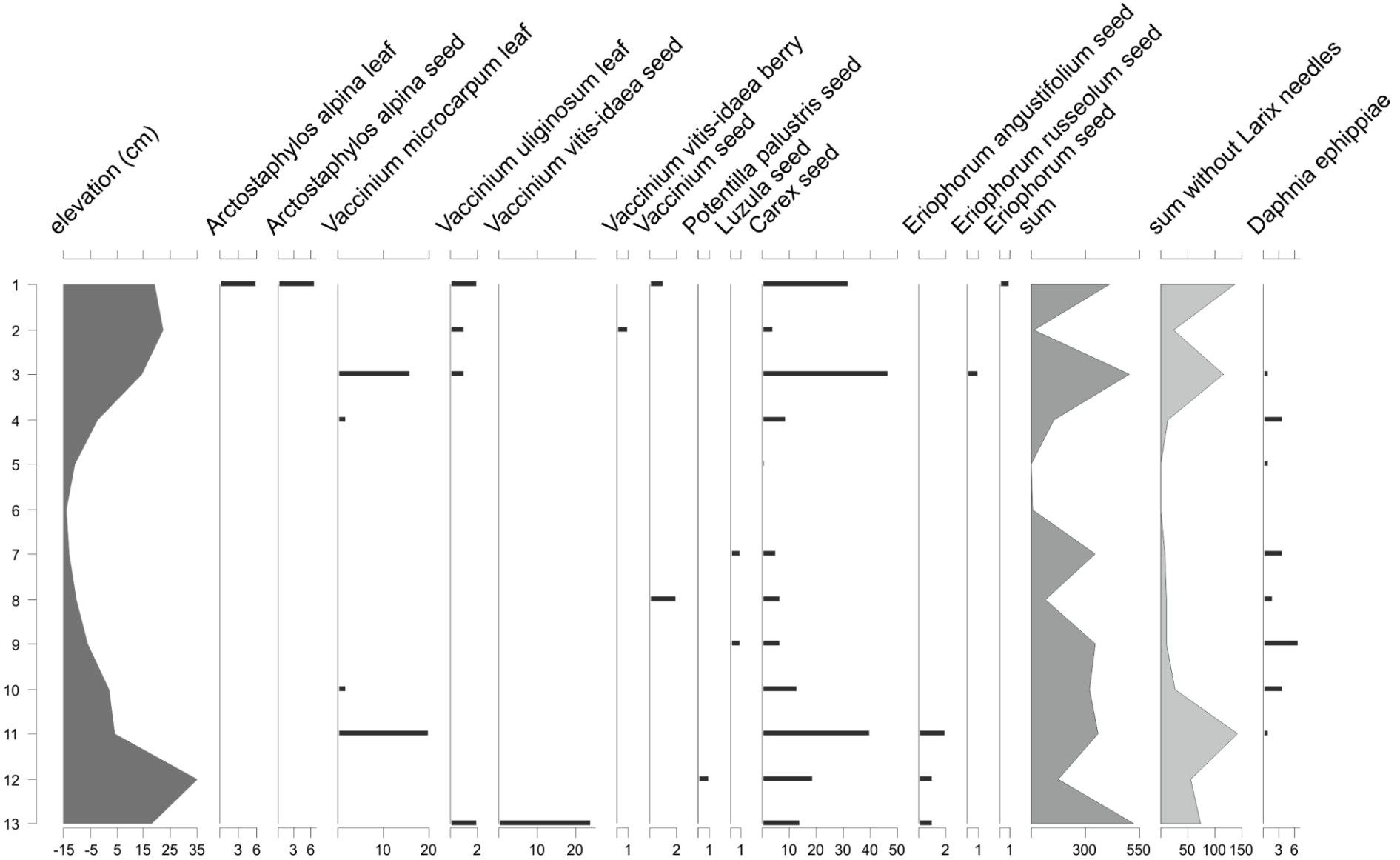

Fig. 14 continued

Grain size

Sand is dominant (>50 vol %) in eight of the samples, three of the samples are dominated by silt. In two samples, both silt and sand reach values between 40 and 50 vol %. Sand contents range from 38 vol % to 78.7 vol %. Silt contents range from 17.9 to 55 vol %. Clay contents range from 3.4 to 17 vol %. The most frequent lithological class (after Shepard 1954) is silty sand (7 samples: 02, 04, 05, 07-09 & 13), followed by sandy silt (5 samples: 03, 06 & 10-12) (see Fig. 15). Sample 01 from the ridge of the polygon belongs to the class sand. The grain size distribution of sample 02 is very similar to that of sample 01.

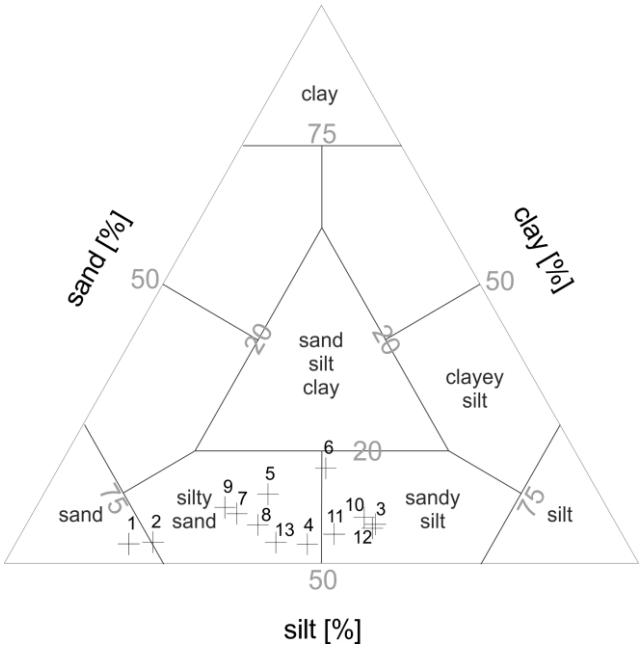

Fig. 15 Lithological classes after Shepard (1954) in the surface transect; crosses represent samples 1-13

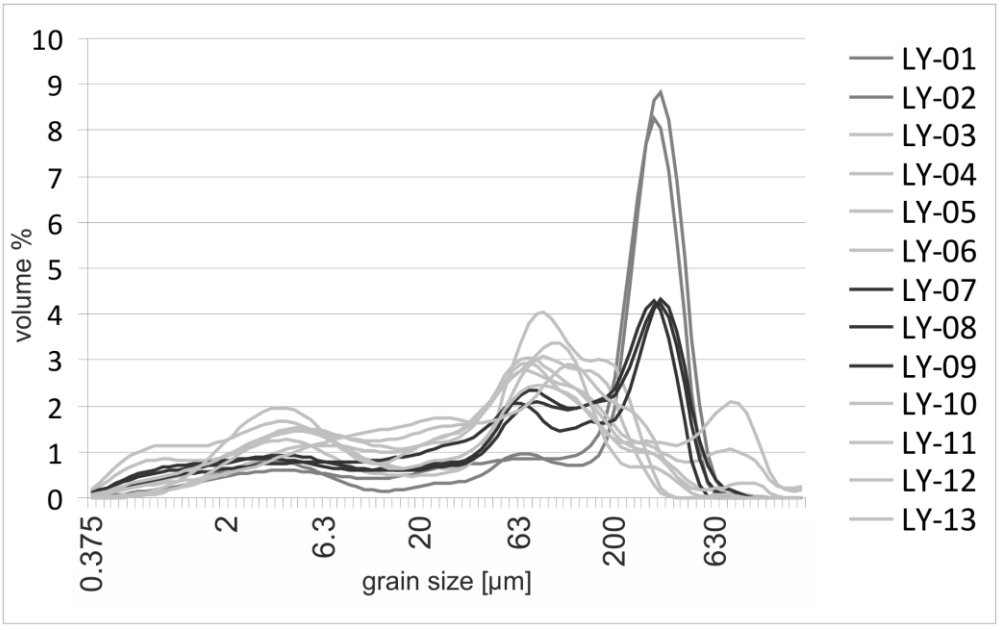

Fig. 16 Grain size distribution in the surface transect

Three types of distributions can be visually distinguished in Fig. 16: the samples 01 and 02 from one of the ridges clearly have a similar grain size distribution, as do samples 07, 08 and 09 from the middle of the mire. Samples from transitional ranges, the upper part of the polygon centre and the other ridge (samples 03-06 and 10-13) can be distinguished as a third group, which shows a little more variance. The ridge samples 01 and 02 are the best sorted samples with a very pronounced peak in the medium sand fraction (for grain size fractions see Table 1). The samples 07, 08 and 09 from the middle of the polygon have a less pronounced peak in the medium sand fraction and another very slight peak around the boundary between coarse silt and fine sand. The samples 03-06 and 10-13 peak slightly in the fine sand fraction and have an even less pronounced peak in the fine silt fraction. The ridge sample 13 has a third peak in the coarse sand fraction. Results of the grain size analysis are given in Fig. 17.

Stable carbon isotopes

$\delta^{13}C$ values lie within a close range between -28.2 in the transition (sample 10) and -30.3 on one of the ridges (sample 13). Generally, $\delta^{13}C$ ratios are slightly higher in transitional ranges and lower in both the lowest and highest ranges. The results of the stable carbon isotope analysis are given in Fig. 17.

Organic matter composition

TC percentages range from 7.08 to 38.84 wt %. They are lower in the centre and higher on one of the ridges. On the other ridge, however, the lowest value was measured (in sample 01). TOC contents closely resemble TC contents and range from 5.26 to 39.49 wt %. TN concentrations are 0.22 % to 1.47 wt %. C/N ratios lie between 15.82 in a centre sample (sample 07) and 51.33 in a ridge sample (sample 12). They follow the elevation of the ground surface, being higher on the highest parts of the polygon and lower in the depression. The results of the organic matter analysis are illustrated in Fig. 17.

Conductivity and pH

The electric conductivity ranges from 16 mS/cm in sample 08 from the polygon centre to 84 mS/cm in sample 1 from the ridge. Values are highest on the ridges, lowest in the centre and intermediate in the transition. pH ranges from 5.7 in a sample from the transition (sample 03) to 6.25 in the three centre samples 07-09. pH values are moderately acidic on the ridges and in the transition and close to neutral in the polygon centre. Conductivity and pH are shown in Fig. 17.

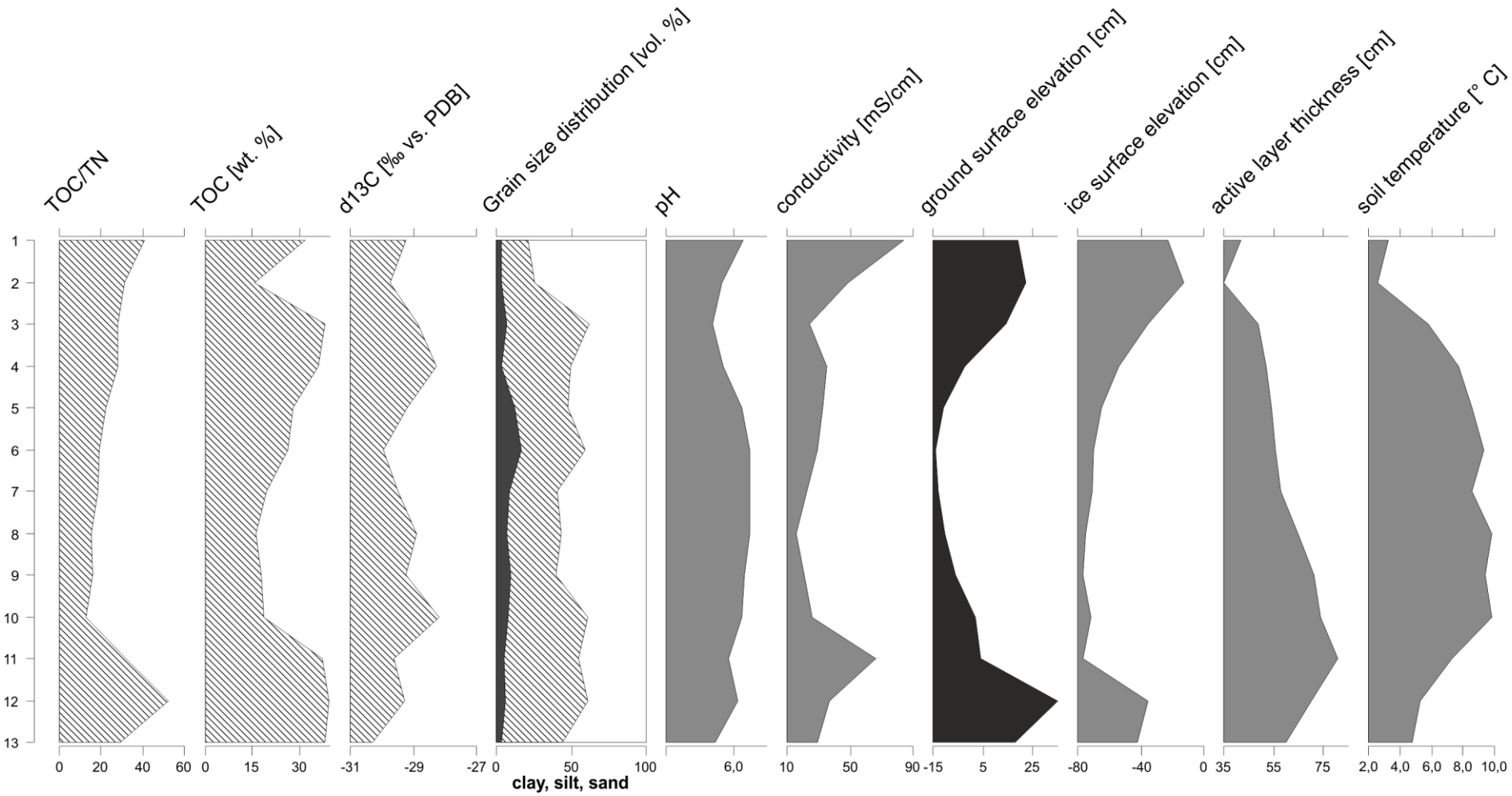

Fig. 17 Stratigraphic diagram of sedimentological and morphological parameters along the surface transect, ground and ice surface elevation relative to the water level in the polygon

4.3 Profile A

Profile A was dug in grid cell G1 on the ridge of the polygon 19 cm above the water table. The recent vegetation consists of *Betula nana*, *Salix* type B, *Arctostaphylos alpina*, *Dryas octopetala*, *Ledum palustre*, *Andromeda polifolia*, *Carex* Type A and the moss type B. *Vaccinium* grows in the adjacent grid cells. No *Larix* grows in the immediate vicinity of profile A.

The bottommost sample (A-18) and a sample from the middle of the profile (A-09) were dated to 1585 ± 25 years BP and 425 ± 25 years BP, respectively. In calibrated calendar years this is around 500 AD and around 1450 AD. The profile is 42 cm deep, and the mean sedimentation rate is about 2.7 mm per year.

Plant macrofossils

There is a conspicuous change in macrofossil composition between the top and lower half of the profile (see macrofossil diagram in Fig. 18). *Larix* needles were found in abundancy only in the two topmost samples, and *Larix* seeds occur nowhere else. Fossils of *Betula nana* decline towards the middle of the profile and are absent from the lower half. *Andromeda polifolia* and *Vaccinium vitis-idaea* are solely present in the most recent samples. Approximately from the middle of the profile downwards leaves of *Dryas octopetala* become the dominant plant remains, with especially pronounced peaks in the samples A-09 and A-14. *Carex* and *Saxifraga* seeds are the only herb macrofossils present. While *Carex* seeds are ubiquitous in the samples, only one *Saxifraga* seed was obtained from sample A-04. *Daphnia* ephippiae are virtually missing from the samples, with only a single occurrence in sample A-12.

Grain size distribution

Sand is dominant (>50 vol %) in all but two samples, in which both silt and sand reach values between 40 and 50 vol %. Sand contents range from 46.1 to 95.2 vol %. Silt contents range from 4.1 to 47.1 vol %. Clay contents are generally low in all samples and do not exceed 9 vol %. The most frequent lithological class (after Shepard 1954; see Fig. 19) is sand (11 samples: A 03-11, 14 & 16), followed by silty sand (6 samples: A-02, 12, 13, 15, 17 & 18). The top sample A 01 belongs to the class sandy silt.

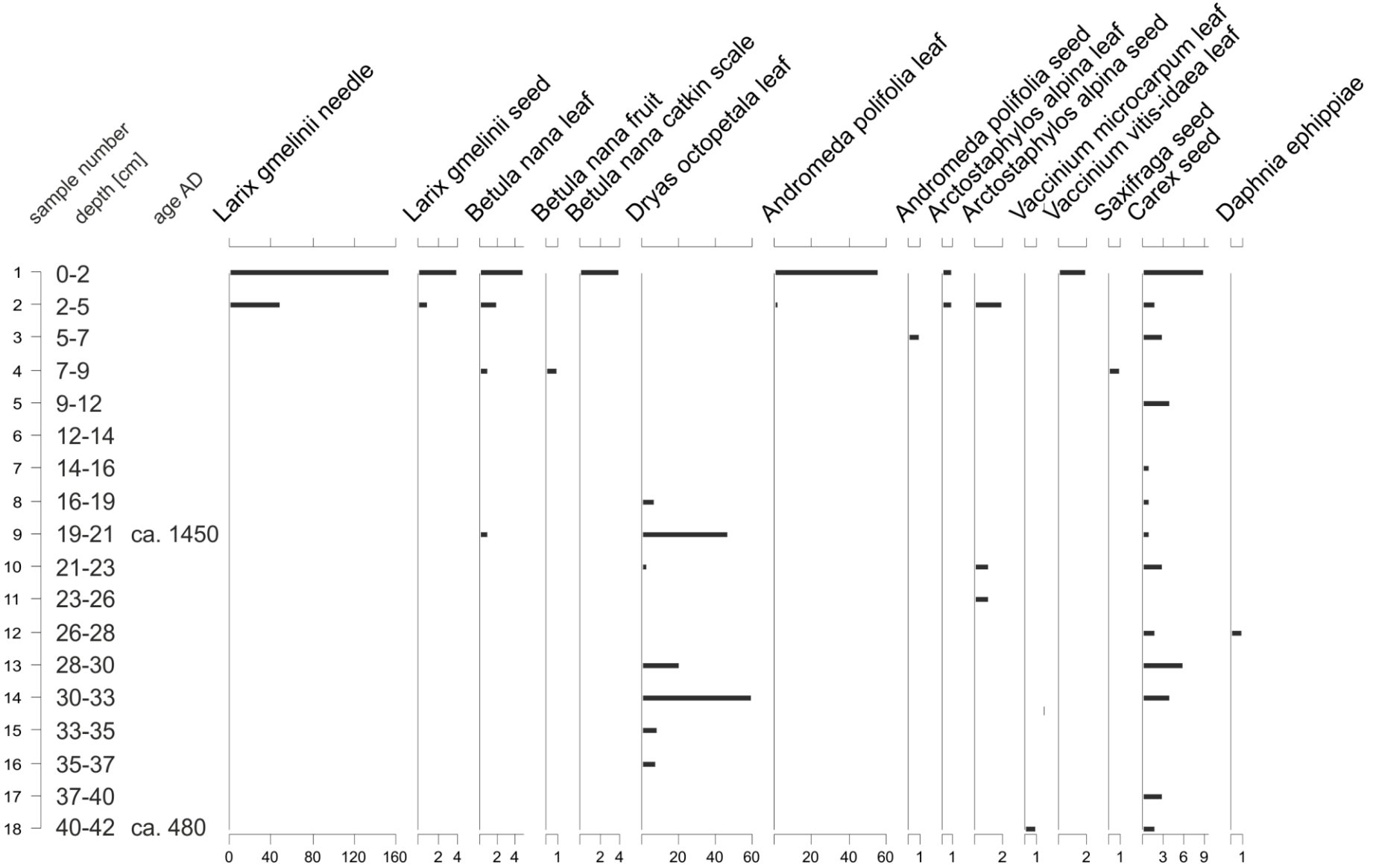

Fig. 18 Plant macrofossil diagram from profile A (polygon ridge)

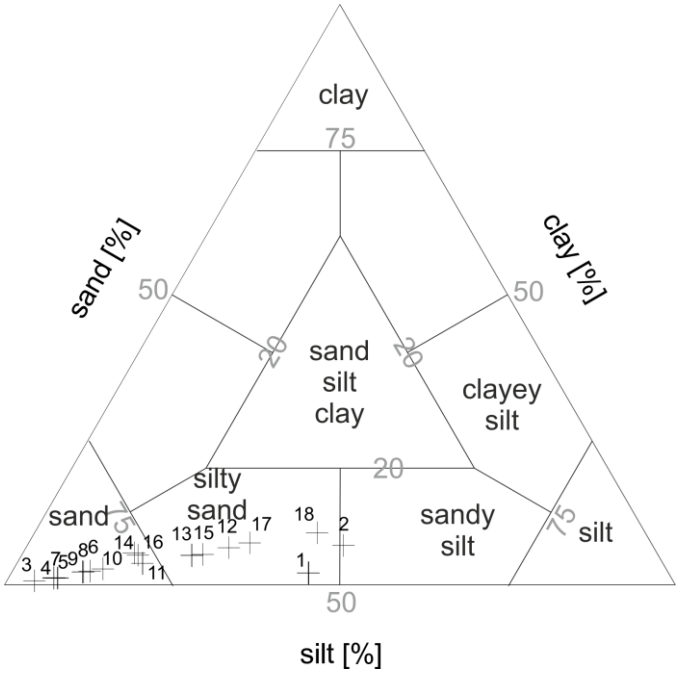

Fig. 19 Lithological classes after Shepard (1954) in profile A; crosses represent samples A-01 to A-18

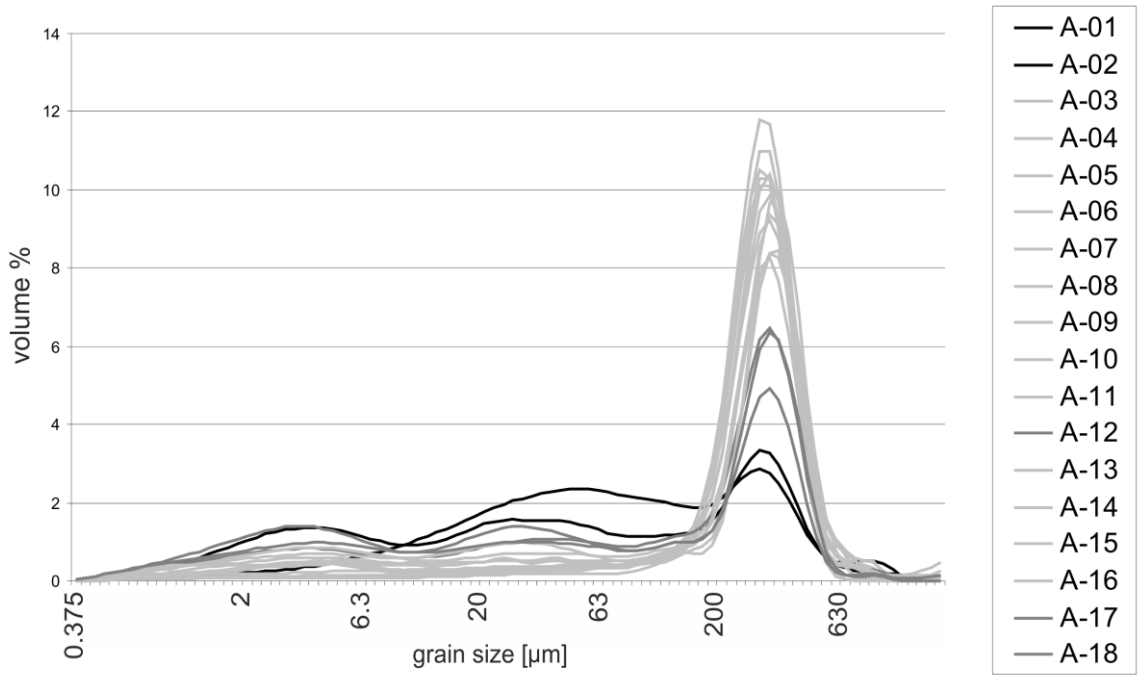

Fig. 20 Grain size distribution in profile A

The top two samples (A-01 and 02) have a similar grain size distribution (see black lines in Fig. 20). From sample A-03 downwards there is a gradual change from coarse-grained to rather finer grained sediment (see gray lines in Fig. 20). The grain size distribution is also illustrated in Fig. 21.

Stable carbon isotopes

$\delta^{13}C$ values are slightly higher than in most of the surface samples. The minimum ratio was found in the topmost sample (A-01), and the maximum value was found in a sample from the middle of the profile (A-09). Due to measurement problems no value could be obtained from the sample A-12. $\delta^{13}C$ values are given in Fig. 21.

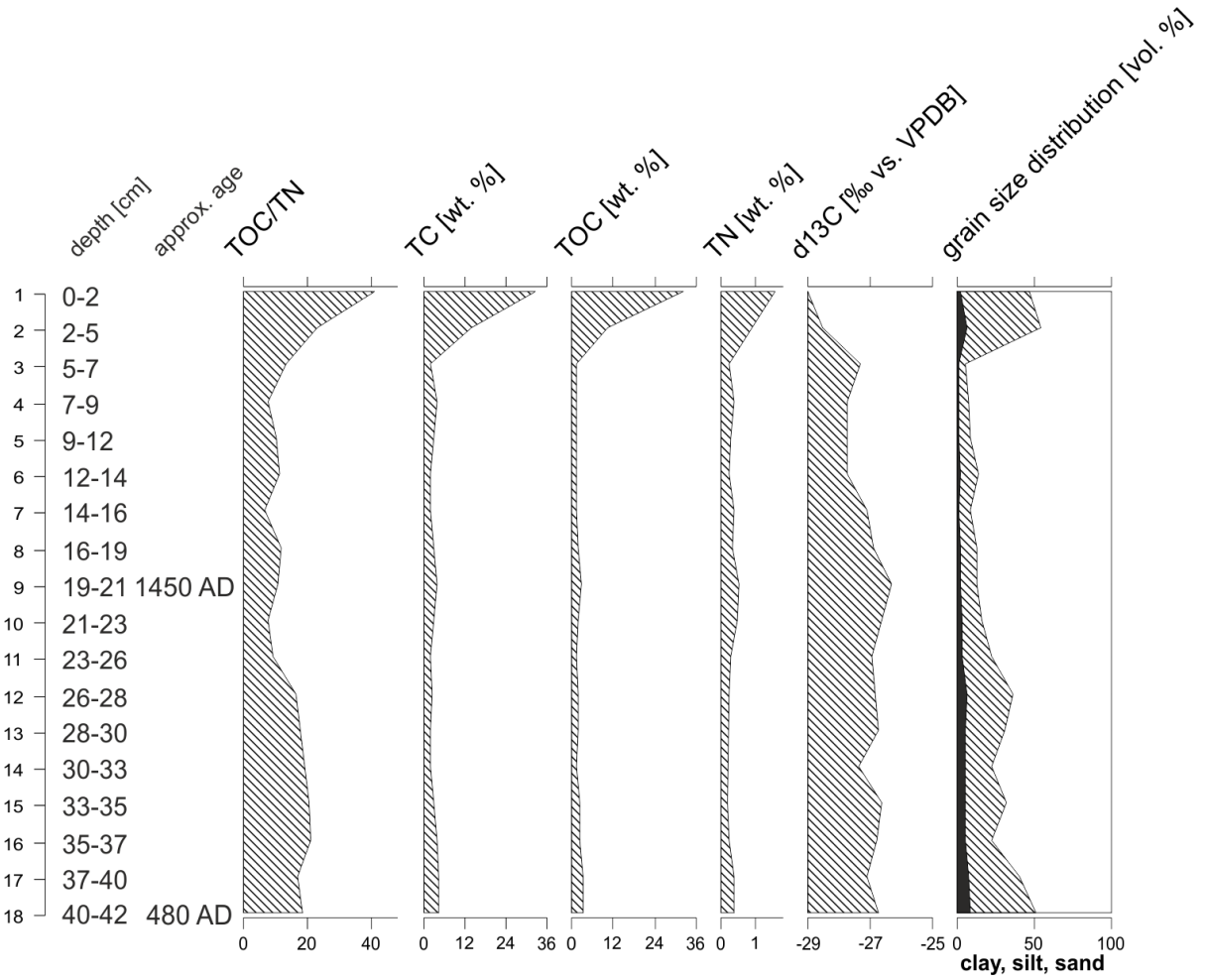

Fig. 21 Stratigraphic diagram of sedimentological parameters in profile A (polygon ridge)

Organic matter composition

TC contents range from 1.74 wt % in the lower half (sample A-13) to 32.61 wt % in the topmost sample (A-01). The values are increasing sharply towards the top in the upper three samples. They are rather uniformly low from sample 03 to 18, staying between 1.74 wt % and 4.49 wt %. The distribution of TOC contents follows that of TC. TOC ranges from 1.195 wt % to 32.08 wt %. TN ranges from 0.11 wt % to 0.78 wt %. In the top two samples values are slightly increased (0.45 wt % and 0.78 wt % in samples A-02 and A-01, respectively). The remainder of the values does not exceed 0.26 wt %. TN values below the

detection limit of 0.01 wt % were excluded from the analysis (samples A-13 and A-14). C/N ratios lie between 10.68 and 41.7. They are high in samples 01 and 02 from the top of the profile (41.7 and 30.88, respectively), intermediate between A-03 and A-14 (roughly between 10 and 20), and slightly elevated in the bottom samples A-15 to A-18 (about 24 to 32). C/N, TOC, TC and TN are shown in Fig. 21.

4.4 Profile B

Profile B was dug in grid cell G3 in the transition between ridge and centre 14 cm above the water table. The vegetation in this spot consists of *Betula nana*, *Salix* type B, *Vaccinium* sp., *Ledum palustre*, *Andromeda polifolia*, Both *Carex* types, moss type B, *Dicranium* sp. and the aquatic moss type. *Arctostaphylos alpina* and *Dryas octopetala*, which are present in grid cell G1 (ridge), are absent from grid cell G3 (transitional). *Larix* grows on the other ridges.
The bottommost sample of the profile (B-22) was dated to 1565 ± 35 years BP, which corresponds to around the calendar year 500 AD. The profile is 50 cm deep and consists of 22 samples. The mean sedimentation rate is 3.3 mm/year.

Plant macrofossils

Larix needles were found in abundance in the top three samples and almost in the entire profile single needles of *Larix gmelinii* occur. Remains of *Betula nana* and *Salix* were found in the top half of the profile. Leaves of *Andromeda polifolia* are abundant in samples B-02 and B-03, with only single occurrences in other samples (B-05, B-14, B-18). Other Ericaceae found in the samples are *Vaccinium microcarpum*, *Vaccinium uliginosum* and *V. vitis-idaea*, which are restricted to the top three samples. *Carex* seeds occur in all samples, but their numbers are much higher in the upper half. Single seeds of Poaceae, *Luzula* sp., *Polygonum viviparum*, and *Valeriana capitata* were found in the upper six samples, with the exception of one Poaceae seed in sample B-19. *Daphnia* ephippiae were recovered from samples B-04 to B-11. The plant macrofossil diagram for profile B is given in Fig. 24.

Grain size distribution

Sand is dominant (>50 vol %) in 20 of the samples. In the top sample, both silt and sand reach values between 40 and 50 vol %. Sand contents range from 46.5 to 96.2 vol %. Silt contents range from 3.3 to 46.1 vol %. Clay contents do not exceed 8.3 vol %. Distribution of the samples in the lithological classes after Shepard (1954) is rather homogeneous (see Fig. 22):

half of the samples are sand (12 samples: B 04-06, 08 & 13-20), the other 10 samples belong to the class silty sand (B 01-03, 7, 09-12, 21 & 22).

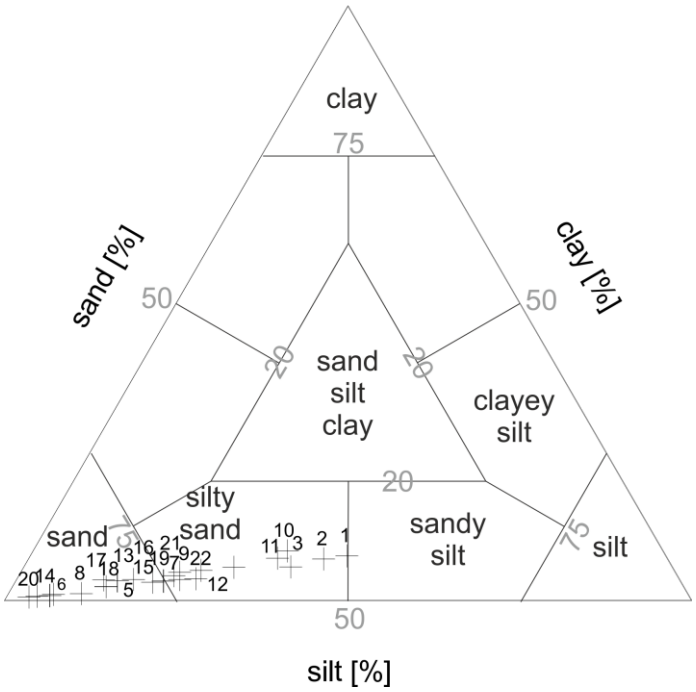

Fig. 22 Lithological classes after Shepard (1954) in profile B; crosses represent samples B-01 to B-22

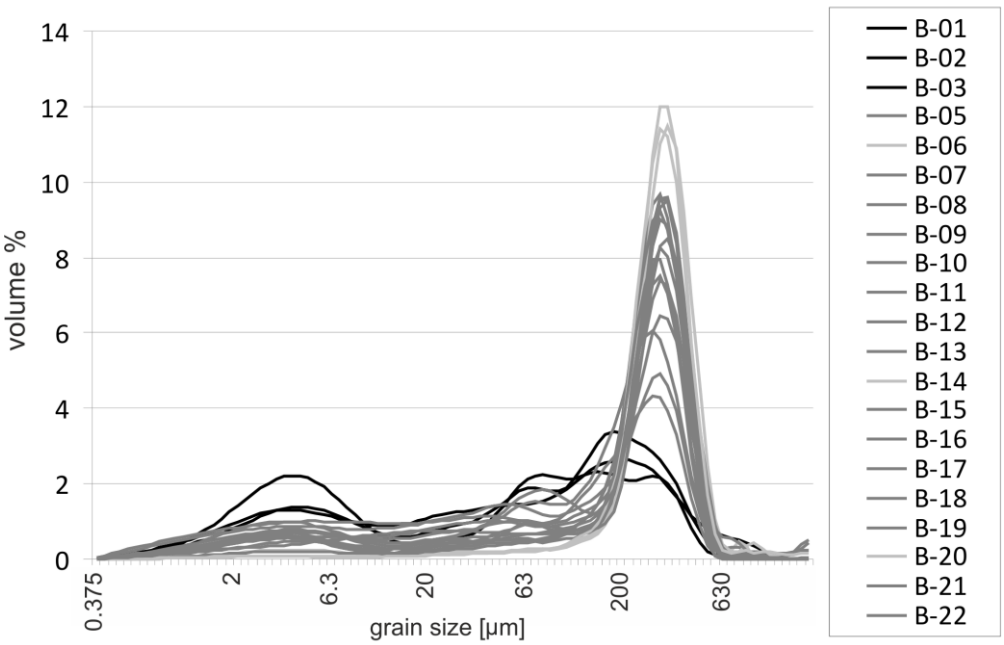

Fig. 23 Grain size distribution in profile B

The top three samples (B-01 to B-03) have a similar grain size distribution (see black lines in Fig. 23). All other samples show one pronounced peak in the medium sand fraction (see gray lines in Fig. 23). The grain size distribution is also illustrated in Fig. 25.

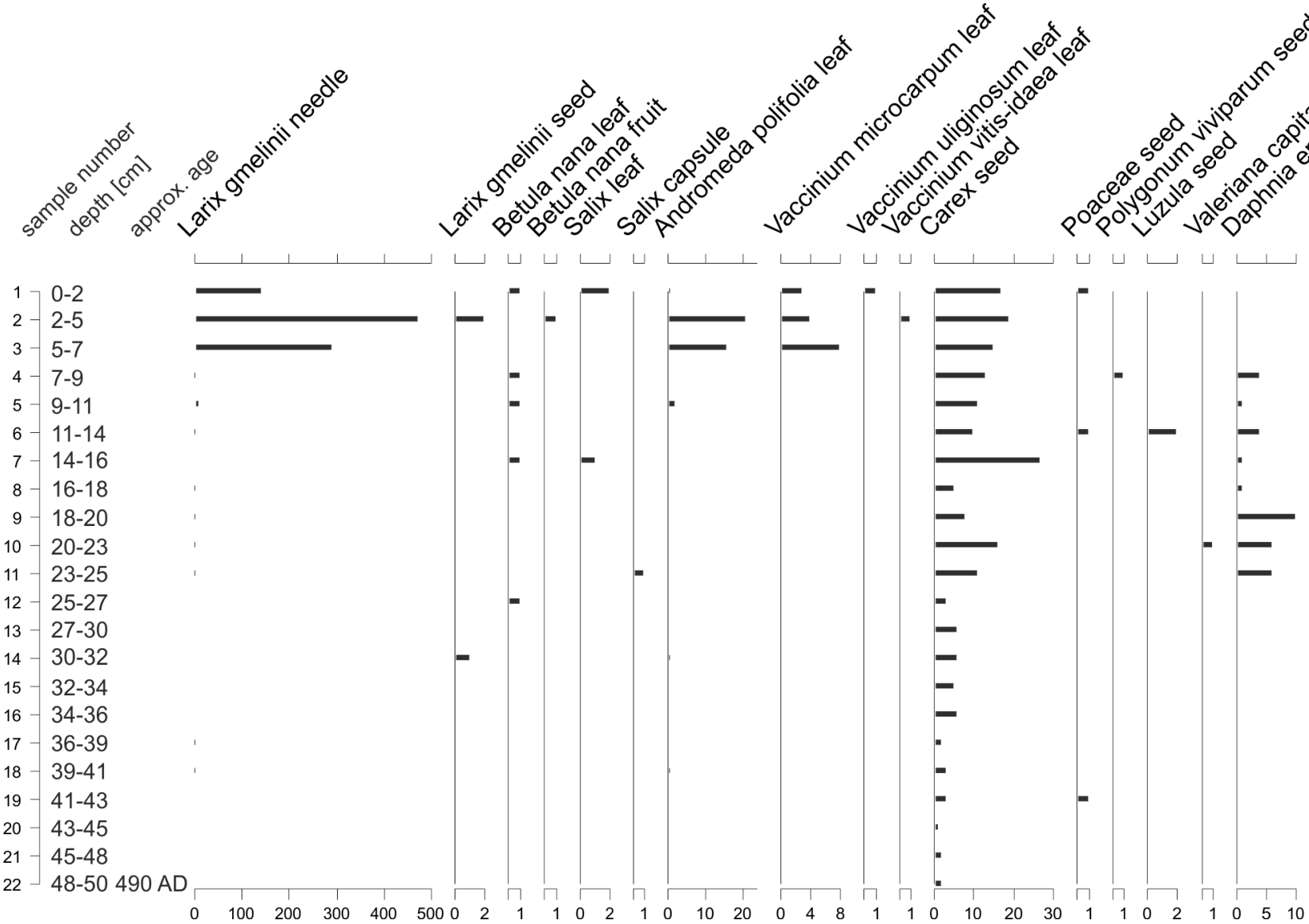

Fig. 24 Plant macrofossil diagram from Profile B (ridge-centre transition)

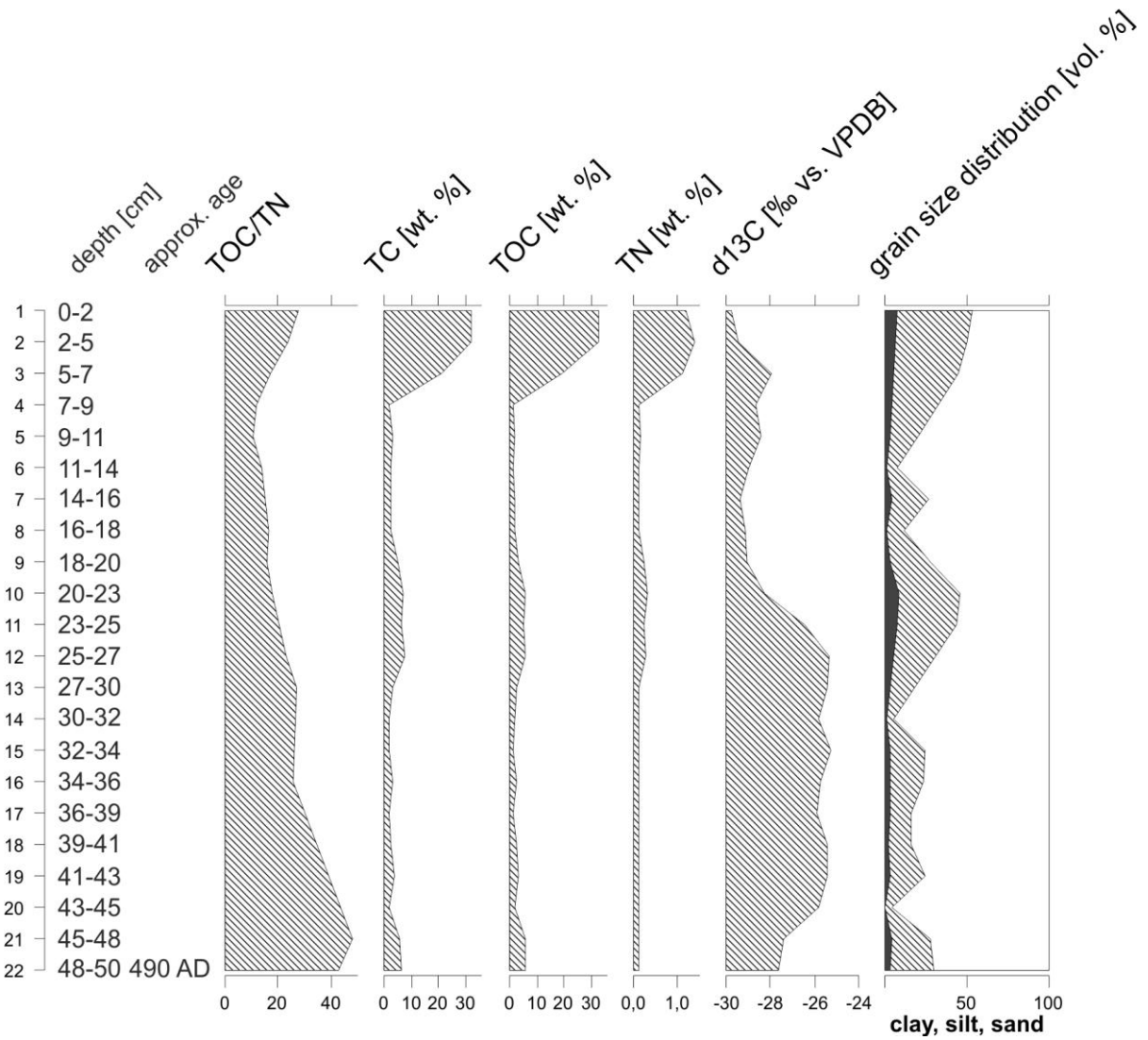

Fig. 25 Stratigraphic diagram of sedimentological parameters in profile B (ridge-centre transition)

Stable carbon isotopes

Stable carbon isotope ratios range from -29.78 to -26.31 ‰. As in profile A, the lowest value was detected in the topmost sample (B-01). The highest value was detected in a sample from the lower middle of the profile (B-15). Generally, $\delta^{13}C$ values are lower in the upper half and higher in the lower half. Stable carbon isotope values are given in Fig. 25.

Organic matter composition

TC contents range from 1.93 wt % to 32.22 wt %. From the bottom up, values decrease slightly in the oldest three samples from 6.48 wt % to 2.05 wt %. Between samples B-20 and B-13 and between B-08 and B-04 values are rather homogeneous (roughly between 2 wt % and 3.5 wt %). Slightly increased values are found in samples B-12 to B-9 (5.19 wt % - 7.76 wt %). The most pronounced increase in TC can be seen at the top of the profile, where

values reach from 21.04 wt % (B-03) to about 32 wt % (B-01 and B-02). TOC values range from 33.08 wt % to 1.31 wt % and follow the pattern observed in TC contents. TN contents are between 0.1 wt % 1.38 wt %, following TC and TOC. Six samples (B-14 & -15, B-17 to B-20) have nitrogen contents below the detection limit of 0.01 wt % and have to be left out of the analysis. As they are all from the bottom half, the C/N record there is rather incomplete. C/N values range from 19.12 near the top (B-03) to 52.08 at the bottom of the profile (B-21). Like the other parameters, they increase in the top three samples: from about 19 to about 26.5. C/N, TOC, TC and TN are illustrated in Fig. 25.

4.5 Core C

Core C was taken from grid cell G8 in the submerged centre of the polygon 10 cm below the water table. The recent vegetation there consists of aquatic mosses. The second lowest sample of the core (sample C-26) was dated to 405 ± 25 years BP, which corresponds to about the year 1460 AD. The profile is 27 cm deep and consists of 27 samples. The average sedimentation rate is 6.7 mm/year.

Grain size distribution

Sand is dominant (>50 vol %) in 25 of the samples. The top two samples are dominated by silt. Sand contents range from 14.7 vol % to 98.7 vol %. Silt contents range from 1.3 to 67.2 vol %. Clay contents range from 0.09 to 18.1 vol %. Distribution of the samples in the lithological classes after Shepard (1954) is displayed in Fig. 26. The majority of the samples are sand (21 samples: C-03 to C-08, C-11, 12 & 15-27), four samples belong to the class silty sand (C-09, 10, 13 & 14), one sample is sandy silt (C-02), and the top sample is clayey silt (C-01).

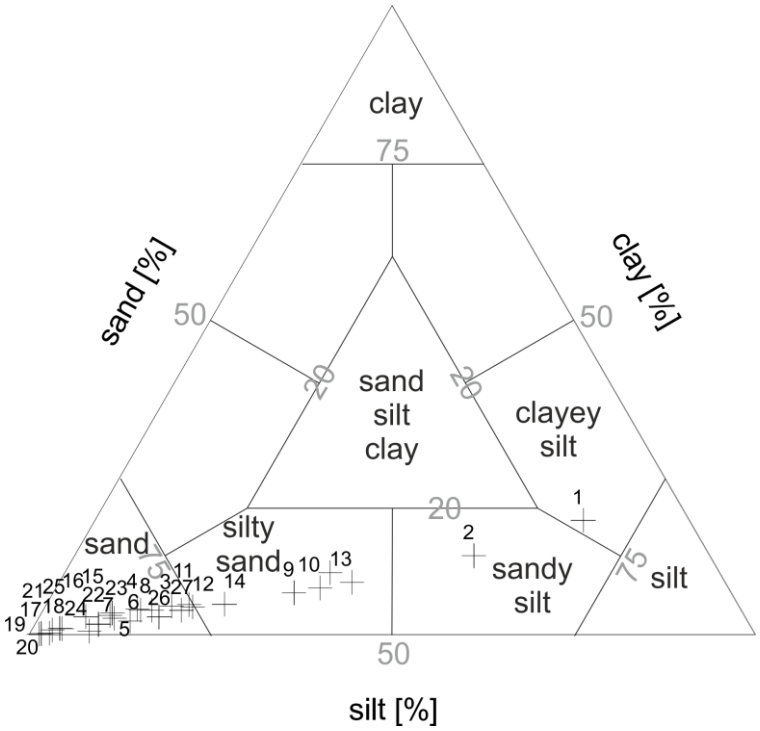

Fig. 26 Lithological classes after Shepard (1954) in core C; crosses represent samples C-1 to C-17

The top two samples (C-01 and C-02) have a similar grain size distribution, showing a peak in the fine silt fraction and another less pronounced one in the medium sand fraction (see black lines in Fig. 27). The other samples have a varyingly pronounced peak in the medium sand fraction (see gray lines in Fig. 27). The grain size distribution is also displayed in Fig. 28.

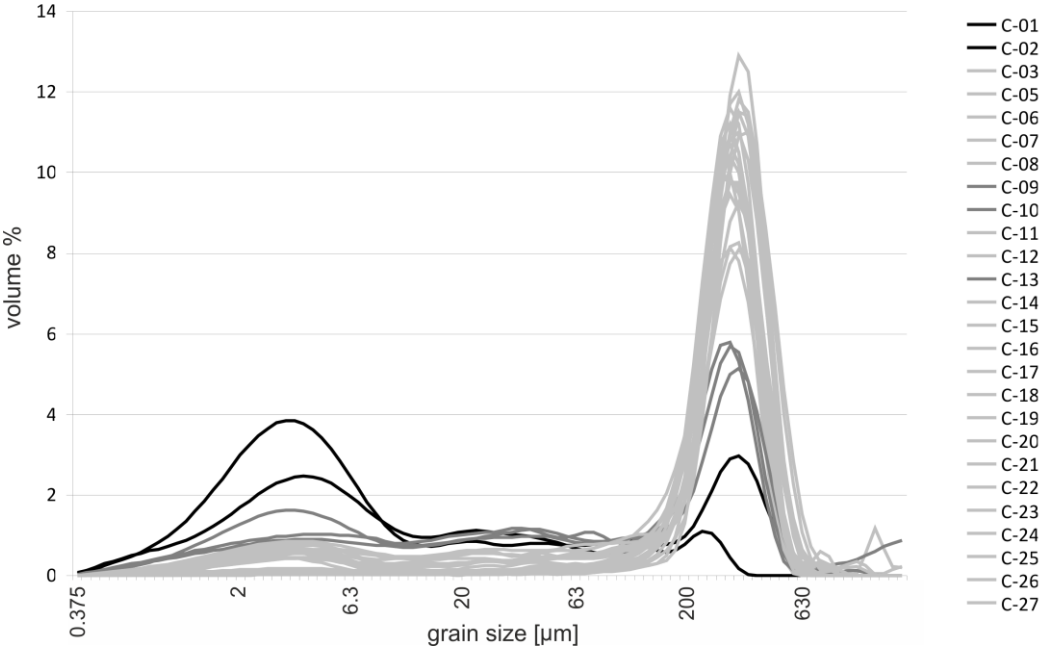

Fig. 27 Grain size distribution in core C

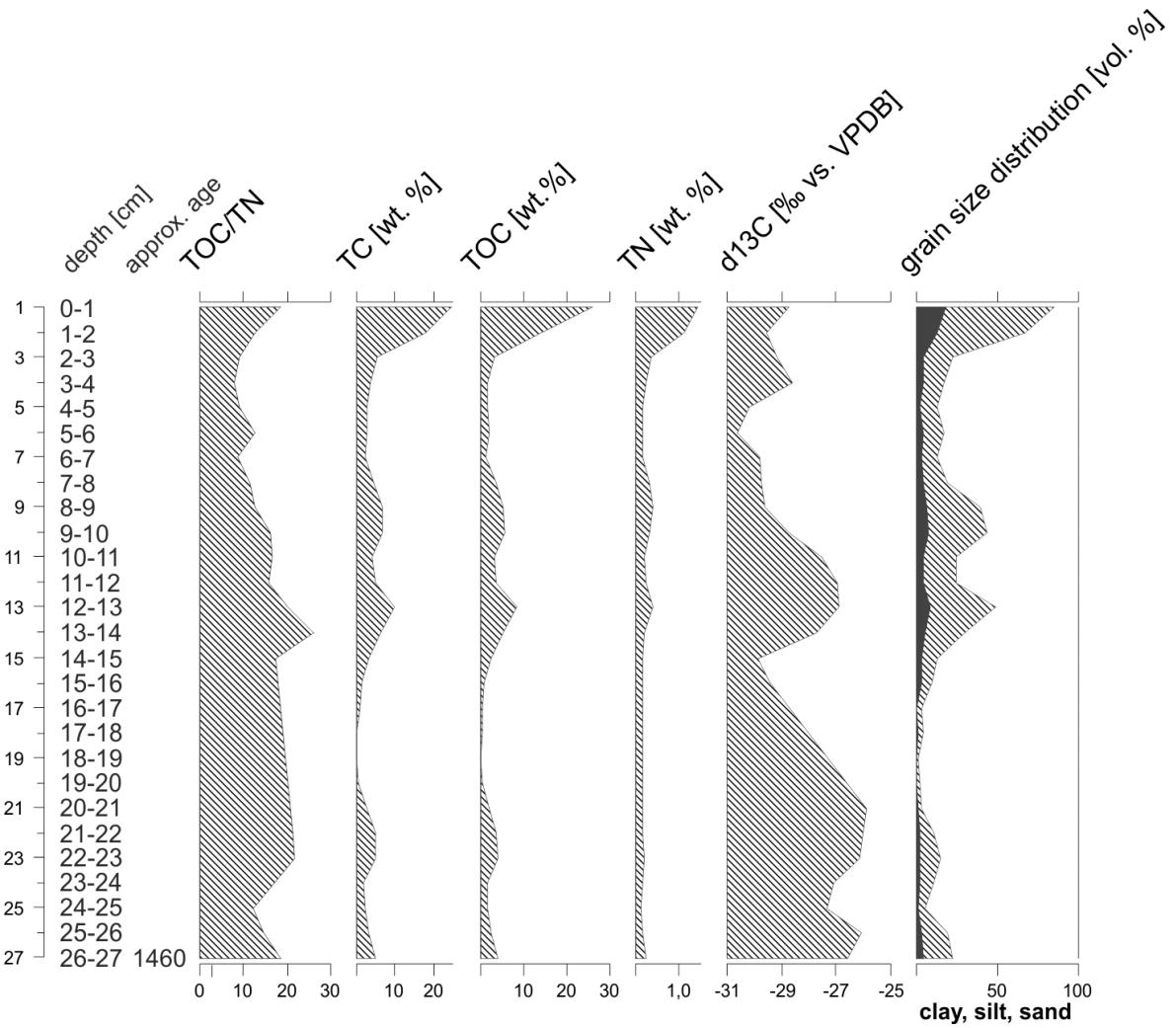

Fig. 28 Stratigraphic diagram of sedimentological parameters in core C (polygon centre)

Stable carbon isotopes

Stable carbon isotope ratios are between -25.87 ‰ and -30.64 ‰. They are generally lower in the upper part from C-01 to C-10 (about -28.5 ‰ to -30.5 ‰) and higher in the lower part of the core (about -25.8 ‰ to -27.7 ‰), with the exception of samples C-15 and C-16, which are within the range of the upper samples. Due to measurement problems no $\delta^{13}C$ values could be obtained from four samples from the lower middle part of the core (C-17 to C-20). Stable carbon isotope ratios are displayed in Fig. 28.

Organic matter composition

TC contents range from 0.13 wt % to 24.46 wt %. About half of the values are below 3.5 wt %, but values rise to between about 4 wt % and 10 wt % in the middle and lower portions of the core (samples C-8 to C-14, C-22, -23 & -27). As in profiles A and B, TC contents increase sharply in the top samples from about 3.5 wt % in sample C-04 to about 24.5 wt % in sample C-01. TOC contents range from 0.2 wt % to 25.94 wt % and follow the

distribution of TC. TN contents are between 0.12 wt % and 1.41 wt % and also follow this distribution. Seven values (from samples C-16 to C-21 & C-24) have to be left out of the analysis because they are below detection level (< 0.1 wt %). The C/N ratio ranges from 13.18 to 31.19. It is lower in the upper part from C-01 to C-09, where values are between about 13 and 17. C/N ratios are incomplete in the lower half of core C due to the lack of nitrogen content values, but the existing ratios are between about 17 and 31. C/N, TOC, TC and TN are displayed in Fig. 28.

5 Discussion

5.1 Polygon setting, morphology and vegetation

Polygon setting and morphology

Ice wedge polygons commonly form under cold and dry conditions on ground with a low topographic gradient (Schirrmeister et al., in press). Floodplains in the arctic tundra provide ideal conditions for their development (Boch 1974). The geographical setting of the studied polygon in an old meander of the river Anabar in Northwest Yakutia is thus quite typical.

Because of these requirements, ice wedges and ice wedge polygons are suitable as evidence for extremely cold and dry winters (Washburn 1980), but also especially susceptible to climate change, which is expected to be most pronounced in the arctic tundra (ACIA 2005). According to Péwé (1966), they are only found where the mean annual air temperature is no higher than -6 °C, although Romanowskii (1985) specifies maximum temperatures according to substrates. He states that ice wedges in clay may occur where the mean annual temperature is as high as -2°C, because ground temperatures are lower in clay than in coarser substrates. Ice wedge polygons diversify the microrelief and ultimately the mosaic of microhabitats in arctic landscapes (ACIA 2005). Especially such environmental parameters as moisture, temperature and active-layer dynamics in different habitats are defined by topography (Brown et al. 1980, Webber et al. 1980) and become the main determining factors in high latitude environments (ACIA 2005).

In size and morphology, the studied polygon is comparable to previously studied ice wedge polygons. While those studied in the North American Arctic usually measure between 15 and 40 m in diameter (French 2007), Siberian polygons range between 7 and 30 m (Chernov & Matveyeva 1997). The studied polygon measures about 12 x 13 m and is one of the smaller polygons. Elevation differences of about 50 cm between ridge and central depression are also typical (French 2007, Boike et al. 2008). The deeper trough in one of the ridges (at coordinates L 3 to L10) is a ridge in state of collapse, with a much lowered frost table and a relative elevation below the water table, providing some drainage to the polygon. Such degraded ridges were long believed to be a sign of degradation and improved drainage conditions. Polygon mires were thought to be hydrologically closed systems in their mature state (French 2007). More recent studies, however, view ice wedge polygons as hydrologically open systems (e.g. Woo & Guan 2006). Minke et al. (2007) found degraded ridges in many of their studied polygons and explained them as a result of water flow mainly

during spring. They conclude that they are natural components of polygon mires, protecting the remaining ridges by allowing some discharge of relatively warm snow melt and rain water from the polygons. Polygon ridges are never static and at times grow or collapse over relatively short time spans of hundreds to thousands of years (Minke et al. 2007, Romanovskii 1977).

The active layer is of central importance to practically all biological and biogeochemical, hydrological and pedogenic processes in cold regions (Hinzmann et al. 1991, Kane et al. 1991). Previous studies have shown a rather large variability in active layer thickness (Walker et al. 2002, Brown et al. 2000, Hinkel & Nelson 2003) on a broad scale. Factors determining the thickness of the summer thaw layer include soil moisture, the thermal properties of the vegetation cover and substrate, surface temperature, snow height and snow cover duration (Hinkel et al. 1997, Paetzold et al. 2000). The diversity of influencing factors causes great variability in active layer thickness in space and time (e.g. Hinkel & Nelson 2003).

The mean active layer thickness in studied sites in Arctic Alaska responds to air temperature forcing on a regional scale and lies between 20 cm and 72 cm (Brown et al. 2000). Boike et al. (2008) found a late summer thaw depth of 70 cm in polygonal tundra in the Lena River Delta, while Minke et al. (2009) measured averages of 34 and 26 cm in two low-centred polygons in the Yana-Indigirka lowlands in Northeast Siberia. Active layer thickness is generally more variable in polygon ridges and more homogeneous in the middle. In the two polygons studied by Minke et al. (2009), average thaw depths were 23 and 31 cm in ridges and 33 and 40 cm in central depressions, but the greatest thaw depths were also found in ridges, probably caused by thermal erosion as a result of water flow. In the ridges, the ground is lifted slightly above the water table. Drier peat is a more effective insulator than wetter peat (Roman 1981, Yershov 1998), and consequently thaw depths are shallower in ridges than in wet depressions. These findings were generally confirmed in this study. Summer thaw depths correspond more closely to those found in the Lena River Delta, which is closest to the studied polygon. Both the highest (83 cm) and the lowest values (21 cm) occur in the ridges. Two of the ridges show the typical shallow thaw depths, while a third exhibits the deepest thaw in the polygon, which may be a sign of initial degradation or else a natural component. In the degraded ridge, the ice surface is not covered by sediments and about as high as in the adjacent part of the polygon centre, underlining the degradation of the ice wedge. In the central depression at or below the water table more homogeneous intermediate values between 52 and 71 cm are found, averaging to about 61 cm.

The elevation of the permafrost table corresponds closely to the ground surface elevation, as do soil temperatures. On the ridges, the active layer surface is highest and soil temperatures are lowest, while in the low-lying centre the active layer surface is lowest and soil temperatures are highest.

Polygon vegetation

The vegetation pattern in the studied polygon is generally consistent with findings from other polygon mires in Yakutia (deKlerk et al. 2008, Minke et al. 2009, Matveyeva 2004, Kutzbach et al. 2004). The distribution of plant taxa in the polygon relates closely to the underlying microrelief. Kutzbach et al. (2004) assigned the vegetation in the centre of a polygon mire in the Lena Delta to the phytosociological association *Meesio triquetris-Caricetum stantis* (Matveyeva 1994), which is found in tundra wetlands. The vegetation on the polygon rims was regarded as a transient type between this association and the association *Carici arctisibiricae-Hylocomietum alaskanii*, which is the typical zonal association of the tundra zone on Taymyr (Matveyeva 1994).

In the studied polygon, not all characteristic species were found, mostly because identification in the field was hindered by lack of flowers on the plants. The species that were identified, however, belong to the above associations.

DeKlerk et al. (2008) studied a similar polygon mire in NE Yakutia. According to them *Betula nana*, Ericales (with the exception of *Andromeda polifolia*), Poaceae, *Polygonum viviparum*, *Ranunculus lapponicus*, *Eriophorum* sp. and most *Sphagnum* species (without *S. subsecundum*) are typical ridge taxa. Taxa preferring the polygon centre *are Comarum palustre* (syn. *Potentilla palustris*), *Pedicularis* sp. and *Carex chordorrhiza*, *Drepanocladus revolvens* dominating the mosses. *Andromeda polifolia*, *Carex rariflora*, *C. rotundata*, cf. *C. orthostachus*, cf. *C. dioica* and *Sphagnum subsecundum* prefer transitional reaches. *Salix* sp., *Carex concolor* (syn. *Carex aquatilis ssp. stans*) and *Saxifraga* sp. grow both on ridges and in the transition. Single individuals of *Valeriana capitata*, *Luzula parviflora* and *Tofieldia coccinea* grow spread across the polygon. Mosses (without *Sphagnum*), as well as liverworts and lichens occur with high dominance across the entire polygon. These findings can be confirmed in most respects. The species composition is comparable, although the vegetation survey is much more detailed in the study by deKlerk et al. (2008). In contrast to this study, no *Eriophorum* was mapped for the studied polygon, but it was observed growing in the polygon. Willows, sedges, and mosses were not identified to species level, but different types were differentiated. Poaceae were not identified in more detail. No *Comarum palustre*,

Saxifraga sp., *Valeriana capitata* or *Luzula parviflora* were mapped, but were found in the macrofossil record. Overall, the vegetation in the two polygons seems to be very similar and findings from the detailed study probably apply to the polygon studied in the Anabar region. Note that there is no *Larix* growing in the NE Yakutian polygon. Distribution of taxa in the polygon and elevational preferences differ only very slightly between the two polygons. Taxa confined to the ridges of the studied polygon are *Larix gmelinii, Salix* type A, *Arctostaphylos alpina, Dryas octopetala, Polygonum viviparum* and Poaceae, while *Betula nana, Salix* type B, *Vaccinium* sp., *Ledum* sp. and *Carex* type A were found both on ridges and in the transition. *Andromeda polifolia* indeed seems to prefer the transition between ridge and centre. In the central depression only the two *Carex* types and mosses were found, while *Pedicularis* sp. favours the transitional reaches. The distribution of plant taxa in the Northeast Yakutian polygon mire studied by deKlerk et al. (2008) and in the studied polygon from Northwest Yakutia is summarized in Table 2.

Table 2 Distribution of plant taxa in polygon mires

	Studied polygon mire in Northwest Yakutia	Polygon mire in Northeast Yakutia (deKlerk et al. 2008)
ridge	*Larix gmelinii*, *Salix* type A, *Arctostaphylos alpina*, *Dryas octopetala*, *Polygonum viviparum*, Poaceae	*Betula nana*, Ericales (with the exception of *Andromeda polifolia*), Poaceae, *Polygonum viviparum*, *Ranunculus lapponicus*, *Eriophorum* and most *Sphagnum* species (without *S. subsecundum)*
Ridge and transition	*Betula nana*, *Salix* type B, *Vaccinium* sp., *Ledum* sp., *Carex* type A	*Salix* sp., *Carex concolor* (*Carex aquatilis ssp. stans*), *Saxifraga*
transition	*Andromeda polifolia*, *Pedicularis* sp.	*Andromeda polifolia*, *Carex rariflora*, *C. rotundata*, cf. *C. orthostachus*, cf. *C. dioica* and *Sphagnum subsecundum*
centre	*Carex* type A and B, aquatic mosses	*Comarum palustre (*syn. *Potentilla palustris)*, *Pedicularis* sp., *Carex chordorrhiza*, mosses (dominated by *Drepanocladus revolvens*)

5.2 Surface transect

Additional data was obtained for 13 samples along a transect through the polygon. Electrical conductivity, pH, TC, TOC, TN, grain size distribution and $\delta^{13}C$ were measured, the C/N ratio was calculated and plant macrofossils were analysed.

The electrical conductivity is positively correlated with the C/N ratio. It is higher on ridges and lower in the submerged centre and exhibits a wide range of values from 16 to 84 mS/cm. Five soil properties have been identified as determinants of the electrical conductivity of soils: porosity, water content, salinity level, cation exchange capacity, and temperature are all positively correlated with soil electrical conductivity (Doerge 1999). High levels of organic matter in a mineral soil have the same effect as high salinity. The presence of dissolved positively charged ions such as Ca, Mg, K, Na, NH_4 or H in moisture-filled soil pores greatly enhances electrical conductivity. Organic matter provides these ions to the soil (Doerge 1999).

pH values show very little variation in the transect. They are close to neutral in the submerged middle (max. 6.25 at G6-8) and moderately acidic on the ridges and in transitional ranges (min. 5.7 at G3). Acidic plant litter generally lowers the pH in a soil. The higher abundance of conifer needles and ericaceous plant litter might explain the slightly lowered pH on the ridges and in the transition.

TOC contents are determined by the production of biomass before deposition and its subsequent decomposition (Meyers and Lallier-Verges 1999). Both production and decomposition rates vary within the polygon due to differences in vegetation composition and differences in soil properties such as soil temperature, water content and oxygen availability. In the waterlogged soils of the polygon centre, anaerobic accumulation of organic matter is expected, while oxic conditions in the polygon ridges should enhance decomposition (Kutzbach et al. 2004). Total organic carbon contents are, however, highest on the ridges and in the transition, and lowest in the submerged middle. This suggests that vegetation composition may be the main explanatory factor for organic matter composition.

When organic matter is decomposed, carbon is gradually released as CO_2 and subsequently lost from the soil, while nitrogen is mostly integrated into the microbial biomass (Scheffer & Schachtschabel 2002). Carbon to nitrogen ratios will thus become narrower during decomposition. C/N ratios may also be used as proxies for the origin of organic carbon in a soil (Meyers and Lallier-Verges 1999). For example, land plants leave higher C/N ratios in soil organic matter than aquatic plants, algae and diatoms (Meyers and Ishiwatari 1993). This effect is clearly seen in the surface sediments across the studied polygon. The largest C/N

ratios are found on the ridges, where shrubs, herbs and mosses grow. The lowest ratios are found in the submerged part of the central depression, where aquatic mosses and some aquatic plants grow, and algae and diatoms are found. In the transition intermediate ratios prevail. This rather large variation in C/N ratios may also be attributed to variability in organic matter decomposition at different sites in the polygon (e.g. Schirrmeister et al. in press). C/N values correlate with the ground surface elevation, however, and wide ratios on the ridges and narrow ratios in the centre indicate that decomposition is higher in the submerged centre, which is not the case. C/N ratios in the surface transect are not determined by decomposition rates, but by vegetation composition, which is probably due to the young age of the peat surface. DeKlerk et al. (2009) found a similarly close relation between C/N and surface elevation, which was attributed to poorer trophic conditions on the ridges (cf. Succow & Stegmann 2001).

Changes in vegetation composition usually lead to relatively strong variations in $\delta^{13}C$ values. According to Schirrmeister et al. (in press), $\delta^{13}C$ values are higher (about -24 to -25 ‰) in submerged polygon centres due to aquatic plants growing in ponds there. Mosses in peat layers as well as grass, herb and shrub communities, however, cause lower values (about -28 to -29 ‰). The $\delta^{13}C$ values vary only slightly across the transect and do not show a conclusive pattern. All values lie within the range for ridge communities. In the studied polygon, $\delta^{13}C$ values are not suitable as proxies for vegetation reconstruction.

Wetlands control the carbon and methane balance of the Arctic (Hobbie et al. 2000, Wagner et al. 2003, 2005, Kutzbach et al. 2004). They contain three to four times more carbon than tundra ecosystems on mineral soil (Joosten, 2008). Wetlands of the arctic tundra contain more than 15 % of the world´s soil carbon (Lal and Kimble 2000), which might be released as carbon dioxide and methane when air temperatures increase and wetlands dry up and decompose.

Plant macrofossil assemblage

Polygon mires provide a variety of habitats within 10 - 30 metres. This is mirrored by small-scale changes in the vegetation, from the arctic and subarctic wetland communities of the low-lying centre to the typical tundra vegetation of the elevated ridges.

Fossil remains of dwarf shrubs such as *Betula nana* fruits were probably blown to the submerged part of the polygon by wind, as they do not grow there. *Larix* needles and even some seeds seem to get transported a short distance as well, as they are found everywhere in the polygon. Numbers of such fossils are higher where the plants actually grow. Another

possible explanation for their presence in the water is that they have fallen into the water at its edge and floated to the middle. Those macrofossils have to be handled with care as their ability to reconstruct the local vegetation at a microscale is limited. Some fossils, however, just fall to the ground due to their weight and lack of aerodynamic features. They are very useful for vegetational reconstruction on a microscale (Birks 1980, Birks and Birks 2000). Short shoots and a cone of *Larix* were found solely under the tree growing in grid cell G12. *Betula nana* catkin scales and an entire catkin also show a very realistic location of the plant from which they originate (Birks 1980). *Salix* capsules, *Dryas octopetala* leaves, *Arctostaphylos alpina* leaves and seeds, *Vaccinium vitis-idaea* and *V. uliginosum* leaves, a *V. vitis-idaea* berry and *V. vitis-idaea* seeds all occur exclusively where presence of the plant was mapped. Leaves of *Vaccinium microcarpum* occur concentrated around two spots and nowhere else. They probably come from plants growing just there, but no data for the species' present dominance in the polygon vegetation is available. Thus, leaves and seeds of *Arctostaphylos alpina*, *Dryas octopetala* leaves and short shoots and cones of *Larix gmelinii* represent the location of ridge vegetation very well, while *Andromeda polifolia* remains will be found in transitional reaches and in their immediate adjacency.

In addition to plant macrofossils, sclerotia of the ectomykorrhizal fungus *Cenococcum geophilum* and cladoceran ephippiae (water flea resting egg pouches) have been taken into account. *Cenococcum geophilum* is present in the ridge samples 01 and 02, and absent from all others. This fungus lives in symbiosis with woody plants, for example with *Dryas octopetala*. Its presence is evidence for relatively dry, ridgelike conditions. *Daphnia* ephippiae have been found in the submerged part of the polygon. Cladocera are found in the open water and littoral zone of standing waters (e.g. Duigan & Birks 2000). Their presence is thus evidence for submerged conditions.

The plant macrofossil record shows a mosaic of taxa growing in wet habitats with surplus moisture under stagnant water conditions interspersed with taxa that require a certain amount of drainage and slightly drier conditions. Taxa with a narrow ecological range are valuable as proxies for environmental and climatic conditions. *Salix polaris* is a typical snowbed species, indicating long snow duration in a sheltered concave portion of the ground. *Dryas octopetala* grows in dry localities with low snow cover (e.g. Ellenberg 1988). *Eriophorum angustifolium* indicates well moistened areas that are drained to some degree and *E. russeolum* thrives under stagnant water conditions on a continuous moss carpet (Tolmachaev et al. 2000). *Potentilla palustris* grows along the water´s edge (Polozhij and Malyschev 2004).

The vegetation represented by macrofossils on the ridges corresponds to the vicariant *Pinguicula villosa* of the association *Carici arctisibirica-Hylocomietum alaskani* (Matveyeva 1994), typical for plakor habitats of the southern tundra subzone on Taymyr. Such habitats are usually moderately wet in summer, and have active layer depths of 55 to 80 cm at the end of summer (Matveyeva 1994). Similar conditions are found on the ridges of the studied polygon. Vegetation of the polygon centres belongs to the association *Meesio triquetris-Caricetum stantis* (Matveyeva 1994). The affiliation to this association cannot be confirmed by the macrofossil record, although at least one differential taxon was identified. As macroremains of mosses were not identified and seeds of *Carex* were not specified, most diagnostic species cannot be ascertained in the macrofossil record. The detailed vegetation survey of a similar polygon mire in NE Yakutia confirmed the affiliation of the polygon centre vegetation to this association (deKlerk 2008). The association occurs in mires of the Siberian tundra zone. The associated habitat has a moist soil for the entire vegetation period and a high ground-water table, especially after snowmelt in spring and after heavy rains in autumn. The mosses are continuously wet or submerged in stagnant water.

The macrofossil record is never complete, as not all plants produce identifiable fossils. Some taxa will always be underrepresented or not show up at all in the macrofossil record. In cold climates with a short growing season, some plants may not flower and resolve to vegetative reproduction (Birks 1980). Others may produce very low numbers of seeds or fruits (Birks 1980). Fragile seeds and leaves will mostly not be preserved, while sturdier fossils produced in abundance such as *Larix* needles and *Betula* fruits may be found in high numbers (Birks and Birks 1980).

Thus, the absence of a taxon in the record does not prove its absence from the vegetation at the time of sedimentation. Its presence, however, proves presence of the plant in the local vegetation. Unlike other palaeoecological proxies such as pollen, wind dispersal of plant macrofossils is of limited importance (Birks and Birks 2000). Many fruits and seeds have developed mechanisms promoting wind transport, but they will not be transported over long distances, especially if they grow close to the ground. Plant macrofossils are thus generally of local origin. Sample sizes need to be rather large, between 50 ml and 200 ml are recommended in order to represent the local vegetation. Samples must be taken in the field, transported and handpicked for macrofossils, however, and manageability of the samples is an issue too. In this study, only 25ml of sediment were used from each sample, as the picking process proved to be rather slow work.

5.3 Profile A - the past 1600 years on the polygon ridge

A soil profile was dug on the polygon ridge (Profile A) in grid cell G1. It corresponds to the surface sample 01. In nearly 1600 years, 42 cm of peat developed in this spot, the average sedimentation rate is about 2.7 mm/year. The range of above-permafrost peat thickness is comparable to that of other low-centred polygons in the Yakutian tundra (Minke et al. 2009).

In the surface transect, a positive correlation between C/N and ground surface elevation was found, with high C/N ratios on the ridges and low C/N ratios in the polygon centre. If this is applied to the C/N curve of the profile, high C/N ratios in the lower und upper parts suggest the prevalence of typical ridge conditions, while low ratios in the upper middle of the profile refer to conditions more alike to the transition or middle parts of the polygon. In the ridge profile, the silt content correlates with TOC, and both TC and TOC correlate with C/N. Silt and TC also show a positive correlation in the surface transect. High silt content accompanied by high TOC and high C/N can thus be associated with ridge conditions, while low silt content, low TOC and low C/N prevail under wetter conditions in the deeper parts of the polygon. This suggests that the polygon wall experienced conditions similar to the present around the end of the 5th century and for some time after that, followed by a phase of transitional, wetter conditions starting around the 15th century (Sample A-09 was dated to about 425 years BP). The sharp decrease in TOC within the top 6 cm of the profile downwards is mostly due to decomposition in the top soil layer. According to Clymo (1984), 80-90 % of dry mass in the peat are lost in the acrotelm (upper peat layer above water level) due to aerobic decay before the peat is incorporated into the catotelm (submerged peat layer). Part of the decrease may also reflect higher bioproductivity due to climatic amelioration in the two most recent samples.

This pattern is mostly supported by the macrofossil record for the site. In the upper two samples of the profile the largest numbers of plant macrofossils and identified taxa are found. This part of the profile is characterized by typical ridge taxa. In older samples, some degree of decomposition must be assumed. The sharp decrease in *Larix* needles appears to be mostly due to decomposition. *Larix* needles seem to be readily decomposed, as frail translucent fragments are the only remains found in samples from greater depth. Such fragments, however, appear across almost the entire profile, proving the presence of *Larix* trees in the polygon for the last 1500 years. *Dryas octopetala* grows in dry localities with low snow cover (e.g. Ellenberg 1988) and can be viewed as a species typical for polygon ridges. Leaves and leaf fragments of *Dryas octopetala* are abundant in the lower part and decrease towards the middle. In the phase of low silt content, low TOC and low C/N described before, leaves are

still present in the beginning, but they are missing from the rest. This can be interpreted as a delayed reaction to unfavourable conditions. A delayed reaction to environmental changes may be the reason why *Dryas* remains are so few in the top samples as well. Further evidence for the existence of ridge conditions in the lower part of the profile is the presence of *Arctostaphylos alpina* seeds not only in the upper samples, but also in the lower middle (in samples A-10 and A-11). *Arctostaphylos alpina* seeds have been shown to be restricted to the polygon ridges in the macrofossil record from the surface transect.

Water level changes in the polygon may either be caused directly by changes in precipitation or flooding events or indirectly by degradation and subsequent build-up of the polygon wall or by a combination of these factors and processes. Flooding can neither be confirmed nor ruled out completely for the last 1500 years. It will not be considered here. The summer water balance of polygonal tundra in the Lena River Delta is mainly controlled by precipitation (Boike et al. 2008). In summers with high precipitation polygonal ponds are constantly refilled, while low precipitation results in the drying of upper soil layers.

On the other hand, alternating collapse and growth of polygon ridges has been observed in polygon mires (Romanowskij 1977, Minke et al. 2007) before. Collapsed ridges have been explained as natural components of polygon mires, which may help stabilizing the polygon pattern by enhancing snowmelt and rain water discharge, providing some protection from the relatively warm water to the remaining ridges (Minke et al. 2007). One of the other ridges of the studied polygon is currently in state of collapse, showing that such thermokarst processes are at work in the polygon today as well, but if a collapsed ridge helps stabilizing the other ridges, it is less likely that they too have collapsed before. A change in climate seems the most likely explanation for the changes in profile A.

Northern Siberia was affected by a cold period from the 17th century until the climatic amelioration in the second half of the 19th century (Borisenkov 1992), and wet and cold summers alternated with extremely cold winters (Shahgedanova 2002). For the Taymyr lowland, warming events inferred from pollen data have been described for ca. 2000 and 1000 ^{14}C yr BP, and a cooling phase is reported for the time between 500 and 200 ^{14}C yr BP (Andreev et al. 2002). The onset of wetter conditions on the ridge coincides with this cooling period, and the drier ridge conditions in the lower part of the profile may have been caused by a warming event.

5.4 Profile B – the past 1500 years in the transition between ridge and centre

Profile B was dug at the transition between ridge and centre of the polygon in grid cell G3, where the surface sample 03 was taken. In about 1500 years, 50 cm of peat accumulated in this spot. The average sedimentation rate of 3.3 mm/year is slightly higher than that of the polygon ridge. The surface is moister there than on the ridges, as it is closer to the water table, impeding decomposition and speeding up sedimentation.

The positive correlation between silt and carbon contents in sediment from the surface transect and profile A is also found in profile B, where there is a strong positive correlation between silt, TC, TOC and TN. While higher silt, carbon and nitrogen contents are related to drier, ridge-like conditions with increased biomass production, wetter and less favourable conditions are accompanied by lower silt, carbon and nitrogen contents. The C/N curve shows a development similar to that of profile A. Those parameters suggest drier and possibly warmer conditions at the bottom of the profile, followed by a phase of wetter conditions. In the three most recent samples, the decomposition in the upper soil layer is seen and possibly drier ridgelike conditions.

The macrofossil record shows a mixture of taxa from wetter and drier habitats, which is typical for the transition between ridge and centre. Some of the macrofossils may originate from the adjacent ridge or the centre, but most will not have been transported far. As in profile A, there is a sharp increase in macrofossil taxa as well as numbers in the topmost samples, which is partly due to decomposition after sedimentation, but also to more favourable environmental conditions. The increase in *Larix* needles observed in profile A is also evident in the transitional profile B (from 1 needle in sample B-04 to 291 needles in sample B-03) and cannot be explained solely by decomposition of the older needles. Clearly, more needles than before were deposited in recent years. The amount of *Carex* seeds is larger than ridge samples, as was expected from the transition from ridge to centre, where sedges are abundant today. Decomposition generally leads to lower seed numbers in older samples, but there is a marked decrease in *Carex* seeds below sample B-11, that may either be the result of stronger decomposition or of reduced seed deposition, both implying drier, ridgelike conditions. The presence of *Daphnia* ephippiae in samples B-04 to B-11 is strong evidence for moist to wet conditions. *Daphnia* lives in aquatic environments and is found in the waterlogged to submerged parts of the surface transect. As in profile A, a change of the water level from dry, ridgelike conditions to wetter conditions with waterlogged peat is implied by the macrofossil record. Recently, a return to a drier and more favourable environment is possible.

$\delta^{13}C$ values show a clear change from higher values in the lower half of the profile to lower values in the phase of wetter conditions in the upper half. Higher values coincide with the phase of drier conditions reconstructed from the macrofossil record.

The vegetation cover of the polygon mire reacts very sensitively to small-scale hydrological changes (deKlerk et al. 2008), and not all of the variation in the macrofossil is necessarily attributed to climatic changes. Local paths of water flow down the ridge sides as a consequence of meltwater runoff over frozen soil or within the active layer (cf. Roulet & Woo 1986, Woo and Guan 2006) may lead to locally increased thawing (Woo and Winter 1993), wetter conditions and changes in the vegetation (Minke et al. 2009). Nevertheless, as the reconstructed development from drier to wetter to drier conditions coincides with those reconstructed from the ridge profile and corresponds to changes in regional climate reconstructed from pollen records (Andreev et al. 2002), past changes in climate are the most probable explanation for the variation in the macrofossil data.

5.5 Core C - the past 450 years in the polygon centre

Core C was taken from the submerged lowest part of the polygon in grid cell G8, and corresponds to the sample 08 from the surface transect. In about 450 years 30 cm of peat accumulated here. The average sedimentation rate is 6.7 mm/year, which is twice as much as in profile B. Decomposition is expected to be slowest in the anaerobic submerged middle, which leads to higher sedimentation rates (e.g. Kutzbach et al. 2004).

As in the two profiles, there is an increase in C/N, TOC, TN and silt content in the upper two samples. As the polygon centre is currently submerged, no aerobic decomposition of organic matter is expected. The increase probably reflects increased bioproductivity in the polygon centre due to climatic amelioration. Apart from that, C/N values are generally lower in the upper half of the core. The C/N signal left by aquatic plants, diatoms and algae is generally low (Meyers and Ishiwatari 1993) and low C/N values were found in the submerged part of the surface transect as well. In the older samples, however, C/N ratios are slightly higher and more alike to ratios from surface samples situated at or near the water table. This may be interpreted as a change from a lower water table to today's submerged conditions some time after 1460 AD.

6. Conclusions

In the studied polygon mire a series of different habitats is created by small-scale changes of the microrelief. Plant macrofossils and sedimentological parameters stored in the peaty sediment of the mire provide a palaeoenvironmental archive of the last 1500 years.

Morphology, sedimentology and vegetation in a Northwest Yakutian polygon mire and their relation to polygon ridge, transition and centre conditions

The polygon mire is situated in an abandoned meander near the eastern bank of the river Anabar in NW-Yakutia, Russia. It is composed of low ridges enclosing a partly submerged low-lying centre, creating height differences of up to 61 cm in an otherwise flat topography. The ground surface elevation follows the elevation of the underlying ice surface. Typical conditions in the upper two centimeters of sediment on the ridges, in the transition and the submerged centre are given in Table 3.

Table 3 Typical conditions in surface sediment in the studied polygon mire

	Active layer depth	Soil temperatures	pH	conductivity	TOC	C/N	$\delta^{13}C$
ridge	Generally shallow, deeper thaw on one ridge	low	moderately acidic	high	high	High	Low
transition	intermediate	intermediate	moderately acidic	intermediate	intermediate	Intermediate	Slightly higher
centre	deep	high	neutral	low	low	low	low

In the deepest parts of the submerged centre of the polygon the plant cover consists solely of aquatic mosses. At or below the water table sedges and mosses are found. Where the ground surface rises a few centimeters above the water table, some few dwarf shrubs (e.g. *Betula nana*, *Andromeda polifolia*) may be found as well as *Pedicularis* sp., sedges and mosses. In the transition between ridge and centre, dwarf shrubs, herbs and mosses grow. The ericaceous dwarf shrub *Andromeda polifolia* favours transitional ranges. Ridge vegetation consists of single *Larix* trees, dwarf shrubs (*Betula nana*, *Salix* sp and various Ericaceae), herbs (e.g. *Polygonum* sp., Poaceae, sedges) and mosses. The dwarf shrubs *Dryas octopetala* and *Arctostaphylos alpina* are restricted to the ridges.

Representation of polygon vegetation in the macrofossil assemblage

The subrecent plant macrofossil assemblage is closely related to the recent vegetation in the polygon. Although the water-filled depression might exert a certain trap effect on macrofossils, the low growth form of most plant taxa prevents seeds, fruits and leaves from being transported far. Only *Larix* needles are distributed over the entire polygon, but they are much more abundant near the actual trees. In the submerged centre, very few plant macrofossils accumulate. Most fossils were found on the ridges and in the transition.

Types of plant macrofossils that are most likely to represent especially ridge communities have been identified. Cones and short shoots of *Larix gmelinii*, leaves and seeds of *Arctostaphylos alpina*, and *Vaccinium uliginosum* and *Dryas octopetala* leaves are very good indicators of ridge conditions, while leaves of *Vaccinium microcarpum* indicate transitional conditions. In the polygon centre, only mosses and sedges may be found, which need to be identified to a lower taxonomic level in order to distinguish them from the mosses and sedges growing higher up. An additional identification and analysis of mosses may be very valuable for reconstructing such small-scale changes in topography and water level, as the species composition of mosses is very different in the centre and on the ridges. Water saturated or submerged soil conditions are indicated by the presence of ephippiae (resting egg pouches) of the cladoceran genus *Daphnia*.

Development of the polygon mire and its vegetation, water regime and climate during the last 1500 years

The two profiles that were dug on one ridge and its side (profiles A and B, respectively) date back to about the 5th century AD and span about 1500-1600 years. The short core from the middle of the mire (core C) reaches about 400 years into the past to about the 16th century AD. The macrofossil and sedimentological evidence suggests that dry ridgelike conditions prevailed from the oldest samples to about 1450 AD, followed by a phase of wetter and probably cooler conditions. Climatic warming is indicated in the most recent samples.

Reaction of polygon mires to a changing climate - outlook

The largest climate change is expected in the Arctic tundra (ACIA 2005). Increased decomposition of soil organic matter due to warmer and drier conditions will lead to substantial carbondioxide and methane release from the soil (e.g. Hobbie et al. 2000, Wagner et al., 2005). In the Siberian Arctic, the corridor between the southern climatic boundary for

active ice wedges and the Arctic Ocean in the North is rather narrow at present, and may disappear entirely if the boundary of polygon mire distribution shifts too far to the north. This would result in the loss of the regulatory peat and plant cover, and with it indispensable habitats for a variety of plant and animal taxa would disappear. The processes that are at work in polygon mires are still not completely understood, and will be worth investigating in a changing world.

7. References

ACIA (2005): Arctic Climate Impact Assessment. Cambridge University Press, Cambridge.

Agricultural Atlas of the Republic Sakha (Yakutia) (1989): Matveev, I.A. (ed.). Nauk, Moscow. 115 pp. In Russian.

Aleksandrova, V.D. (1980): The Arctic and Antarctic: their division into geobotanical areas. Cambridge University Press, Cambridge (English translation by D. Löve of the original Russian book from 1977.).

Anderberg, A.-L. (1994): Atlas of seeds and small fruits of Northwest-European plant species. (Sweden, Norway, Denmark, East Fennoscandia and Iceland) With morphological descriptions. Part 4. Resedaceae-Umbelliferae. Swedish Museum of Natural History, Stockholm.

Andreev, A.A., Siegert, C., Klimanov, V.A., Derevyagin, A.Y., Shilova, G.N. and Melles, M. (2002): Late Pleistocene and Holocene Vegetation and Climate on the Taymyr Lowland, Northern Siberia. Quaternary Research 57: 138-150.

Andreev, A. A., Grosse, G., Schirrmeister, L., Tarasov, P. E., Meyer, H., Kuzmina, S. A., Novenko, E. Y., Bobrov, A. A., Ilyashuk, B. P., Kuznetsova, T. V., Krbetschek, M. and Kunitsky, V. V. (2004): Late Saalian and Eemian palaeoenvironmental history of the Bol'shoy Lyakhovsky Island (Laptev Sea region, Arctic Siberia). Boreas 33: 319–348.

Anisimov, O.A. and Nelson, F.E. (1996): Permafrost distribution in the Northern Hemisphere under scenarios of climate change. Global and Planetary Change 14: 59-72.

Beijerinck, W. (1947): Zadenatlas der Nederlandsche Flora. Veenmann and Zonen, Wageningen.

Berggren, G. (1969): Atlas of seeds and fruits of Northwest-European plant species with morphological descriptions: Part 2. Cyperaceae. Swedish Natural Research Council, Stockholm.

Berggren, G. (1981): Atlas of seeds and fruits of Northwest-European plant species with morphological descriptions: Part 3. Salicaceae-Cruciferae. Swedish Natural Research Council, Stockholm.

Billings, W.D. and Peterson, K.M. (1980): Vegetational change and ice-wedge polygons through the thaw-lake cycle in arctic Alaska. Arctic and Alpine Research 12: 413-432.

Birks, H.H. (1980): Plant macrofossils in Quaternary lake sediments. E. Schweizerbart'sche Verlagsbuchhandlung, Stuttgart. 59 pp.

Birks, H.J.B. and Birks, H.H. (1980): Quaternary Palaeoecology. Edward Arnold, London.

Birks, H.H. and Birks, H.J.B. (2000): Future uses of pollen analysis must include plant macrofossils. Journal of Biogeography 27 (1): 31-35.

Bliss, L.C. and Matveeva, N.V. (1992): Circumpolar Arctic Vegetation. In: Chapin, F.S. (ed.): Arctic Ecosystems in a Changing Climate: An Ecophysiological Perspective. Academic Press, New York. pp. 59-90.

Boch, M.S. (1974): Bolota tundrovoi zony Sibiri (printsipy tipologii). In: Abramova, T.G. (ed.): Tipy bolot SSSR I printsipy ikh klassifikatsii. Nauka, Leningrad. pp. 146-154. In Russian.

Boike, J., Wille,C., Abnizova, A. (2008): Climatology and summer energy and water balance of polygonal tundra in the Lena River Delta, Siberia. Journal of Geophysical Research 113: G03025.

Borisenkov, E.P. (1992): Documentary evidence from the USSR. In: Bradley, R.S. and Jones, P.D. (eds.): Climate since AD 1500. Routledge, London. pp. 171-183.

Botch, M.S. and Masing, V.V. (1983): Mire ecosystems in the U.S.S.R. In: Gore, A.J.P. (ed.): Mires: swamp, bog, fen and moors. Ecosystems of the World 4b. Elsevier, Amsterdam. pp. 95-152.

Brouchkov, A., Fukada, M., Fedorov, A., Konstantinov, P. and Iwahana, G. (2004): Thermokarst as short-term permafrost disturbance, Central Yakutia. Permafrost and Periglacial Processses 15: 81-87.

Brown, J., Everett, K.R., Webber, P.J., MacLean Jr., S.F. and Murray, D.F. (1980): The coastal tundra at Barrow. In: Brown, J., Webber, P.C., Tieszen, L.L. and Bunnell, F.L. (eds.): An Arctic Ecosystem: The Coastal Tundra at Barrow, Alaska. Dowden, Hutchinson and Ross, Pennsylvania. pp. 1-29.

Brown, J., Hinkel, K.M. and Nelson, F.E. (2000): The Circumpolar Active Layer Monitoring (CALM) Program: research designs and initial results. Polar Geography 24 (3): 165-258.

Chernov, Y.I. and Matveyeva, N.V. (1997): Arctic ecosystems in Russia. In: Wielgolaski F.E. (ed.): Ecosystems of the World 3: Polar and Alpine Tundra. Elsevier, Amsterdam. pp. 361-507.

CHNOS Elementaranalysator vario EL III - Bedienungsanleitung (2005).

Clymo, R.S. (1984): The limits of peat bog growth. Philosophical Transactions of the Royal Society, London 303B. pp. 605-654.

deKlerk, P., Donner, N., Joosten, H., Karpov, N.S., Minke, M., Seifert, N. and Theuerkauf, M. (2009): Vegetation patterns, recent pollen deposition and distribution of non-pollen palynomorphs in a polygon mire near Chokurdakh (NE Yakutia, NE Siberia). Boreas 38: 39-58.

Doerge, T. (1999): Soil electrical conductivity mapping. Crop insights 9 (19).

Duigan, C.A. and Birks, H.H. (2000): The late-glacial and early-Holocene palaeoecology of cladoceran microfossil assemblages at Kraakenes, western Norway, with a quantitative reconstruction of temperature changes. Journal of Palaeolimnology 23: 67-76.

Eisner, W.R., Bockheim, J.G., Hinkel, K.M., Brown, T.A., Nelson, F.E., Peterson, K.M. and Jones, B.M. (2005): Palaeoenvironmental analyses of an organic deposit from an erosional landscape remnant, Actic Coastal Plain of Alaska. Palaeogeography, Palaeoclimatology, Palaeoecology 217: 187-204.

Ellenberg, H. (1988): Vegetation ecology of central Europe. 4th edition. Cambridge University Press, New York. 731pp.

Ellis, C.J. and Rochefort, L. (2006): Long-term sensitivity of a High Arctic wetland to Holocene climate change. Journal of Ecology 94: 441-454.

Federal State Statistics Russia (2009): data available from: www.info.gks.ru/eng/about.htm

Fortier, D. and Allard, M. (2004): Late Holocene synergetic ice-wedge polygons development, Bylot Island, Canadian Arctic Archipelago. Canadian Journal of Earth Sciences 41: 997-1014.

Franz, H.J. (1973): Physische Geographie der Sowjetunion. Hermann Haack, Gotha. 535pp. In German.

French, H.M. (2007): The Periglacial Environment. John Wiley and Sons, Chichester.

Gavrilova, M.K. (1993): Climate and Permafrost. Permafrost and Periglacial Processes 4: 99-111.

Geokryologiya SSSR (1989): Vostochnaya Sibir i Dalny Vostok (Geocryology of the USSR: Eastern Siberia and the Far East). Nedra Publishers, Moscow. 514 pp. In Russian.

Harris, S.A., French, H.M., Heginbottom, J.A., Johnston, G.H., Ladanyi, B., Sego, D.C. and van Everdingen, R.O. (1988): Glossary of permafrost and related ground ice terms. Ottawa. 156 pp.

Hinkel, K.M. and Nelson, F.E. (2003): Spatial and temporal patterns of active layer depth at CALM sites in northern Alaska, 1995-2000. Journal of Geophysical Research 108 (D2): 8168.

Hinkel, K.M., Outcalt, S.I. and Taylor, A.E. (1997): Seasonal patterns of coupled flow in the active layer at three sites in northwest North America. Canadian Journal of Earth Sciences 34: 667-678.

Hinzmann, L.D., Kane, D.L., Gieck, R.E. and Everett, K.R. (1991): Hydrologic and thermal properties of the active layer in the Alaskan Arctic. Cold Regions Science and Technology 19 (2): 95-110.

Hobbie, S.E., Schimel, J.P., Trumbore, S.E. and Randerson, J.R. (2000): Control over carbon storage and turnover in high-latitude soils. Global Change Biology 6 (1): 196-210.

Huh, Y. & Edmond, J.M. (1999): The fluvial geochemistry of the rivers of Eastern Siberia: III. Tributaries of the Lena and Anabar draining the basement terrain of the Siberian Craton and the Trans-Baikal highlands. Geochimica et Cosmochimica Acta 63 (7/8): 967-987.

International Permafrost Association (1998): Circumpolar Active-layer Permafrost System (CAPS). UNEP/GRID Arendal.

IUSS Working Group WRB (2007): World Reference Base for Soil Resources 2006. first update 2007. World Soil Resources Reports No. 103. FAO, Rome.

Joosten, H. (2008): Peatlands and carbon. In: Parish, F., Sirin, A., Charman, D., Joosten, H., Minaeva, T. and Silvius, M. (eds.): Assessment on peatlands, biodiversity and climate change. Global Environment Centre/Wetlands International: Kuala Lumpur/Wageningen. pp. 99-117.

Kane, D.L., Hinzmann, L.D. and Zarling, J.P. (1991): Thermal response of the active layer to climate warming in a permafrost environment. Cold Regions Science and Technology 19 (2): 111-122.

Katz, N. Ya., Katz, S.V.and Kipiani, M.G. (1965): Atlas and keys of fruits and seeds occurring in the quaternary deposits of the USSR. Nauka, Moscow. In Russian.

Kienel, U., Siegert, C. and Hahne, J. (1999): Late Quaternary palaeoenvironmental reconstruction from a permafrost sequence (North Siberian Lowland, SE Taymyr peninsula): A multi-disciplinary case study. Boreas 28: 181-193.

Konert, M. and Vandenberghe, J. (1997): Comparison of laser grain size analysis with pipette and sieve analysis: a solution for the underestimation of the clay fraction. Sedimentology 44: 523-535.

Koronkevich, N. (2002): Rivers, lakes, inland seas and Wetlands. In: Shagedanova, M. (ed.): The Physical Geography of Northern Eurasia. Oxford University Press, Oxford. pp. 122-148.

Koronovsky, N. (2002): Tectonics and Geology. In: Shagedanova, M. (ed.): The Physical Geography of Northern Eurasia. Oxford University Press, Oxford. pp. 1-35.

Kunitsky, V.V. (1989): Kriolitologiya nizov'ya Leny (Kryolithogenesis of the lower Lena). Russian Academy of Science, Siberian branch, Permafrost Institute Yakutsk. 164pp. In Russian.

Kutzbach, L., Wagner, D. and Pfeiffer, E.-M. (2004): Effect of microrelief and vegetation on methane emission from wet polygonal tundra, Lena Delta, Northern Siberia. Biogeochemistry 69: 341-362.

Lal, R. and Kimble, J.M. (2000): Soil C pool and dynamics in cold regions. In: Lal, R., Kimble, J.M. and Stewart, B:A. (eds.): Global climate change and cold regions ecosystems. Advances in Soil Science. Lewis Publishers, Boca Raton, FL, USA. pp. 3-28.

Loizeau, J.-L., Arbouille, D. Santiago, S. and Vernet, J.-P. (1994): Evaluations of a wide range laser diffraction grain-size analyzer for use with sediments. Sedimentology 41: 353-361.

Mackay, J.R. (2000): Thermally induced movements in ice-wedge polygons, Western Arctic Coast: A long-term study. Geogaphie physique et Quaternaire 54: 41-68.

Marchand, P.J. (1996): Life in the cold: An introduction to winter ecology. University Press of New England, Hanover. 304pp.

Matveyeva, N.V. (1994): Floristic Classification and Ecology of Tundra Vegetation of the Taymyr Peninsula, Northern Siberia. Journal of Vegetation Science 5 (6): 813-828.

Meyer, H. (2003): Studies on recent cryogenesis. In: Grigoriev, M.N., Rachold, V., Bolshiyanov, D.Y., Pfeiffer, E.M., Schirrmeister, L., Wagner, D. and Hubberten, H.-W. (eds.): Russian-German Cooperation System Laptev Sea. The Expedition LENA 2002. Berichte zur Polar-und Meeresforschung 466: 29-48.

Meyers, P.A. and Ishitawari, R. (1993): Lacustrine organic geochemistry - An overview of indicators of organic matter sources and diagenesis in lake sediments. Organic Geochemistry 20: 867-900.

Meyers, P.A. (1994): Preservation of elemental and isotopic identification of sedimentary organic matter. Chemical Geology 114: 289-302.

Meyers, P.A. and Lallier-Verges, E. (1999): Lacustrine sedimentary organic matter records of late quaternary palaeoclimates. Journal of Palaeolimnology 21: 345-372.

Minke, M., Donner, N., Karpov, N.S., de Klerk, P. and Joosten, H. (2007): Distribution, diversity, development and dynamics of polygon mires: examples from NE Yakutia (NE Siberia). Peatlands International 1/2007: 36-40.

Minke, M., Donner, N., Karpov, N., deKlerk, P. and Joosten, H. (2009): Patterns in vegetation composition, surface height and thaw depth in polygon mires in the Yakutian Arctic (NE Siberia): A microtopographical characterisation of the active layer. Permafrost and Periglacial Processes 20: 357-368.

Mock, C.J., Bartlein, P.J. and Anderson, P.M. (1998):Atmospheric circulation patterns and spatial climatic variations in Beringia. International Journal of Climatology 10: 1085-1104.

Naumov, Y.M.. (2004): Soils and soil cover of northeastern Eurasia. In: Kimble, J.M. (ed.): Cryosols. Springer, Berlin. pp. 161-183.

Nicholson, F.H. and Granberg, H.B. (1973): Permafrost and snow cover relationships near Schefferville. In: Proceedings of the Second International Conference on Permafrost, Yakutsk, USSR. North American contribution, National Academy of Science, Washington DC. pp. 151-158.

Paetzold, R.F., Hinkel, K.M., Nelson, F.E., Osterkamp, T.E., Ping, C.L. and Romanovsky, V.E. (2000): Temperature and thermal properties of Alaskan soils. In: Lal, R. and Kimble, J.M. and Stewart, B.A. (eds.): Global climate change and cold regions ecosystems. Lewis Publishers, Boca Raton, FL, USA. pp. 223-245.

Péwé, T.L. (1966): Ice wedges in Alaska - classification, distribution and climatic significance. In: Proceedings, 1st International conference on Permafrost. National Academy of Science: National Research Council of Canada, Publication 1287. pp. 76-81.

Polozhij, A.V. and Malyschev, L.I. (Eds.) (2004): Flora of Siberia, Vol. 8: Rosaceae. Science Publishers Inc., Enfield, NH, USA. 197pp.

Popp, S. (2006): Late quaternary environment of Central Yakutia (NE Siberia): Signals in frozen ground and terrestrial sediments. PhD thesis, Universität Potsdam.

Reimer, P.J., Baillie, M.G.L., Bard, E., Bayliss, A., Beck, J.W., Bertrand, C.J.H., Blackwell, P.G. and Buck, C.E. (2004): IntCal04 Terrestrial Radiocarbon Age Calibration, 0-26 Cal Kyr BP. Radiocarbon 46: 1029-1058.

Rivas-Martínez, S. (2007): Global bioclimatics. Data set. Phytosociological Research Center, Madrid, Spain (published online: http://www.globalbioclimatics.org)

Roman, L.T. (1981): Fiziko-mekhanicheskie svojstva merzlykh torfyanykh gruntov. Nauka, Novosibirsk. 237 pp. In Russian.

Romanovskij, N.N. (1977): Formirovanie Polygonalno-Zhilnykh Struktur. Nauka, Novosibirsk. In Russian.

Romanovskii, N.N. (1985): Distribution of recently active ice and soil wedges in the USSR. In: Church, M. and Slaymaker, O. (eds.): Field and theory. Univ. B.C. Press, Vancouver, BC, Canada. pp. 154-165.

Roulet, N.T., Woo, M.K. (1986): Hydrology of a wetland in the continuous permafrost region. Journal of Hydrology 89: 73-91.

Sachs, T., Wille, C., Boike, J. and Kutzbach, L. (2008): Environmental controls on ecosystem-scale CH_4 emission from polygonal tundra in the Lena River Delta, Siberia. Journal of Geophysical Research 113: G00A03. 12 pp

Scheffer, F. and Schachtschabel, P. (2002): Lehrbuch der Bodenkunde. Spektrum Akademischer Verlag, Heidelberg, Berlin. 593 pp. In German.

Schirrmeister, L., Siegert, C., Kuznetsova, T., Kuzmina, S., Andreev, A. A., Kienast, F., Meyer, H. and Bobrov, A. A. (2002): Paleoenvironmental and paleoclimatic records from permafrost deposits in the Arctic region of Northern Siberia. Quaternary International 89: 97–118.

Schirrmeister, L. , Kunitsky, V.V., Grosse, G. Wetterich, S., Meyer, H., Schwamborn, G., Babiy, O., Derevyagin, A.Y: and Siegert, C. (in press): Sedimentary characteristics and origin of the Late Pleistocene Ice Complex on north-east Siberian Arctic coastal lowlands and islands: A review. Quaternary International.

Schleser, G.H. (1995): Parameters determining carbon isotope ratios in plants. In: Frenzel, B., Stauffer, B. and Weiss, M.M. (eds.): Paläoklimaforschung/Palaeoclimate Research 15: 71-96.

Shahgedanova, M. (2002): The climate at present and in the historical past. In: Shahgedanova, M. (ed.): The physical geography of northern Eurasia. Oxford University Press, Oxford. pp. 70-102.

Shahgedanova, M. and Kuznetsov, M. (2002): The Arctic Environments, in: Shahgedanova, M. (ed.): The Physical Geography of Northern Eurasia. Oxford University Press. pp. 191-215.

Smol, J.P. and Douglas, M.S.V. (2007): Crossing the final ecological threshold in high Arctic ponds. Proceedings of the National Academy of Sciences (PNAS) 104: 12395-12397.

Sokolov, I.A., Ananko, T.V. and Konyushkov, D.Y. (2004): The Soil Cover of Central Siberia. In: Kimble, J. M. (ed.): Cryosols - Permafrost-Affected Soils. Springer, Berlin. pp. 303-338.

Stuiver, M. and Polach, H.A. (1977): Discussion - Reporting of $_{14}$C data. Radiocarbon 19 (3): 355-363.

Succow, M. and Stegmann, H. (2001): Nährstoffökologisch-chemische Kennzeichnung. In: Succow, M. and Joosten, H. (eds.): Landschaftsökologische Moorkunde. Schweizerbart'sche Verlagsbuchhandlung (Nägele und Obermiller), Stuttgart. pp. 75-85.

Svendsen, J.I., Alexanderson, H., Astakhov, V.I., Demidov, I., Dowdeswell, J.A., Funder, S., Gataulling, V., Henriksen, M., Hjort, C., Houmark-Nielsen, M., Hubberten, H.W., Ingólfsson, O., Jakobsson, M., Kjær, K., Larsen, E., Lokrantz, H., Lunkka, J.P., Lysså, A., Mangerud, J., Matiouchkov, A., Murray, A., Möller, P., Niessen, F., Nikolskaya, O., Polyakh, L., Saarnisto, M., Siegert, C., Siegert, M.J., Spielhagen, R.F. and Stein, R. (2004): Late Quaternary ice sheet history of northern Eurasia. Quaternary Science Reviews 23: 1229-1271.

The World Factbook (2008): The World Factbook. Central Intelligence Agency, Washington, D.C., USA. (available online: https://www.cia.gov/library/publications/the-world-factbook/geos/rs.html).

Tolmachaev, A.I., Packer, J.G., Griffith, J.C.D (1996): Flora of the Russian Arctic, Vol. II: Cyperaceae-Orchidaceae. University of Alberta Press, Edmonton, AB, Canada. h

USDA (1998): Keys to soil taxonomy. United States Department of Acriculture, Natural Resources Conservation Service, Soil Survey Staff, Washington, D.C., USA.

Wagner, D., Kobabe, S., Pfeiffer, E.-M. and Hubberten, H.-W. (2003): Microbial controls on methane fluxes from a polygonal tundra of the Lena Delta, Siberia. Permafrost and Periglacial Processes 14: 173-185.

Wagner, D., Lipski, A., Embacher, A. and Gattinger, A. (2005): Methane fluxes in extreme permafrost habitats of the Lena Delta: Effects of microbial community structure and organic matter quality. Environmental Microbiology 7: 1582-1592.

Walker, D.A, Gould, W.A., Maier, H.A. and Raynolds, M.K. (2002): The Circumpolar Arctic Vegetation Map: AVHRR-derived base maps, environmental controls, and integrated mapping procedures. International Journal of remote sensing 23: 4551-4570.

Washburn, A.L. (1980): Permafrost features as evidence of climatic change. Earth-Science Reviews 15: 327-402.

Webber, P.J., Miller, P.C., Chapin III, F.S. and McCown, B.H. (1980): The vegetation: pattern and succession. In: Brown, J., Miller, P.C., Tieszen, L.L. and Bunnell, F.L. (eds.): An Arctic Ecosystem: The Coastal Tundra at Barrow, Alaska. Dowden, Hutchinson and Ross, Pennsylvania, USA. pp. 186-218.

Weischet, W. and Endlicher, W. (2000): Regionale Klimatologie Teil 2 - Die alte Welt: Europa, Afrika, Asien. B.G. Teubner, Stuttgart. In German.

Wetterich, S. (2008): Freshwater ostracods as bioindicators in Arctic periglacial regions. PhD thesis, Alfred Wegener Institut Potsdam.

Woo, M.K. and Guan, X.J. (2006): Hydrological connectivity and seasonal storage change on tundra ponds in a polar oasis environment, Canadian High Arctic. Permafrost and Periglacial Processes 17: 309-323.

Woo, M.K. and Winter, T.C. (1993): The role of permafrost and seasonal frost in the hydrology of northern wetlands in North America. Journal of Hydrology 141: 5-31.

Yershov, E.D. (1998): General Geocryology, Cambridge University Press, Cambridge. 580 pp.

Zoltai, S.C. and Tarnocai, C. (1975): Perennially frozen peatlands in the western arctic and subarctic of Canada: Canadian Journal of Earth Sciences 12: 28-43.

Zoltai, S.C. and Pollett, F.C. (1983): Wetlands in Canada: Their classification, distribution, and use. In: Gore, A.J.P. (ed.): Mires: Swamp, bog, fen and moors. Ecosystems of the World 4b. Elsevier, Amsterdam. pp. 245-268.

A Appendix

A.1 Morphological data

Table 4 Ground surface elevation [cm] relative to the water level

	A	B	C	D	E	F	G	H	I	J	K	L
01	15	21	27	27	24	19	19	28	25	25	25	21
02	24	29	32	29	27	29	22	21	11	21	18	0
03	15	35	37	32	27	19	14	4	9	13	12	-61
04	12	39	43	27	3	-1	-2	4	6	10	11	-62
05	13	44	40	10	-2	-6	-11	0	5	6	9	-53
06	15	44	32	1	-12	-15	-14	0	3	9	6	-50
07	15	39	32	-6	-17	-15	-13	2	3	9	4	-52
08	14	37	28	-10	-17	-14	-10	-6	4	9	4	-62
09	16	31	15	-11	-14	-11	-6	-5	2	7	4	-54
10	8	27	20	-5	-7	-2	2	-2	4	6	7	-56
11	7	23	19	15	10	18	4	14	15	11	11	0
12	6	19	25	14	16	14	35	22	25	26	27	19
13	2	19	16	5	17	10	18	9	2	4	15	9

Table 5 Ice surface elevation [cm] relative to the water surface

	A	B	C	D	E	F	G	H	I	J	K	L
01	-8	-15	-13	-13	-12	-20	-23	-13	-8	-11	-22	-23
02	3	-10	-4	-4	-12	-12	-13	-23	-26	-19	-34	-49
03	-9	-1	2	-4	-22	-24	-35	-46	-43	-35	-46	-61
04	-15	5	22	-21	-53	-54	-54	-49	-47	-44	-53	-62
05	-20	5	18	-43	-60	-66	-65	-57	-49	-50	-49	-53
06	-18	15	-13	-57	-67	-71	-70	-60	-49	-44	-45	-50
07	-17	10	-18	-60	-72	-75	-71	-58	-51	-50	-54	-52
08	-21	0	-36	-70	-81	-80	-75	-69	-55	-49	-56	-62
09	-25	-5	-42	-72	-82	-79	-77	-72	-60	-54	-60	-54
10	-39	-5	-34	-67	-72	-71	-72	-72	-57	-53	-60	-56
11	-36	-12	-30	-58	-69	-65	-77	-56	-51	-52	-51	0
12	-41	-15	-30	-43	-46	-50	-35	-38	-32	-23	-21	-49
13	-50	-29	-39	-47	-48	-49	-42	-45	-46	-48	-35	-56

Table 6 Active layer thickness [cm]

	A	B	C	D	E	F	G	H	I	J	K	L
01	23	36	40	40	36	39	42	41	33	36	47	44
02	21	39	36	33	39	41	35	44	37	40	52	49
03	24	36	35	36	49	43	49	50	52	48	58	0
04	27	34	21	48	56	53	52	53	53	54	64	0
05	33	39	22	53	58	60	54	57	54	56	58	0
06	33	29	45	58	55	56	56	60	52	53	51	0
07	32	29	50	54	55	60	58	60	54	59	58	0
08	35	37	64	60	64	66	65	63	59	58	60	0
09	41	36	57	61	68	68	71	67	62	61	64	0
10	47	32	54	62	65	69	74	70	61	59	67	0
11	43	35	49	73	79	83	81	70	66	63	62	0
12	47	34	55	57	62	64	70	60	57	49	48	68
13	52	48	55	52	65	59	60	54	48	52	50	65

Table 7 Soil temperatures [° C]

	A	B	C	D	E	F	G	H	I	J	K	L
01	1.2	2.5	2.4	2.5	1.8	2.1	3.3	3	2.6	2.3	3.1	3.7
02	1.2	1.7	2.2	1.8	2.6	3	2.6	4.7	3.5	3.2	4.5	
03	1.4	1.4	1.5	2.5	2.7	4.7	5.8	5.7	4.8	4	5.4	
04	1.5	1.4	1	4.4	5.2	6.9	7.7	6.2	6.2	5.7	7.1	
05	1.5	2	1.8	4.5	7.3	8.3	8.6	7.6	6.2	6.6	9.1	
06	1.8	2.1	2.5	7.2	8.2	8.1	9.3	9.5	6.6	6.3	8.2	
07	1.7	1.4	4.6	8.1	8.5	8.4	8.6	8.5	6.2	6.3	8	
08	1.8	2.3	6.1	8.2	10.2	10.4	9.8	8.9	7.9	7.3	7.5	
09	2.7	2	6.4	8.5	9.1	10.2	9.4	8.6	7.2	7.2	7.7	
10	2.3	1.7	6.1	8.5	9	9.2	9.8	9.1	7.2	6.9	7.9	
11	2.6	2	3.2	5.3	5.9	5.5	7.3	6.7	5.8	6.4	5	6.7
12	3	3.5	2.6	3.8	3.7	4.9	5.3	4.9	3.9	3.4	4.1	4.6
13	4.1	3.5	4.1	3.2	4.6	3.7	4.8	3.8	4.4	5	3.9	4.5

A.2 Vegetation survey data

Table 8 Distribution of *Larix gmelini* in cover-abundance classes after Braun-Blanquet (1964); location of trees is indicated in bold numbers

	A	B	C	D	E	F	G	H	I	J	K	L
13						**40-50**		**40-50**	20-30			**10**
12		**20**				5	**100**	30-40				
11												
10												
9												
8												
7												
6												
5	2-5											
4	60	**100**	40									
3	5	50	20									
2											**40**	40-50
1											40-50	**50-60**

Table 9 Distribution of *Betula nana* in cover-abundance classes after Braun-Blanquet (1964)

	A	B	C	D	E	F	G	H	I	J	K	L
13	10	5	20	20	5-10	5	5-10	20				5-10
12	10	5	20	30	30	20	20	30	5			
11	10	10	40	40	30	30-40	10		30-40	10	10-20	20
10	10	10	20	5						30	30	
9	20	30	20	10						5-10	5	
8	20	20	10									
7	30	10	30							10	10	
6	10-20	5	10						5	30-40	30	10
5	5	20	20	20						30	10	10
4	5-10			5	10				5	30	30	5
3	20		30	20	40	10	10	10	5-10	30	20	5
2	10	5	20	10	10	10-15	20	20-30	10-20	30	30	10-20
1	20	5	10	20	10	30	10	10	10-20	10	30	10

Table 10 Distribution of *Salix* type A in cover-abundance classes after Braun-Blanquet (1964)

	A	B	C	D	E	F	G	H	I	J	K	L
13	10	2-5				5						
12												
11							2-5				30-40	
10	5											
9												
8	5											
7												
6	2-5											
5												
4	2-5											
3	2-5											
2	5	2-5	1	2-5								
1	10		10					20				

Table 11 Distribution of *Salix* type B in cover-abundance classes after Braun-Blanquet (1964)

	A	B	C	D	E	F	G	H	I	J	K	L
13	5	20	30	30	2-5	20	20	30-40	30	30	80	70-80
12		20	10	20-30	20	5-10	20	30	20	20	20	30
11	5	20-25	20	20	30	20	5	5	20	10		
10		30	40-50	10						10	10-20	5
9	10	20	20	5						5	20	
8	5-10	10	5							5-10	10	
7	5	20								30	10-20	
6	30	30	20	10					5	5-10		5
5	50	10	60	30					5-10	5-10		
4	20	5-10	30	5	5				5	2-5	5	
3	20	20	5		10	30	30	5-10	5	10	5-10	
2	5	10		5	5	5	10	20	10	10	10	
1	20	5		10	30	30	2-5		5	2-5	40	60

Table 12 Distribution of *Dryas octopetala* in cover-abundance classes after Braun-Blanquet (1964)

	A	B	C	D	E	F	G	H	I	J	K	L
13		2-5		1	5		2-5					
12		5	5	2-5	5	5-10	2-5	5-10	5-10	5	5	5
11		5			1	5	2-5	5	5			
10		10										
9		10										
8	1	10										
7		1										
6		5										
5												
4												
3		1			5-10							
2		10	5	5	5	5	2-5	2-5	2-5			
1	1	1	1	10	10		2-5	2-5	5	5	5	

Table 13 Distribution of *Andromeda polifolia* in cover-abundance classes after Braun-Blanquet (1964)

	A	B	C	D	E	F	G	H	I	J	K	L
13	5	2-5	5	5	2-5							
12	10-20			5	2-5	2-5		5-10		2-5	2-5	5
11	10	5	10	5	10	5-10	5	5-10	10-20	5-10	5-10	5
10	5-10	5	5							5	5-10	1
9	5	1	1									
8	1	1										
7	5									5-10	5	
6	5			5						5-10	10-15	1
5	5-10			5					5	20	20-30	
4	5-10			10-15	5				5-10	20-30	10-20	
3	5	1				20	5	5	10-20	5-10	5-10	2-5
2	2-5				2-5	2-5	5	5	5-10	5-10	5	2-5
1					10	5	5-10	5-10	5			5

Table 14 Distribution of *Arctostaphylos alpina* in cover-abundance classes after Braun-Blanquet (1964)

	A	B	C	D	E	F	G	H	I	J	K	L
13		2-5	5									
12		2-5		5			5-10		5		5	5
11								1	2-5			
10		5										
9												
8												
7												
6	1											
5												
4												
3												
2								1				
1	2		1			2-5	5		1		1	2-5

Table 15 Distribution of *Ledum palustre* in cover-abundance classes after Braun-Blanquet (1964)

	A	B	C	D	E	F	G	H	I	J	K	L
13												10
12				1	5	5		10			5-10	40
11			5								5	10
10			10								2-5	
9	5											
8												
7												
6	1											
5		5										
4				2-5						5-10		
3				5		20	5-10		5-10	10	10	
2						1		5-10	2-5	20	20	
1			2-5			2-5	5		5	2-5		

Table 16 Distribution of *Vaccinium* sp. in cover-abundance classes after Braun-Blanquet (1964)

	A	B	C	D	E	F	G	H	I	J	K	L
13		5	5	40	30-40	20	10	20	10	5	10	
12		10	10	30	40	10	30	20	40	30	10	
11		5	5	10	20	20	30	20		20		5-10
10												
9	5	20	30									
8	5	30	70	10								
7	40	50	60	15-20								
6	20	60	60	10								
5	10	30	30	10								
4		5-10	20	50	20						10-20	
3	5-10	5	10	20	10	20	20	10	20	20	10	
2	10					5-10	30	30	30	30	5-10	20
1	5				5	20		30	5	5-10	20	20

Table 17 Distribution of *Pedicularis* sp. in cover-abundance classes after Braun-Blanquet (1964)

	A	B	C	D	E	F	G	H	I	J	K	L
13			2-5	1								
12	1											
11	1									1		
10										1	1	
9											2-5	
8		1										
7	2-5											
6										1		
5	1			1						2-5	2-5	
4					1						1	
3								1				
2												
1	1							1				

Table 18 Distribution of *Polygonum* sp. in cover-abundance classes after Braun-Blanquet (1964)

	A	B	C	D	E	F	G	H	I	J	K	L
13	1	1	1	1	2-5							
12	1	1		1	1	1						
11	1		1						2-5	1		
10												
9												
8	1											
7												
6												
5	1											
4												
3						1						
2												
1	1								1			

Table 19 Distribution of Poaceae in cover-abundance classes after Braun-Blanquet (1964)

	A	B	C	D	E	F	G	H	I	J	K	L
13												
12												
11	1											
10												
9												
8	5											
7		5-10										
6												
5												
4												
3												
2	5		5									
1	5									5-10		
	A	**B**	**C**	**D**	**E**	**F**	**G**	**H**	**I**	**J**	**K**	**L**

Table 20 Distribution of *Carex* type A in cover-abundance classes after Braun-Blanquet (1964)

	A	B	C	D	E	F	G	H	I	J	K	L
13	20	20	20	10	5-10	10	20	20-30	10	20-30	20	20
12	10	10	20	30	20	20	10	20	10-20	40	20	10
11	30	20	5	20	20	20	10	20	10	5-10	5	20
10	20	30	20	5	2-5	10	5-10	10-20	20	5-10	5	20
9		20-30	20	10				2-5	30	20	10	30
8	20	20	10	10				2-5	40	30-40	5	20
7	20	10	10-20	20	5			10-20	30	20	10	20
6	20	10	10	30	5-10			2-5	20-30	20	5	20-30
5	10	20	10	20	5-10		20	10	10-20	30	5-10	30
4	5	5	5	10	10	20	30-40	40-50	20-30	10-20	5	20
3	20	5-10	10	10	5	20	10-20	20-30	20	10-20	2-5	20-30
2	5	10	10	10	20	5	10	5-10	20	10	5	10
1	10	30	30	20	20	20	20	10-20	10	2-5	10	10

Table 21 Distribution of *Carex* type B in cover-abundance classes after Braun-Blanquet (1964)

	A	B	C	D	E	F	G	H	I	J	K	L
13	1											
12	5	1										
11			5	10	10	5	20	5-10	5-10		10-20	5-10
10		1	5	10	30	5	20-30	20-30	40	20	40	10
9			5	5	2-5			10	40	20	30-40	10
8		1		10				10	10-20	20-30	50-60	10
7				10			2-5	10	10	30	30-40	10
6	1	5		20	10-20		5-10	20-30	10-20	30	30-40	10-20
5	1			20	20-30	50	30	20-30	10-20	20	10-20	10
4					10	60	40-50	30-40			5	10
3							30	5-10			5	10-20
2					10						2-5	5
1	1				5-10						5	2-5

Table 22 Distribution of *Dicranium* sp. in cover-abundance classes after Braun-Blanquet (1964)

	A	B	C	D	E	F	G	H	I	J	K	L
13		10					10-20					
12												
11												
10												
9		10										
8												
7	15											
6				10						5-10		
5												
4					5							
3	10						5-10	5				
2										5-10		
1						10		10				

Table 23 Distribution of Moss type A in cover-abundance classes after Braun-Blanquet (1964)

	A	B	C	D	E	F	G	H	I	J	K	L
13												
12												
11												
10	5											
9												
8												
7												
6												
5	5											
4	5-10											
3												
2	2-5											
1	10											

Table 24 Distribution of Moss type B in cover-abundance classes after Braun-Blanquet (1964)

	A	B	C	D	E	F	G	H	I	J	K	L
13	30	10	40	10	20	5	10	10-20	5	5	10	10
12	20	10	20	10	20	10	20	20		10	10	10
11	10	10	2-5	5	10	10	5-10	5-10	30	10	20	
10	20	5	10							5-10	10	
9	10-20	50	20									
8	40	5	20									
7	10-15	5	10								10	
6	10-20	20	60							10		
5	40	20	10	20						10-20		
4	30	40	10	40	10					5-10	30	
3	10-20	40	10-20	70	20	50				10	30	
2	60	20	10	5	10	10	10	10	10	10	30	5
1	60	20	20	40	80	20	5-10	10-20		30-40	10-20	

Table 25 Distribution of the aquatic moss in cover-abundance classes after Braun-Blanquet (1964); bold numbers indicate sole presence of aquatic moss

	A	B	C	D	E	F	G	H	I	J	K	L
13												
12												
11							20-30					20-30
10				50-60	60	100	60	60	30-40	30-40		30-40
9				80	70	**50**	**100**	100	40	20	20	40-50
8				70	70	**40**	**100**	100	20-30	20-30	20-30	50-60
7				50	100	**100**	100	90-100	50-60	20	20-30	50-60
6					80-90	**100**	90	100	20-30		20-30	30
5	1				40	100	60-70	80-90			20-30	40-50
4						40	40					50-60
3							30				10	30-40
2											20	30
1												5-10

A.3 Results from the surface transect

Table 26 Sediment properties in the surface transect

Sample number	**Sand** [vol %]	**Silt** [vol %]	**Clay** [vol %]	**TC** [wt %]	**TIC** [wt %]	**TOC** [wt %]	**TN** [wt %]	**TOC/TN**	**$\delta^{13}C$** [‰ vs. PDB korr.]	**pH**	**Electric conductivity** [mS/cm]
07-SA-LY 01	78.66	17.88	3.47	32.61	0.53	32.08	0.78	41.03	-29.23	6.14	84
07-SA-LY 02	74.68	21.57	3.76	21.17	5.51	15.66	0.51	31.01	-29.74	5.83	49
07-SA-LY 03	38.01	55.03	6.96	38.1	-0.3	38.41	1.36	28.35	-28.84	5.7	24
07-SA-LY 04	50.49	46.07	3.4	34.32	-1.81	36.13	1.3	27.84	-28.25	5.85	35
07-SA-LY 05	52.24	35.4	12.36	28.4	0.48	27.93	1.25	22.38	-29.2	6.13	33
07-SA-LY 06	40.82	42.21	17.04	26.59	0.26	26.33	1.39	18.99	-29.95	6.25	29
07-SA-LY 07	58.86	32.22	8.87	16.7	-2.93	19.63	1.06	18.6	-29.5	6.25	23
07-SA-LY 08	56.54	36.52	6.89	17.81	1.65	16.15	1.05	15.44	-28.88	6.25	16
07-SA-LY 09	60.24	29.79	10.01	20.01	1.95	18.07	1.14	15.8	-29.25	6.17	21
07-SA-LY 10	39.16	52.66	8.2	35.89	16.99	18.9	1.47	12.89	-28.2	6.12	26
07-SA-LY 11	45.36	49.38	5.2	38	0.35	37.65	1.18	32.05	-29.62	5.92	66
07-SA-LY 12	38.86	54.92	6.26	38.84	-0.65	39.49	0.76	52.19	-29.28	6.06	37
07-SA-LY 13	55.33	40.96	3.71	36.89	-1.55	38.44	1.3	29.59	-30.3	5.74	29

Table 27 Plant macrofossils in the surface transect

Sample number	*Larix gmelinii* needle	*Larix gmelinii* seed	*Larix gmelinii* short shoot	*Larix gmelinii* cone	*Betula nana* leaf	*Betula nana* fruit	*Betula nana* catkin scale	*Betula nana* catkin	*Salix* sp. leaf	*Salix polaris* leaf	*Salix* sp. capsule	*Dryas octo-petala* leaf	*Andro-meda polifolia* leaf	*Andro-meda polifolia* seed	*Arcto-staphylos alpina* leaf
07-SA-LY-01	273	8	0	0	1	2	2	1	2	0	0	0	58	13	6
07-SA-LY-02	40	2	0	0	8	0	0	0	1	0	0	1	3	1	0
07-SA-LY-03	386	3	0	0	1	0	0	0	2	0	0	0	46	1	0
07-SA-LY-04	142	0	0	0	1	0	0	0	0	0	0	0	1	0	0
07-SA-LY-05	51	0	0	0	0	0	0	0	0	0	0	0	0	0	0
07-SA-LY-06	54	0	0	0	0	1	0	0	0	0	0	0	0	0	0
07-SA-LY-07	339	1	0	0	0	0	0	0	1	0	0	0	0	0	0
07-SA-LY-08	102	0	0	0	1	0	0	0	0	0	0	0	1	0	0
07-SA-LY-09	332	2	0	0	0	0	0	0	0	0	0	0	1	0	0
07-SA-LY-10	295	2	0	0	1	0	1	0	0	0	0	0	8	0	0
07-SA-LY-11	218	3	0	0	11	3	0	0	8	0	0	1	48	5	0
07-SA-LY-12	121	3	7	0	3	0	1	0	2	0	1	0	18	0	0
07-SA-LY-13	448	3	0	1	6	0	0	0	14	1	1	0	4	2	0

Table 27 continued

Sample number	*Arcto-staphylos alpina* seed	*Eriophorum* sp. seed	*Eriophorum angusti-folium* seed	*Erio-phorum russeolum* seed	*Vaccinium vitis-idaea* seed	*Vaccinium vitis-idaea* berry	*Vaccinium uliginosum* leaf	*Vaccinium* sp. seed	*Oxycoccus microcarpus* leaf	*Luzula* sp. seed	*Comarum palustre* seed	*Carex* sp. seed	*Daphnia* ephippiae
07-SA-LY-01	7	1	0	0	0	0	2	1	0	0	0	32	0
07-SA-LY-02	0	0	0	0	0	1	1	0	0	0	0	4	0
07-SA-LY-03	0	0	0	1	0	0	1	0	16	0	0	47	1
07-SA-LY-04	0	0	0	0	0	0	0	0	2	0	0	9	4
07-SA-LY-05	0	0	0	0	0	0	0	0	0	0	0	1	1
07-SA-LY-06	0	0	0	0	0	0	0	0	0	0	0	0	0
07-SA-LY-07	0	0	0	0	0	0	0	0	0	1	0	5	4
07-SA-LY-08	0	0	0	0	0	0	0	2	0	0	0	7	2
07-SA-LY-09	0	0	0	0	0	0	0	0	0	1	0	7	7
07-SA-LY-10	0	0	0	0	0	0	0	0	2	0	0	13	4
07-SA-LY-11	0	0	2	0	0	0	0	0	20	0	0	40	1
07-SA-LY-12	0	0	1	0	0	0	0	0	0	0	1	19	0
07-SA-LY-13	0	0	1	0	24	0	2	0	0	0	0	14	0

A.4 Results from profile A

Table 28 Sediment properties and plant macrofossils from profile A

Sample number	**Sand** [vol %]	**Silt** [vol %]	**Clay** [vol %]	**TC** [wt %]	**TIC** [wt %]	**TOC** [wt %]	**TN** [wt %]	**TOC/TN**	**$\delta^{13}C$** [‰ vs. PDB korr.]	***Larix gmelinii*** needle	***Larix gmelinii*** seed	***Betula nana*** leaf	***Betula nana*** fruit	***Betula nana*** catkin scale
07-SA-LY A-01	53.7	44.28	2.04	32.61	42.24	32.08	0.78	1.32	-28.98	155	4	5	0	4
07-SA-LY A-02	46.13	47.1	6.75	13.87	40.35	10.26	0.45	3.93	-28.55	49	1	2	0	0
07-SA-LY A-03	95.2	4.101	0.71	2.1	3.39	1.48	0.11	2.29	-27.31	2	0	0	0	0
07-SA-LY A-04	92.13	6.731	1.18	3.63	5.55	1.492	0.2	3.72	-27.73	0	0	1	1	0
07-SA-LY A-05	91.62	7.26	1.14	2.76	6.12	1.55	0.15	3.95	-27.75	0	0	0	0	0
07-SA-LY A-06	86.06	11.51	2.36	2.09	9.15	1.414	0.12	6.47	-27.76	1	0	0	0	0
07-SA-LY A-07	91.51	7.31	1.22	2	6.09	1.211	0.19	5.03	-27.1	1	0	0	0	0
07-SA-LY A-08	87.24	10.51	2.23	2.69	8.28	1.866	0.16	4.44	-26.91	0	0	0	0	0
07-SA-LY A-09	87.12	10.65	2.25	4.04	8.41	2.797	0.26	3.01	-26.31	0	0	1	0	0
07-SA-LY A-10	83.93	13.28	2.76	2.67	10.52	1.844	0.24	5.7	-26.65	0	0	0	0	0
07-SA-LY A-11	77.57	18.7	3.71	1.9	15	1.261	0.13	11.89	-26.93	1	0	0	0	0
07-SA-LY A-12	63.43	30.21	6.36	2.31	23.85	1.913	0.12	12.47		1	0	0	0	0
07-SA-LY A-13	69.58	25.34	5.07	1.74	20.27	1.716	<0.1		-26.76	0	0	0	0	0
07-SA-LY A-14	77.91	16.53	5.5	1.81	11.04	1.195	<0.1		-27.37	2	0	0	0	0
07-SA-LY A-15	67.87	26.91	5.22	3.05	21.69	2.141	0.11	10.13	-26.64	0	0	0	0	0
07-SA-LY A-16	77.62	17.31	5.11	3.66	12.2	2.411	0.11	5.06	-26.77	0	0	0	0	0
07-SA-LY A-17	59.9	32.9	7.23	4.38	25.67	3.085	0.18	8.32	-27.11	0	0	0	0	0
07-SA-LY A-18	49	42.07	8.94	4.49	33.13	3.326	0.18	9.96	-26.76	0	0	0	0	0

Table 28 continued

Sample number	*Andromeda polifolia* leaf	*Andromeda polifolia* seed	*Dryas octopetala* leaf	*Vaccinium microcarpum* leaf	*Vaccinium vitis-idaea* leaf	*Arctostaphylos alpina* leaf	*Arctostaphylos alpina* seed	*Saxifraga* sp. seed	*Carex* sp. seed	*Daphnia* ephippiae
07-SA-LY A-01	56	0	0	0	2	1	0	0	9	0
07-SA-LY A-02	2	0	1	0	0	1	2	0	2	0
07-SA-LY A-03	0	1	0	0	0	0	0	0	3	0
07-SA-LY A-04	0	0	0	0	0	0	0	1	0	0
07-SA-LY A-05	0	0	1	0	0	0	0	0	4	0
07-SA-LY A-06	0	0	0	0	0	0	0	0	0	0
07-SA-LY A-07	0	0	0	0	0	0	0	0	1	0
07-SA-LY A-08	0	0	7	0	0	0	0	0	1	0
07-SA-LY A-09	0	0	47	0	0	0	0	0	1	0
07-SA-LY A-10	0	0	3	0	0	0	1	0	3	0
07-SA-LY A-11	0	0	0	0	0	0	1	0	0	0
07-SA-LY A-12	0	0	0	0	0	0	0	0	2	1
07-SA-LY A-13	1	0	21	0	0	0	0	0	6	0
07-SA-LY A-14	1	0	60	0	0	0	0	0	4	0
07-SA-LY A-15	0	0	9	0	0	0	0	0	0	0
07-SA-LY A-16	0	0	8	0	0	0	0	0	0	0
07-SA-LY A-17	0	0	1	0	0	0	0	0	3	0
07-SA-LY A-18	0	0	1	1	0	0	0	0	2	0

A.5 Results from profile B

Table 29 Sediment properties and plant macrofossils from profile B

Sample number	Sand [vol %]	Silt [vol %]	Clay [vol %]	TC [wt %]	TIC [wt %]	TOC [wt %]	TN [wt %]	TOC/TN	$\delta^{13}C$ [‰ vs. PDB korr.]	*Larix gmelinii* needle	*Larix gmelinii* seed	*Betula nana* leaf	*Betula nana* fruit	*Salix* sp. leaf	*Salix* sp. bud
07-SA-LY B-01	46.5	46.12	7.4	32	14.1	33.08	1.2	2.35	-29.8	143	0	1	0	2	0
07-SA-LY B-02	50.13	42.97	6.87	32.2	10.75	32.59	1.38	3.03	-29.5	474	2	0	1	0	0
07-SA-LY B-03	55.58	38.89	5.56	21	17.85	18.98	1.1	1.06	-28	291	0	0	0	0	0
07-SA-LY B-04				2.22		1.31	0.11	-0.59	-28.6	1	0	1	0	0	0
07-SA-LY B-05	79.52	17.1	3.41	3.49	13.61	1.92	0.18	0.14	-28.5	10	0	1	0	0	0
07-SA-LY B-06	93.04	6.21	0.77	2.47	3.75	1.5	0.11	0.4	-29	1	0	0	0	0	0
07-SA-LY B-07	73.33	22.63	4.06	2.42	20.21	1.73	0.11	0.09	-29.3	3	0	1	0	1	0
07-SA-LY B-08	88.26	10.65	1.06	2.84	7.81	1.86	0.11	0.24	-29.1	1	0	0	0	0	0
07-SA-LY B-09	72.82	23.77	3.41	5.19	18.58	3.53	0.22	0.19	-29	1	0	0	0	0	0
07-SA-LY B-10	54.72	37.04	8.26	7.13	29.91	5.55	0.31	0.19	-28.2	1	0	0	0	0	0
07-SA-LY B-11	56.81	36.17	7.04	6.35	29.82	4.89	0.24	0.16	-26.5	1	0	0	0	0	1
07-SA-LY B-12	68.92	26.11	4.96	7.76	18.35	5.99	0.26	0.33	-25.4	3	0	1	0	0	0
07-SA-LY B-13	81.99	14.82	3.21	3.4	11.42	2.78	0.1	0.24	-25.5	2	0	0	0	0	0
07-SA-LY B-14	95.01	4.4	0.6	2.15	2.25	1.72	<0.1		-25.8	3	1	0	0	0	0
07-SA-LY B-15	75.25	21.51	3.19	2.04	19.47	1.49	<0.1		-25.3	2	0	0	0	0	0
07-SA-LY B-16	76.99	20.07	2.97	3.28	16.8	2.63	0.1	0.16	-25.7	0	0	0	0	0	0
07-SA-LY B-17	83.93	12.75	3.37	1.93	10.82	1.58	<0.1		-25.9	1	0	0	0	0	0
07-SA-LY B-18	84.1	13.68	2.24	2.6	11.08	2.38	<0.1		-25.4	1	0	0	0	0	0
07-SA-LY B-19	75.3	21.54	3.17	3.66	17.88	3.02	<0.1		-25.4	0	0	0	0	0	0
07-SA-LY B-20	96.17	3.34	0.48	2.05	1.29	1.65	<0.1		-25.8	0	0	0	0	0	0
07-SA-LY B-21	72.19	23.18	4.65	5.98	17.2	5.51	0.12	0.32	-27.4	0	0	0	0	0	0
07-SA-LY B-22	70.4	26.02	3.54	6.48	19.54	5.74	0.14	0.29	-27.6	0	0	0	0	0	0

Table 29 continued

Sample number	*Andromeda polifolia* leaf	*Vaccinium microcarpum* leaf	*Vaccinium uliginosum* leaf	*Vaccinium vitis-idaea* leaf	*Carex* sp. seed	Poaceae seed	*Polygonum viviparum* seed	*Luzula* sp. seed	*Valeriana capitata* fruit	Daphnia ephippiae
07-SA-LY B-01	1	3	1	0	17	1	0	0	0	0
07-SA-LY B-02	21	4	0	1	19	0	0	0	0	0
07-SA-LY B-03	16	8	0	0	15	0	0	0	0	0
07-SA-LY B-04	0	0	0	0	13	0	1	0	0	4
07-SA-LY B-05	2	0	0	0	11	0	0	0	0	1
07-SA-LY B-06	0	0	0	0	10	1	0	2	0	4
07-SA-LY B-07	0	0	0	0	27	0	0	0	0	1
07-SA-LY B-08	0	0	0	0	5	0	0	0	0	1
07-SA-LY B-09	0	0	0	0	8	0	0	0	0	10
07-SA-LY B-10	0	0	0	0	16	0	0	0	1	6
07-SA-LY B-11	0	0	0	0	11	0	0	0	0	6
07-SA-LY B-12	0	0	0	0	3	0	0	0	0	0
07-SA-LY B-13	0	0	0	0	6	0	0	0	0	0
07-SA-LY B-14	1	0	0	0	6	0	0	0	0	0
07-SA-LY B-15	0	0	0	0	5	0	0	0	0	0
07-SA-LY B-16	0	0	0	0	6	0	0	0	0	0
07-SA-LY B-17	0	0	0	0	2	0	0	0	0	0
07-SA-LY B-18	1	0	0	0	3	0	0	0	0	0
07-SA-LY B-19	0	0	0	0	3	1	0	0	0	0
07-SA-LY B-20	0	0	0	0	1	0	0	0	0	0
07-SA-LY B-21	0	0	0	0	2	0	0	0	0	0
07-SA-LY B-22	0	0	0	0	2	0	0	0	0	0

A.5 Results from core C

Table 30 Sediment properties from core C

Sample number	Sand [vol %]	Silt [vol %]	Clay [vol %]	TC [wt %]	TIC [wt %]	TOC [wt %]	TN [wt %]	TOC/TN	$\delta^{13}C$ [‰ vs. PDB korr.]
07-SA-LY C-01	14.67	67.21	18.15	24.5	-1.47	25.94	1.41	18.37	-28.7
07-SA-LY C-02	32.53	54.98	12.53	17.9	3.75	14.18	1.12	12.65	-29.6
07-SA-LY C-03	78.12	17.33	4.51	5.58	2.23	3.35	0.36	9.22	-29.2
07-SA-LY C-04	83.06	12.84	4.06	3.57	1.8	1.77	0.23	7.76	-28.6
07-SA-LY C-05	87.02	10.42	2.59	2.73	1.12	1.61	0.17	9.25	-30.2
07-SA-LY C-06	82.75	13.38	3.89	2.86	0.78	2.09	0.17	12.46	-30.6
07-SA-LY C-07	86.82	9.69	3.45	2.1	0.72	1.38	0.16	8.66	-29.8
07-SA-LY C-08	81.2	14.92	3.89	4.4	0.89	3.51	0.31	11.49	-29.7
07-SA-LY C-09	60.22	33.13	6.66	6.7	1.7	5	0.4	12.6	-29.6
07-SA-LY C-10	56.26	36.31	7.42	6.8	1.39	5.4	0.33	16.33	-28.8
07-SA-LY C-11	75.64	19.62	4.77	3.89	0.87	3.02	0.18	16.54	-27.6
07-SA-LY C-12	75.31	20.31	4.38	4.83	1.15	3.68	0.24	15.65	-26.9
07-SA-LY C-13	51.5	40.25	8.32	9.89	1.67	8.22	0.41	20.05	-26.9
07-SA-LY C-14	70.68	24.48	4.8	6.35	1.06	5.29	0.2	25.98	-27.7
07-SA-LY C-15	87.42	9.6	3.05	3.16	0.66	2.5	0.14	17.43	-29.9
07-SA-LY C-16	90.8	6.36	2.82	1.13	0.26	0.87	< 0.1		-29.4
07-SA-LY C-17	97.05	2.68	0.24	0.83	0.24	0.59	< 0.1		
07-SA-LY C-18	95.2	3.72	0.96	0.15	-0.09	0.25	< 0.1		
07-SA-LY C-19	98.73	1.28	0.09	0.13	-0.07	0.2	< 0.1		
07-SA-LY C-20	98.39	1.57	0.15	0.56	0.07	0.49	< 0.1		
07-SA-LY C-21	96.37	2.82	0.75	2.78	0.69	2.08	< 0.1		-25.9
07-SA-LY C-22	89.63	8.73	1.62	4.73	1	3.73	0.17	21.42	-26
07-SA-LY C-23	85.03	12.84	2.12	4.77	0.74	4.03	0.19	21.72	-26.1
07-SA-LY C-24	89.65	8.66	1.66	1.97	0.52	1.45	< 0.1		-27.1
07-SA-LY C-25	95.05	4.06	0.92	2.01	0.54	1.47	0.1	12.07	-27.3
07-SA-LY C-26	80.73	16.45	2.82	3.19	0.8	2.39	0.16	14.71	-26.1
07-SA-LY C-27	77.17	19	3.84	4.85	0.82	4.04	0.22	18.37	-26.6

A.6 Results from Accelerator Mass Spectrometry (AMS) dating

Table 31 Radiocarbon dates

Laboratory number	Sample number	Elevation [cm above water level]	Description	^{14}C age [yrs BP]	Calibrated calendar age, two sigma range [yrs AD]
KIA 39094	07-SA-LY A-09	Ridge	Plant remains	425 ± 25	1426-1495
KIA 38752	07-SA-LY A-18	Ridge	Seeds and wood	1585 ± 25	420-539
KIA 38753	07-SA-LY B-22	Ridge-centre transition	Seeds	1565 ± 35	417-568
KIA 39095	07-SA-LY C-26	Centre	Plant remains	405 ± 25	1436-1516

Selbständigkeitserklärung

Hiermit erkläre ich, dass ich die vorliegende Arbeit selbständig und nur unter Verwendung der angegebenen Literatur und Hilfsmittel angefertigt habe. Aus fremden Quellen direkt oder indirekt übernommene Inhalte sind als solche gekennzeichnet.
Diese Arbeit wurde bisher keiner anderen Prüfungsbehörde in gleicher oder ähnlicher Form vorgelegt und auch nicht veröffentlicht.

Ort, Datum Unterschrift